COPY 1

DOT/FAA/CT-83/28

FAA WJH Technical Center
00093454

Radiative Ignition and Opposed Flow Flame Spread Measurements on Materials

Margaret Harkleroad
James Quintiere
William Walton

FEDERAL AVIATION ADMINISTRATION
SEP 2 1983
TECHNICAL CENTER LIBRARY
ATLANTIC CITY, N.J. 08405

August 1983

Final Report

This document is available to the U.S. public through the National Technical Information Service, Springfield, Virginia 22161.

US Department of Transportation
Federal Aviation Administration
Technical Center
Atlantic City Airport, N.J. 08405

NOTICE

This document is disseminated under the sponsorship of the Department of Transportation in the interest of information exchange. The United States Government assumes no liability for the contents or use thereof.

The United States Government does not endorse products or manufacturers. Trade or manufacturer's names appear herein solely because they are considered essential to the object of this report.

Technical Report Documentation Page

1. Report No.	2. Government Accession No.	3. Recipient's Catalog No.
DOT/FAA/CT-83/28		

4. Title and Subtitle	5. Report Date
RADIATIVE IGNITION AND OPPOSED FLOW FLAME SPREAD MEASUREMENTS ON MATERIALS	August 1983
	6. Performing Organization Code
7. Author(s) Margaret Harkleroad, James Quintiere and William Walton	8. Performing Organization Report No.
9. Performing Organization Name and Address National Bureau of Standards Department of Commerce Washingtion, D.C. 20234	10. Work Unit No. (TRAIS)
	11. Contract or Grant No. 181-350-100
12. Sponsoring Agency Name and Address U.S. Department of Transportation Federal Aviation Administration Technical Center Atlantic City Airport, New Jersey 08405	13. Type of Report and Period Covered March 1981 - Sept. 1982
	14. Sponsoring Agency Code

15. Supplementary Notes

16. Abstract

The purpose of this study is to develop a fire-testing method that relates material ignitability and flame spread in the creeping mode. The analytical approach involves parameters and solutions arising from transient heat condition to a semi-infinite solid. Experimental data are generated on an apparatus employing a radiant panel to provide a varying heat flux to test specimens. Flame-spread rates and ignition events are measured against incident radiation and exposure time. The flame-spread data for given materials are correlated for varying exposure conditions by plotting the inverse square root of the flame-spread velocity against a product of the heat flux and a time function. The test and analysis results are shown for six diverse materials representative of aircraft (interior panels, carpeting, and seat cushions) and buildings (plywood, polymethyl methacrylate, and rigid foam).

17. Key Words	18. Distribution Statement
Flame Spread Ignition Fire Safety Aircraft Interior Materials	Document is available to the U.S. public through the National Technical Information Service, Springfield, Virginia 22161

19. Security Classif. (of this report)	20. Security Classif. (of this page)	21. No. of Pages	22. Price
Unclassified	Unclassified		

Form DOT F 1700.7 (8-72) Reproduction of completed page authorized

METRIC CONVERSION FACTORS

Approximate Conversions to Metric Measures

Symbol	When You Know	Multiply by	To Find	Symbol
		LENGTH		
in	inches	*2.5	centimeters	cm
ft	feet	30	centimeters	cm
yd	yards	0.9	meters	m
mi	miles	1.6	kilometers	km
		AREA		
in^2	square inches	6.5	square centimeters	cm^2
ft^2	square feet	0.09	square meters	m^2
yd^2	square yards	0.8	square meters	m^2
mi^2	square miles	2.6	square kilometers	km^2
	acres	0.4	hectares	ha
		MASS (weight)		
oz	ounces	28	grams	g
lb	pounds	0.45	kilograms	kg
	short tons (2000 lb)	0.9	tonnes	t
		VOLUME		
tsp	teaspoons	5	milliliters	ml
Tbsp	tablespoons	15	milliliters	ml
fl oz	fluid ounces	30	milliliters	ml
c	cups	0.24	liters	l
pt	pints	0.47	liters	l
qt	quarts	0.95	liters	l
gal	gallons	3.8	liters	l
ft^3	cubic feet	0.03	cubic meters	m^3
yd^3	cubic yards	0.76	cubic meters	m^3
		TEMPERATURE (exact)		
°F	Fahrenheit temperature	5/9 (after subtracting 32)	Celsius temperature	°C

*1 in = 2.54 (exactly). For other exact conversions and more detailed tables, see NBS Misc. Publ. 286, Units of Weights and Measures, Price $2.25, SD Catalog No. C13.10:286.

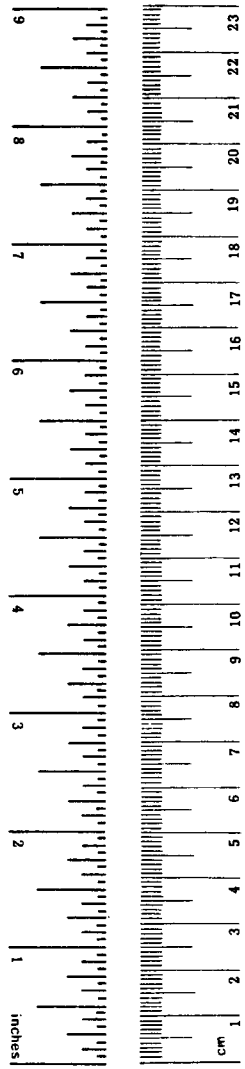

Approximate Conversions from Metric Measures

Symbol	When You Know	Multiply by	To Find	Symbol
		LENGTH		
mm	millimeters	0.04	inches	in
cm	centimeters	0.4	inches	in
m	meters	3.3	feet	ft
m	meters	1.1	yards	yd
km	kilometers	0.6	miles	mi
		AREA		
cm^2	square centimeters	0.16	square inches	in^2
m^2	square meters	1.2	square yards	yd^2
km^2	square kilometers	0.4	square miles	mi^2
ha	hectares (10,000 m^2)	2.5	acres	
		MASS (weight)		
g	grams	0.035	ounces	oz
kg	kilograms	2.2	pounds	lb
t	tonnes (1000 kg)	1.1	short tons	
		VOLUME		
ml	milliliters	0.03	fluid ounces	fl oz
l	liters	2.1	pints	pt
l	liters	1.06	quarts	qt
l	liters	0.26	gallons	gal
m^3	cubic meters	35	cubic feet	ft^3
m^3	cubic meters	1.3	cubic yards	yd^3
		TEMPERATURE (exact)		
°C	Celsius temperature	9/5 (then add 32)	Fahrenheit temperature	°F

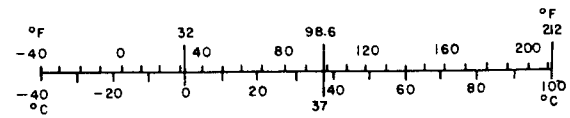

PREFACE

The authors wish to acknowledge the advice of Dr. A.F. Robertson in using the test apparatus, Mr. C. Veirtz for constructing a new apparatus, and Dr. T. Eklund of the Federal Aviation Administration Technical Center for his support as technical monitor for this study.

NOMENCLATURE

a	$h^2/k\rho c$
b	constant, Eq. (16)
c	specific heat
C	flame heat transfer modulus Eq. (7)
Gr	Grashof number
h	heat transfer coefficient
h_c	convective heat transfer coefficient
k	thermal conductivity
$\dot{q}''$	heat transfer per unit area per unit time
Pr	Prandtl number
t	time
t_m	characteristic time, Eq. (16)
T	Temperature
V_f	flame spread speed
x	horizontal coordinate
δ_f	flame heat transfer length
ρ	density
ϕ	parameter, Eq. (1)

Subscripts

e	external
f	flame
i	initial or ambient
ig	ignition
o	minimum
s	surface
max	maximum
min	minimum

EXECUTIVE SUMMARY

A test method concept is explored. The test is intended to provide data which would allow the prediction of downward or lateral flame spread on a vertical surface. A radiant heat source incorporated in the apparatus provided pre-heating ahead of the advancing flame front. Results are presented which show the prediction of flame spread velocity as a function of irradiance or surface temperature.

In addition to flame spread, piloted ignition data were recorded under irradiance levels of up to nominally 6 W/cm^2. An empirical relationship was found to approximately describe the time to ignite as a function of heat flux. The flame spread results are shown to be complementary to piloted ignition in that spread velocity at thermal equilibrium and time to ignite are both asymptotic and unbounded at a critical irradiance (the minimum flux for piloted ignition).

For a given material various conditions of heating were imposed during the flame spread tests. For each material, those results were correlated suggesting the generality of the derived parameters. Those parameters consist of a phenomenological constant which incorporates flame heat transfer and the thermal properties of the material, and minimum and maximum irradiances (or surface temperatures) for the spread limits. An ignition parameter or thermal-time response factor is also derived.

A primary aspect of this study was to explore the applicability of the test results to describe the flame spread and ignition processes on a diverse range of materials. These materials were selected to be representative of applications in aircraft (aircraft interior paneling, carpeting, and seat cushion foam) and buildings (wood particle board, polymethymethacrylate and rigid low density foam). Although experiments outside the scope of the test apparatus were not conducted, the analyses and results suggest that the data would be generally applicable under similar environmental conditions and material orientation.

INTRODUCTION

PURPOSE.

The purpose of this study is to seek new flame spread test method concepts. The test procedures should be suitable for a diverse range of materials including those used in aircraft and building interiors. The data derived from such tests should be capable of quantitatively estimating a material's flame spread characteristics for a specific mode of spread. The form of these results should provide an improved basis for fire risk analyses.

OBJECTIVE.

Specifically this report will outline a procedure for deriving flame spread parameters related to the phenomena of downward or lateral spread on a vertical surface. These parameters consist of an effective ignition temperature, the minimum surface temperature to permit spread, and a flame heat transfer modulus. When taken together in an appropriate formula, they provide a basis for computing flame spread rates as a function of surface temperature or imposed radiant heat flux. Six distinctly different materials, representative of aircraft and building interior applications, were examined in the study.

BACKGROUND.

Common interior furnishings can provide many avenues for fire growth. For example, typical aircraft cabin furnishings consist of seats composed of cushions covered by fabric, carpeted floors, and lightweight structural paneling for its interior shell. Although one may attempt to limit the fuel content of such furnishings, their continuity over large areas still presents a risk of surface flame spread. Flame spread is an extremely complex process which is affected by many physical, geometrical and chemical parameters. These factors include surface orientation, direction of flame spread, specimen size, initial fuel temperature, external radiant flux, surface roughness, flow velocity of the environment, composition of material, composition of the atmosphere, and more. The only way to effectively deal with these factors in

evaluating the performance of materials, is to integrate appropriate material data with a mathematical model of the particular process. Currently such data are not generally available, although many flammability test methods exist. Indeed, a large number of flame spread test methods have evolved over the past 30 years. These tests were undoubtedly developed without allowance for the numerous factors influencing flame spread rate. Yet, each test was probably developed with a conceptual model in mind with regard to its intended application. This conceptual process is a form of modeling, but it is likely only to have been based on qualitative data. For these reasons, the test methods developed usually yield results that are not consistent with each other nor do they necessarily reflect behavior in actual fires. Examples of inconsistencies among flammability test methods have been cited by Quintiere and Huggett [1], Tustin [2] and Nicholas [3]. However, test method correlation with full-scale fire experiments, although desirable, is not generally achievable [4]. To achieve proper correlation, the processes present in full-scale must be well understood, appropriate data must be derived for the materials involved, and mathematical models must be developed to provide a framework for analysis. This report shall focus on the aspect of data derivation for one type of flame spread process; namely, lateral or downward spread on vertical surfaces. This process is only one link in the complex array of fire dynamic phenomena possible in fire growth. Yet the successful derivation of meaningful data for this process could provide the basis for improved correlations.

The approach taken in this study is founded on existing flame spread theories for the case in which the spread velocity is opposite to the bulk flow velocity of the ambient. In the case of the test apparatus used in the study and in most fire applications, this opposed ambient flow is induced by the spreading fire itself, and therefore, is not independent. The effect of an imposed flow speed and other factors have been explored in numerous studies which taken together provide a fairly complete understanding of the opposed flow flame spread problem. Some of those investigations will be cited to illustrate the present scope and state of that research. They include: Magee and McAlevy [5] who investigated the effects of initial solid temperature and ambient oxygen concentration; deRis [6] who developed one of the first complete mathematical treatments; Fernandez-Pello, Ray and Glassman [7] who correlated the effects of oxygen and opposed flow velocity in terms of a

Damköhler number in a range leading to extinction; Frey and Tien [8] who demonstrate a model which includes extinction; and Fernandez-Pello and Santoro [9] who analyzed the forward heat transfer processes promoting flame spread. The results of these and other studies suggest that the rate of spread (V_f) is related to the ignition temperature (T_{ig}) (a critical surface temperature) and the surface temperature (T_s) just upstream of the solid region not yet affected by the flame heat transfer. For a thermally thick solid, this relationship has the form

$$V_f = \Phi/(T_{ig} - T_s)^2 \tag{1}$$

where Φ depends on the thermal properties of the solid, the ambient oxygen concentration and velocity, and on the heat flux ahead of the advancing flame. Although the forward heat flux may take various paths (solid or gas phase, conduction or radiation), it only significantly affects the solid approximately 2 mm ahead of the pyrolysis ("flame") front [9]. Morever, theoretical results which include finite rate gas-phase kinetics show a minimum surface temperature is required for propagation and V_f is lower than that predicted by infinite kinetics [10]. Some of these characteristics have been utilized by Quintiere [11] in developing a simpler flame spread theory as the basis for interpreting test results on materials. That analysis will serve as a framework for defining and deriving parameters from tests of downward and lateral flame spread on materials.

The method of analysis used and the results achieved for six materials will be related in the following discussion. A presentation of the theoretical flame spread model will provide a framework for analysis of the data and identify several parameters for measurements. The hypothesis is that those parameters for a given material will not change under a range of conditions. Hence, flame spread tests were conducted for various conditions. Also supporting experiments were performed to measure the ignition times and surface temperature response under radiant heating. The simplified theory used in the analysis of these data suggests that the flame spread and ignition properties should be consistent. This will be examined for the six materials. The conclusions drawn from those results bear on the feasibility of extracting a practical test procedure for deriving material flame spread properties.

DISCUSSION

THEORETICAL MODEL.

The general problem being addressed is opposed flow flame spread in which a thermally thick solid is heated by an arbitrary time and space dependent external radiant heat flux ($\dot{q}''_e$). This is shown schematically in figure 1. A solution to this problem has been previously derived [11] and is displayed below:

$$T_{ig} - T_i = \frac{\dot{q}''_f}{h} \frac{2}{\sqrt{\pi}} \sqrt{\frac{a\delta_f}{V_f}} \left(1 - \frac{\sqrt{\pi}}{2} \sqrt{\frac{a\delta_f}{V_f}}\right)$$

$$+ \frac{\sqrt{a}}{h\sqrt{\pi}} \int_0^t \frac{\dot{q}''_e(x_f,s)}{\sqrt{t-s}} \, ds$$

$$- \frac{a}{h} \int_0^t \dot{q}''_e \, (x_f,s) \exp(a(t-s)) \operatorname{erfc}\sqrt{a(t-s)} \, ds \qquad (2)$$

The following assumptions were utilized:

(1) the flame provides a constant forward surface heat flux ($\dot{q}''_f$) over a small distance (δ_f),

(2) a constant convective-radiative heat transfer coefficient (h) is used,

(3) the solid is semi-infinite with conduction only normal to its surface, and

(4) the position of the flame front (x_f) must satisfy the condition that the surface temperature (T_s) is equal to the ignition temperature (T_{ig}).

Also the parameter, a, is given as

$$a = h^2/k\rho c \qquad (3)$$

with $k\rho c$ being the properties of the solid, and the flame spread velocity V_f is given as

$$V_f = \frac{dx_f}{dt} . \tag{4}$$

In this form, eq. (2) presents an integro-differential equation to solve. This will not be necessary if it is recognized that eq. (2) can be considered as the sum of two temperature rises,

$$T_{ig} - T_i = (T_{ig} - T_s) + (T_s - T_i) . \tag{5}$$

The term $T_{ig} - T_s$ represents the rise due to flame heating ($\dot{q}''_f$). This is the first term in eq. (2) and can be simplified, since $a\delta_f/V_f$ is usually small [11], so that

$$T_{ig} - T_s = (2/\sqrt{\pi})\ (\dot{q}''_f/h)\ \sqrt{a\delta_f/V_f} . \tag{6}$$

Because δ_f is small, the flame heating occurs over a small depth; hence the temperature of the solid, ahead of δ_f, may be considered uniform over that depth. This means that the surface temperature time history before the arrival of the flame is not very important [12]. Therefore, the most appropriate means of predicting T_s due to external heating should be used, not necessarily that corresponding to eq. (2). Also, since δ_f is small, a prediction for T_s (due to external radiation) at $x = x_f + \delta_f$ can be regarded at x_f as an approximation. In anticipation of the analysis of the test apparatus results, the thermally thick heating problem of eq. (2) is considered with $\dot{q}''_e$ regarded as a function of x only. Thus, the surface temperature rise due to external heating is given by

$$T_s - T_i = (\dot{q}''_e/h)\ F(t) \tag{7a}$$

with

$$F(t) = 1 - \exp(at)\ \mathrm{erfc}\ \sqrt{at} . \tag{7b}$$

For the application of predicting flame spread, $\dot{q}''_e$ should be regarded as the external radiant flux at the position of the flame (x_f) and t is the time over which the constant flux $\dot{q}''_e$ has been imposed at x_f. Alternatively the phenomenon of ignition due to radiant heating could also be described by eqs. (7a,b). In particular, since flame spread might be viewed as a succession of piloted ignitions, it will prove advantageous to conduct a corresponding analysis of piloted ignition data based on

$$T_{ig} - T_i = (\dot{q}''_e/h)\ F(t) \tag{8}$$

where t is the ignition time. Also, since $F(t) \to 1$ as $t \to \infty$, it follows from eq. (8) that the minimum external flux required for ignition is

$$\dot{q}''_{o,ig} = h\ (T_{ig} - T_i) \tag{9}$$

Thus, from an analysis of ignition data it will be possible to derive an effective ignition temperature, and perhaps a better functional form for F(t).

Having decomposed the flame spread process into heating from the flame and heating from the surroundings, the two effects can be now coupled to derive a relationship for the spread rate, V_f. eq. (6) and eq. (7a) are substituted into eq. (5) so that

$$T_{ig} - T_i = 1/Ch\sqrt{V_f} + (\dot{q}''_e/h)\ F(t). \tag{10}$$

where the parameter C can be regarded as a flame heat transfer factor,

$$C = \sqrt{\pi}/(2\dot{q}''_f\ \sqrt{a\delta_f}). \tag{11}$$

For this mode of spread under natural convection conditions and in a normal air environment, the parameters T_{ig}, C, and a (or $k\rho c$) should be constant for a given material. These may be regarded as "flame spread properties." They are not to be confused with fundamental physical constants. They depend on the process as well as the material; however, their relative invariance for this flame spread process makes them useful. Moreover, these particular parameters are restricted to the approximate flame spread analysis considered

here; they may not be compatible with a more sophisticated spread model. Finally, success in arriving at a reasonably constant and consistent set of flame spread properties for the materials tested will provide evidence to support these ideas. Several forms of eq. (10) will be useful in deriving these properties from the test results. From eq. (10), solving for $V_f^{-1/2}$ yields

$$V_f^{-1/2} = Ch\ ((T_{ig} - T_i) - (\dot{q}''_e/h)\ F(t)). \tag{12}$$

From eq. (7) an alternative form follows:

$$V_f^{-1/2} = Ch(T_{ig} - T_s), \tag{13}$$

and applying eq. (8) to eq. (12) yields

$$V_f^{-1/2} = C\ (\dot{q}''_{o,ig} - \dot{q}''_e\ F(t)), \tag{14}$$

At thermal equilibrium (long-time heating, $F(t) \rightarrow 1$), eq. (14) can be expressed as

$$V_{f,max}^{-1/2} = C(\dot{q}''_{o,ig} - \dot{q}''_e) \tag{15}$$

where $V_{f,max}$ is the maximum possible flame spread speed corresponding to an imposed external flux $\dot{q}''_e$.

These equations (8-15) constitute the basis for interpreting the test data on ignition and flamespread, and serve as guidance in establishing test procedure. The parameters C, T_{ig} (or $\dot{q}''_{o,ig}$), and the limiting surface temperature for propagation ($T_{s,min}$) will be sought. Several procedures will be used with the objective to identify the most expeditious manner to achieve these results. Both external heat flux and its time of application will be varied in the flame spread tests. From ignition data the quantity $\dot{q}''_{o,ig}$ can be found along with the parameter "a" corresponding to eq. (7b). Moreover, the ignition phenomenon will be examined to assess whether or not eq. (7b) is valid, or whether an alternative F(t) is needed in eq. (7a). Indeed, it will be shown that an empirical function does better:

$$F(t) = \begin{cases} b\sqrt{t}, & t \leq t_m \\ 1, & t \geq t_m \end{cases} \tag{16}$$

These experiments and their results will be described subsequently. Before doing that, some comments on the evaluation of the heat transfer coefficient (h) will be given.

HEAT TRANSFER COEFFICIENT.

A complete expression of the surface heat loss should include radiative as well as convective heat loss. Fortunately, emissivities and absorptivities of common combustible materials are nearly unity for the radiation characteristic of fires or for the gas-fired heater used in the tests. Consequently the total heat transfer coefficient can be expressed as

$$h = \frac{\sigma(T_s^4 - T_i^4)}{(T_s - T_i)} + h_c \tag{17}$$

where

$$h_c = 0.13 \ \frac{k}{x} \ (Gr_x Pr)^{1/3}, \ Gr > 10^9 \tag{18}$$

is the convective coefficient as given in Krieth [13]. Also, an attempt was made to measure the convective coefficient for a plate mounted in the sample holder of the test apparatus [14]. Those results were compared to that computed by eq. (18) and are displayed in figure 2. Also displayed in figure 2 are results for h using eq. (17) with the measured values for h_c. Despite the nonlinear effect of radiation, a useful approximate representation for h is

$$h = 0.01 \ (1 + 8.5 \times 10^{-3} \ (T_s - T_i)) \text{ in } kW/m^2K \tag{19}$$

for the range of surface temperatures expected ($T_s < 600^oC$). Thus, in evaluating h, an effect of surface temperature should be accounted for in the linearized theory. In the subsequent analyses, eq. (19) was substituted into

eq. (9) in order to derive T_{ig} from an experimental value for $\dot{q}''_{o,ig}$. Furthermore, it was decided to use the corresponding value for h (i.e., $h = h(T_{ig})$) in eq. (13). In evaluating the minimum surface temperature for spread ($T_{s,min}$) from the incident radiative flux at extinction ($\dot{q}''_{o,f}$), the equation

$$\dot{q}''_{o,f} = h\ (T_s - T_i) \tag{20}$$

was used with h taken from eq. (19). In this way, nonlinear heat loss effects were accounted for.

It can be observed that h is independent of scale since the x dependence cancels in eq. (18), and no significant radiative property variation among non-metallic materials is likely. Hence the results to be derived from the tests should be applicable to similar fire situations provided ambient conditions (e.g., natural convection, oxygen concentration, etc.) are the same. This suggests that the small-scale test results should apply to large-scale fires.

EXPERIMENTAL PROCEDURE.

Six materials were selected for study. They vary in material type and structure. Their selection was based on a desire to challenge the analysis with a diverse array of materials. Three are typical of aircraft interior materials and three are typical building materials. The six are described in table 1, and will be referred to throughout the report as follows: (1) particle board, (2) poly(methyl methacrylate) PMMA, (3) rigid foam, (4) flexible foam, (5) carpeting, and (6) aircraft interior paneling. The materials were maintained at 55 percent relative humidity before testing by storing them in a conditioning room or in a desiccator.

The apparatus consists of a radiant heat source and a sample holder. It is essentially the apparatus developed by Robertson [15] for study under ISO (International Standards Organization) and IMCO (Intergovernmental Maritime Consultative Organization) interests. A schematic is shown in figure 3. The sample was either oriented so that the 162 mm dimension was vertical or the 800 mm dimension was vertical. The former arrangement recorded lateral spread

Table 1. Description of Materials

Material	Description	Thickness (cm)
Particle board	Douglas Fir wood with particle size range of 0.97-2.6 mm and urea-formaldehyde binder	1.28
Poly(methyl methacrylate) [PMMA]	Rohm & Haas* - Type G two 0.635 cm thick samples bonded with methyl ethyl ketone	1.28
Rigid foam	Polyurethane low density rigid foam - GM 31+	2.54
Flexible foam	Polyurethane low density flexible foam - Custom Products, Inc.* HD54CA low density	2.54
Carpet	Wool-nylon looped fibers with a rubberized backing	0.634
Aircraft panel	Aircraft interior lining (#2), a composite material consisting of a phenolic-polyamide honeycomb core with epoxy fiberite face sheets and a Tedlar®* coating on the exposed face.	2.54

---

* Use of trade names implies no endorsement by the National Bureau of Standards.

+ GM 31 is a material from the Material Bank of the Product Research Committee currently maintained at the National Bureau of Standards ("Materials Bank Compendium of Fire Property Data", Product Research Committee, February 1980).

while the latter arrangement recorded downward spread. In the lateral orientation the radiant panel imposed a distribution of radiant heat flux to the face of the sample as shown in figure 4. The results there have been normalized in terms of the incident flux at x = 50 mm.

A series of ignition and flame spread experiments were conducted with the apparatus on the six designated materials. Ignition was measured using a sample mounted in the region shown in figure 3. A pilot flame was used to trigger the process. The flame spread tests were run either laterally or downward; ignition always occurring at the high irradiation end and flame spread proceeded along the material to extinction at some lower flux. In some flame spread tests, fine wire (0.13 mm dia.) chromel-alumel thermocouples were used to monitor the rise in surface temperature before the onset of flame heating. Since the flame heat transfer zone is small (0 to 2 mm), this surface temperature could easily be correlated with the local flame spread velocity.

IGNITION EXPERIMENTS. Ignition experiments were conducted in a vertical orientation with sample face dimensions of 155 x 110 mm wide. The back and sides were wrapped with aluminum-foil. This was mounted in the sample holder such that the back side was bounded by 12.8 mm thick calcium silicate board and the exposed face was 130 x 90 mm. The sample was mounted at the hot end of the lateral spread apparatus. It is seen from figure 4 that the flux was nearly constant over the face of the sample. The flux was varied at the face over a range of 1.5 to 6.5 W/cm^2. With the pilot flame on, the sample holder was moved into place to initiate the radiant exposure. The time to ignite was then recorded. A definition of ignition, most relevant to flame spread, was taken to be the onset of sustained surface burning. Any departure from this was noted. Ignition data were also taken during lateral flame spread tests, and these data were added to the results for the smaller sample.

The onset of ignition depends on the location and temperature of the pilot flame. Simms [16] found that the distance of the pilot flame from the surface of a vertical specimen under laminar conditions affected the time to ignite. Kashiwagi [17] found that the temperature of a heated wire pilot for an upward facing horizontal sample had an effect. Different pilot flame configurations

and locations were used in this study. They are described in table 2. Each was located within 1 cm of the sample face plane. In general each seemed to give equivalent results for most conditions. Typically when a peculiar ignition behavior occurred, variations with the pilot flame were made to determine whether the pilot configuration was responsible. If it was, a new pilot arrangement was adopted, and the anomalous data discarded. In this fashion an optimum pilot flame was developed and subsequently used. The objective was to provide a hot region in the mixture of air and fuel gases with a minimal disturbance. An additional criterion for the pilot was that it should not provide any heat transfer to the surface of the specimen. It should only act as a source of heat to the mixture of pyrolysis products and air. The optimum pilot flame was found to consist of a premixed flame positioned above the specimen to intercept the hot boundary layer plume generated by sample decomposition. For this sample configuration that boundary layer was expected to be turbulent or in the transition region. That pilot configuration consisted of an acetylene (C_2H_2)-air flame supplied through two 1.5 mm diameter openings in a ceramic cylinder mounted as shown in figure 5. The pilot was adjacent to a vertical flange mounted flush with the sample in order to maintain continuity in the wall boundary layer. The pilot tube was positioned 5 mm from the flange surface and 25 mm above the top edge of the sample. Its conical blue flame extended about 140 mm horizontally (see figure 5.)

FLAME SPREAD EXPERIMENTS. The samples for flame spread had a 155 x 800 mm face dimension. Their back and edge surfaces were covered with aluminum-foil, and they were backed by a 12.8 mm thick calcium silicate board. Their exposed face in the sample holder was 130 x 775 mm. Two apparatuses were used so that lateral and downward spread could be measured on a sample positioned in a vertical plane. The initial heat flux with its corresponding distribution and the application time of the pilot flame were two conditions varied in the experiments. Flame position was visually recorded. From these data flame velocity could be computed. An extensive series of experiments investigating the effect of these conditions was conducted for the lateral flame spread mode. This was done less extensively in downward spread; however, surface temperatures were measured during those flame spread experiments.

Table 2. Pilot Flame Configurations

Position reported with specimen positioned for horizontal spread

Number	Flame	Burner Head	Orientation	Position
1	Conical acetylene - air premixed flame	Two 1.5 mm dia. holes in a 6.4 mm O.D. ceramic tube	Horizontal	Top edge of sample, spaced 5 mm from sample holder
2	Conical acetylene - air premixed flame	Two 1.5 mm dia. holes in a 6.4 mm O.D. ceramic tube	Horizontal	25 mm above top edge of sample, 5 mm from the face of a flange flush with the sample holder
3	Conical acetylene - air premixed flame	Two 1.5 mm dia. holes in a 6.4 mm O.D. ceramic tube	Vertical	25 mm below lower exposed edge of sample
4	Conical natural gas air premixed flame	Two 1.5 mm dia. holes in a 6.4 mm O.D. ceramic tube	Horizontal	Top of sample, spaced 5 mm from sample holder
5	Fan-shaped acetylene - air premixed flame	Rectangular diffuser	Horizontal	Top of sample, spaced 5 mm from sample holder
6	Fan shaped acetylene - air premixed flame	Rectangular diffuser	Horizontal	Centered at side edge of sample
7	Finepoint acetylene - air premixed flame	Small Converging nozzle	Horizontal	Centered at side edge of sample 6.25 mm from sample surface

IGNITION RESULTS AND ANALYSIS.

Data were compiled on the time to ignite under radiant heating for the six materials. These results are tabulated in tables 3-8. Analysis consisted of identifying the flux ($\dot{q}''_{o,ig}$) below which sustained surface ignition would not occur, and in seeking a functional form for F(t) in eq. (8). Either the parameter "a" of eq. (7b) was found by a "best" fit of the data for small ignition times; or the parameters "b" and "t_m" of eq. (16) were found. The latter functional form is empirical and tends to fit the data better. The data and F(t) fits are displayed for all six materials in figures 6-11. Some observations and characteristics of each will be discussed.

PARTICLE BOARD. Several pilot flame configurations were used in the ignition experiments. Both acetylene and natural gas were premixed with air and supplied through small burner heads located in various positions near the heated sample. The range of exposure radiant heat fluxes varied from nominally 1.4 to 6.5 W/cm^2. The results are tabulated in table 3 along with the pilot flame configuration used. Variation in results among the different pilot flames is similar to differences in results using the same pilot. Hence with the scatter of these data, these pilot flames have no significant effect. The pilot flame position above the sample appears to offer the best combination of no direct heat transfer to the sample and full exposure to the fuel gases released by the sample. However, the ignition behavior for this pilot position shows, first an ignition of the gases at the pilot, followed by downward propagation through the boundary layer to sustained ignition over the sample surface. This is probably due to flame stability effects in which the local burning velocity of the pyrolysis gas-air mixture must be greater than the upward gas speed in the boundary layer before downward propagation can occur. Since opposed flow flame spread is being considered, it is felt that the definition of ignition most consistent with that flame spread phenomenon is sustained ignition at the surface following flashback from the pilot. Those times are recorded in table 3 along with some measurements of the incipient ignition above the sample. There it is seen that the gas-phase ignition times precede the surface ignition times by as much as 20% until the flux is below 1.55 W/cm^2. At fluxes of 1.69 and 1.55 W/cm^2 the flame did not propagate to the lower edge of the sample, and for fluxes below 1.55 W/cm^2,

Table 3. Particle Board Ignition Tests

Test	Pilot Flame Configuration	Flux (W/cm^2)	Time (s)	Time of Gas Phase Ignition Above the Sample (s)
27	2	1.37	∞	410
26	2	1.49	∞	359
29	2	1.49	∞	300
30	2	1.50	∞	274
31	2	1.54	∞	278
23	1	1.55	626	--
28	1	1.69	373	316
L-19	2	1.7	292	--
25	1	1.82	284	--
24	1	1.85	323	--
1	4	2.00	242	195
L-11	2	2.0	240	--
L-10	2	2.07	225	--
L-18	2	2.1	166	--
19	1	2.15	228	205
20	1	2.20	218	--
2	4	2.45	184	156
21	1	2.50	181	161
22	1	2.50	155	141
18	1	2.77	93	--
17	1	2.78	101	--
5	1	2.95	93	--
4	3	2.95	92	90
32	1	2.96	113	--
6	4	3.00	105	87
7	1	3.05	110	100
8	1	3.06	79	--
10	1	3.62	68	--
9	1	3.62	69	--
12	1	4.45	47	40
11	1	4.45	49	--
L-1	2	5.15	41	--
L-2	2	5.2	24	--
L-16	2	5.32	30	--
13	1	5.35	28	--
14	1	5.45	29	--
15	1	6.45	23	--
16	1	6.48	19	--

FAA WJH Technical Center
00093454

ignition occurs at the pilot but does not flashback to the sample surface at all. Hence, the critical flux for piloted ignition ($\dot{q}''_{o,ig}$) was taken as 1.55 W/cm^2.

The sustained surface ignition times are plotted against incident radiative heat flux in figure 6. The data follow the form of eq. (8) and eq. (9) in which $\dot{q}''_{o,ig}/\dot{q}''_e = F(t)$ where F = 0 at t = 0 and asymptotically approaches 1 as t becomes large. An attempt to fit the data using two functional forms of F(t) was made. The empirical form for F(t) given by eq. (16) is able to fit the data much better than the exact solution for an inert thermally thick solid described by eq. (7b). Attempts at fitting eq. (7a) to the ignition data were always done favoring the shortest times since the assumption of an infinitely thick solid would be valid. It appears that variability in thermal properties due to temperature variation and decomposition, plus perhaps the need to predict the rate of fuel gas release limit the applicability of a simple inert model. Nevertheless, the value of "a" used to fit the short time data, found to be 0.00455^{-1}, is consistent with thermal property data for the particle board. From $\dot{q}''_{o,ig}$ = 1.55 W/cm^2 and eq. (9), T_{ig} = 393°C and the corresponding h = 0.042 kW/m^{2}K. Since $k\rho c = h^2/a$, the derived value for $k\rho c$ is 0.392 (kW/m^{2}K)^2, compared to a literature value [14] of 0.255 (kW/m^{2}K)^{2}s at T = 393°C. Of course, the effect of charring was not included in estimating the literature value for $k\rho c$. In view of the fact that $k\rho c$ can vary by several orders of magnitude for common materials, these deviations may not be so significant for particle board. Moreover, both results for F(t) may be good enough in the correlation of flame spread data per eq. (14), since only the transient response of the material needs to be predicted. That is, the characteristic heating time for F(t) to go from 0 to 1 is significant.

PMMA. Table 4 displays the results of ignition times for PMMA under irradiance levels of 1.55 to 6.4 W/cm^2. On heating, tiny bubbles appear to form within the PMMA near the surface. Also, before ignition significant bulging and deformation of the sample occurred for fluxes below 4 W/cm^2. In table 4 it can be seen that the use of a pilot flame at the edge of the sample produced a variety of results. This can be attributed in part to the type and displacement of the pilot from the sample face. However, the large gradient in fuel concentrations at the edge of the boundary layer makes ignition times

Table 4. PMMA Ignition Tests

Test	Pilot Flame Configuration	Flux W/cm^2	Time s	Notes
27	5	1.55	1050.	
28	5	1.95	348.	
16	5	2.1	312.	
15	5	2.1	270.	
14	5	2.35	194.	
13	5	2.38	220.	
L-1	2	2.75	97.	
12	5	2.8	120.	
11	5	2.8	161.	
10	5	3.2	88.	
9	5	3.2	107.	
8	5	3.8	66.	
7	5	3.8	68.	
6	6	3.8	158.	Pilot 5 mm from sample
5	7	3.8	57.	Pilot 5 mm from sample
2	6	3.94	76.	Pilot < 5 mm from sample
4	7	3.94	79.	Pilot 5 mm from sample
3	7	3.94	99.	Pilot 10 mm from sample
1	6	4.2	125.	Pilot 10 mm from sample
24	5	4.2	52.	
23	5	4.3	53.	
26	5	4.78	45.	
25	5	4.8	44.	
22	5	5.25	36.	
21	5	5.32	32.	
17	5	5.8	23.	
18	5	5.85	22.	
19	5	6.4	21.	
20	5	6.4	21.	

very dependent on pilot position. This is one reason for ultimately selecting a pilot configuration above the sample.

All of the results are shown plotted in figure 7 along with curve fits for F(t). The data suggest that the critical flux for ignition ($\dot{q}''_{o,ig}$) is less than or equal to 1.5 W/cm^2. Since this flux was the lowest operating level of the apparatus, it was taken as $\dot{q}''_{o,ig}$. The curve fits were based on this value. The empirical form of F(t) given by eq. (16) yields a better fit than the exact inert solution, eq. (7b). Based on $\dot{q}''_{o,ig}$ = 1.5 W/cm^2, an effective ignition temperature is calculated to be 388°C. Thus, the value of $k\rho c$ = 0.42 (kW/m^{2}K)^{2}s follows from a best fit value for a = 0.0040 s^{-1} and h = 0.041 kW/m^{2}K. This can be compared to a value at 22°C estimated from the literature of $k\rho c$ = 0.61 (kW/m^{2}K)^{2}s.

RIGID FOAM. Ignition experiments were conducted for the polyurethane rigid foam material (GM-31) using only the pilot flame configuration as shown in figure 5 (number 2 of table 2). The results are tabulated in table 5 and include results derived from the lateral flame spread experiments. Based on these data, the critical flux for ignition ($\dot{q}''_{o,ig}$) was estimated at 2.0 W/cm^2. The very short ignition times are subject to some error since it takes about 1 s to insert the sample for exposure to the radiant source. It can be seen from figure 8 that, except for the data taken during flame spread tests, the empirical form of F(t) again does a better fit of the data. Based on $\dot{q}''_{o,ig}$ = 2.0 W/cm^2, T_{ig} is calculated as 453°C. From the "best fit" value for a = 0.75 s^{-1}, $k\rho c$ = 0.0032 (kW/m^{2}K)^{2}s compared to literature value of 0.0014 (kW/m^{2}K)^{2}s.

FLEXIBLE FOAM. The polyurethane flexible foam exhibits a complex response to heating. This is manifested by its rapid surface regression and its melting. The vertical test orientation also promotes dripping. Of the materials tested, the behavior by this material is the most incongruous with the theoretical basis of the data analysis. Nevertheless, it was useful to perform the standard analysis to see where problems might lie. The results are tabulated in table 6. Above 4 W/cm^2, nearly instant ignition occurred above the sample at the pilot upon insertion of the sample. Subsequent flash-back to the surface occurred within 20 s. Below 2.5 W/cm^2, significant

Table 5. Rigid Foam Ignition Tests*

Test	Flux W/cm^2	Time s
5	1.41	∞
6	1.73	∞
8	2.12	∞
9	2.25	8
3	2.45	7
4	2.45	8
7	2.68	7
1	2.97	4
2	2.97	6
L-3	3.03	4
L-4	3.04	2
L-2	3.04	3
L-6	3.05	3
L-1	3.05	4
10	5.5	2

Table 6. Flexible Foam Ignition Tests

Test	Flux (W/cm^2)	Time (s)
15	1.51	no ignition
19	1.64	no ignition
18	1.79	81.
17	1.83	68.
13	2.04	58.
14	2.04	56.
12	2.13	49.
11	2.2	30.
10	2.2	42.
9	2.4	35.
8	2.86	23.
6	3.62	18.
4	4.81	18.
3	4.85	14.
1	5.5	8.
2	5.53	14.

* All tests used pilot flame configuration 2.

regression took place with sustained ignition preceded by periodic ignition on the sample. A cavity is formed by the sample holder as the material vaporized and formed a melted pool at the bottom. At 1.64 W/cm^2, no ignition occurred; however, the material was completely depleted due to heating by 120 s. As the surface regressed the minimum flux at the rear face of the sample was 1.3 W/cm^2. Although 1.6 W/cm^2 was taken as the critical flux for ignition ($\dot{q}''_{o,ig}$), it is seen from these results that the rapid decomposition of this material precludes a precise determination of $\dot{q}''_{o,ig}$. It could be 1.3 W/cm^2 or even lower. The data are plotted in figure 9 using the flux values at the initial face of the sample. The curve fits based on F(t) were derived using $\dot{q}''_{o,ig}$ = 1.6 W/cm^2. Again, the empirical form of F(t) enables a better fit.

CARPET. Ignition behavior of the wool/nylon pile carpet with an integral rubberized backing reflects its composite construction. Indeed, on heating, the fibers charred and volatilized, but subsequent ignition appeared to be more attributable to the rubberized backing. Also, ignition manifested itself in several ways. Above an irradiance of 5 W/cm^2, ignition resulted in complete combustion over the sample surface. Between approximately 3.5 to 5 W/cm^2, ignition occurred only over the upper half of the sample surface. At lower heat fluxes, ignition would only occur at discrete regions or "spots." Below 1.6 W/cm^2 ignition did not occur. The data are displayed in table 7. At low heat fluxes, near the critical value, a fair degree of scatter is present. This probably reflects the non-homogenity of the spot-like ignition. In exploring the effects of pilot location several data show the effect of pilot flame heating of the sample directly on the sample holder. Also, two data points were taken with another apparatus in which the sample was horizontally oriented. These horizontal results are within the scatter of the overall data so that no conclusion can be made on the effects of orientation.

The results are plotted in figure 10 along with the curve fits. Even if a fit, using eq. (7b) for F(t), is based on mid-time results it does not match the data. The empirical function, eq. (16) yields a fair fit.

AIRCRAFT PANEL. The multi-layered composite construction of the aircraft interior panel leads to unusual ignition behavior. On heating, the decorative surface coating would swell, then split or burst depending on the irradiance

Table 7. Carpet Ignition Tests

Test	Pilot Flame Configuration	Flux W/cm^2	Time s
12	2	1.55	∞
10	2	1.73	269
9	2	1.75	350
8	1*	1.75	169
11	2	1.76	437
1C	+	2.0	180
13	2	2.03	240
14	2	2.05	152
15	1*	2.05	103
L-2	2	2.35	94
6	2	2.37	87
7	2	2.37	93
26	2	2.39	92
2C	+	2.65	103
4	1**	2.75	65
5	2	2.75	91
3	2	2.75	91
25	2	3.01	43
1	2	3.25	45
2	2	3.25	52
17	2	3.85	24
18	2	3.87	32
21	2	5.01	20
19	2	5.08	25
L-3	2	5.1	37
20	2	5.15	23
22	2	5.15	19
23	2	6.13	23
24	2	6.15	20

* Pilot flame touching sample holder.
** Pilot flame touching sample face.
\+ Horizontal sample orientation.

level. At heat fluxes below 5 W/cm^2, the coating would burst and a flammable gas cloud could be released which momentarily would ignite. The intensity of this release increased as the flux was lowered, or the heating time was longer. Following this behavior, the fiberite face sheet over the honeycomb core was exposed, and sustained ignition occurred over its surface subsequently. For example, at 2.8 W/cm^2, the surface coating bursts at 27 s, ejecting a jet of flames. This flame extinguishes and the coating delaminates and rolls off to the side exposing the fiberite face. At 54 s a combustible mixture results and ignition occurs above the sample with flashback to the sample surface at 79 s. The results for sustained surface ignition are tabulated in table 8 along with ignition times in the gas-phase above the sample. At 2.5 W/cm^2 sustained ignition did not occur, and 2.7 W/cm^2 was estimated as the critical flux. The data are plotted in Figure 11 and the F(t) curve fits are displayed. Significant scatter exists in the data; however, the range of ignition times is less than 80 s. Hence the material requires a high heat flux for ignition, but ignites quickly.

Table 8. Aircraft Panel Ignition Tests*

Test	Flux W/cm^2	Time s	Gas Phase Ignition Above the Sample
10	2.1	∞	∞
20	2.5	∞	85.
19	2.8	79.	--
9	2.93	60.	38.
8	3.38	45.	43.
12	3.9	28.	27.
11	3.9	40.	39.
13	4.18	39.	16.-28.
14	4.35	25.	24.
17	4.6	25.	14.
4	5.0	24.	--
L-1	5.05	19.	--
6	5.3	24.	11.
2	5.38	15.	--
5	5.4	26.	23.
3	5.4	20.	--
16	5.7	20.	13.
7	6.3	10.	8.

* All tests used pilot flame configuration 2.

SUMMARY OF IGNITION PARAMETERS. The parameters derived from these analyses can be classed into two categories. First, there is the thermal condition necessary to produce a flammable mixture necessary for piloted ignition. Second, there is the thermal response of the material or the time necessary to achieve ignition. The parameters which reflect the thermal requirement are the minimum flux for ignition ($\dot{q}''_{o,ig}$) or the derived effective ignition temperature (T_{ig}) based on eq. (9) and eq. (19). The temporal parameters can be expressed by the parameters used in F(t); either a of eq. (7b) or b and t_m of eq. (16). Indeed, since 1-exp(at) erfc $\sqrt{at}$ is approximately $\sqrt{at}$ for small (at) values, it can be shown that all of these parameters are related, i.e., $a \sim b^2 \sim 1/t_m$. The smaller a or b are, the longer it will take to ignite. These parameters are summarized in table 9 where the temporal parameters tend to correspond. Also it should be noted that the thermal requirement for ignition is independent of its characteristic time for ignition.

Table 9. Summary of Ignition Parameter

	Minimum Flux for Ignition $\dot{q}''_{o,ig}$	Ignition Temperature T_{ig}	Parameters for F(t) Eq. (7b) a	Eq. (16) b	Eq. (16) t_m
Material	W/cm^2	^oC	s^{-1}	$s^{-1/2}$	s
PMMA	$\leq$ 1.5	$\leq$ 388	0.0040	0.047	456
Particle Board	1.55	395	0.0045	0.0504	393
Carpet	1.55	395	0.015	0.063	243
Aircraft Panel	2.7	536	0.05	0.131	57
Flexible Foam	$\leq$ 1.6	$\leq$ 407	0.07	0.114	81
Rigid Foam	2.1	464	0.7	0.321	10

FLAME SPREAD RESULTS AND ANALYSIS.

The flame spread data consist of flame front position as a function of time. From the known external radiant distribution along the sample (figure 4), the flux ($\dot{q}''_e$) at the flame position can be found. Hence flame spread velocity as a function of external flux was derived. That velocity was computed using a numerical differential formula based on a three-point parabolic fit of the position-time data.

Several methods were examined to determine the flame spread parameters. These methods are based on alternative forms of the flame spread equation given in eqs. (12)-(15). From eq. (14) it follows that by plotting the data as $V^{-1/2}$ versus $\dot{q}''_e$ F(t), the intercept on the abscissa is $\dot{q}''_{o,ig}$ and the slope of a straight line fit through the data is C. The time, t, is the total external heating time up until the arrival of the flame front. At the point where the flame ceases to propagate, the corresponding abscissa value is $\dot{q}''_{o,f}$, the minimum external flux for flame spread. In aligning a straight line fit to these data the center core of the data points should be favored. This is advised because near extinction, this simple theory is not likely to hold and departures from a linear result are expected. At the other end of the data set, errors are likely since the spread velocity is very rapid and early transient effects may not be well accounted for by the function F(t). As time increases, F(t) approaches 1 and the analysis has more reliability.

Three methods of analysis based on eq. (14) will be presented to derive the parameters: C, $\dot{q}''_{o,ig}$, $\dot{q}''_{o,f}$ and T_{ig} and $T_{s,min}$, respectively. First, data from "long preheating" tests were examined. These "long preheating" times were based on experience in the thermal response of materials developed during ignition tests. Therefore, F(t) was assumed to be equal to 1 in this analysis. The other two methods were based on using F(t) in the form of eq. (7b) or eq. (16) with parameters for these formulae derived from the ignition tests (table 9). Although eq. (7b) does not perform well in the ignition data fits, it might be sufficiently accurate here, since for "long" duration tests F(t) will approach 1. That is, for long enough times, it is the ability of F(t) to express the thermal equilibrium time, not its functional form, that is important.

The flame spread behavior and the results of these analyses will be described for each material. Following that, those results will be converted in eq. (13) and compared to the measured results for flame spread velocity as a function of surface temperature.

PARTICLE BOARD. The range of flame spread experiments conducted for Douglas fir particle board are shown in table 10. In the lateral tests (L) the pilot configuration above the sample (figure 5) was used; it was moved into that position following a set "pre-heating" or exposure time of the sample to the radiant heater. Subsequently, ignition and flame spread occurred. In the downward tests (D), a contacting pilot flame was applied to the sample after a specified exposure time. The preheating times and initial flux levels were selected based on the ignition results for particle board. The ignition data suggest that 400 to 600 s may be sufficient heating times to reach thermal equilibrium. Also, if the sample is heated too long, as in tests L-17 and D-3, ignition may not occur due to excessive charring or ablation. Hence, some judgement must be exercised in initiating flame spread after a sample has been heating for a "long" time. The ideal distribution of flux is to have the maximum initial flux be slightly above the critical flux for ignition.

The results of the data analysis are displayed in figures 12 to 16. The flame front position as a function of time, figure 12, reflects the variations in incident radiant flux as well as the pre-heating times. The plot of velocity versus external flux is included to show the wide range of possible results. A unique relationship is not possible since the spread velocity is primarily a function of surface temperature and that depends on the external flux and its duration. However, the results converge, as in figure 13, as sufficient time has transpired. In figure 14, these data are replotted in terms of $V^{-1/2}$ and $\dot{q}''_e$. The data from a given test shifts downward on the plot as the heating time is increased before the flame arrival. Several tests (L-14, D-4, 5, 6) constitute "long preheating" runs, and a close examination of the data set of L-14 in figure 12c, yields an intercept, $\dot{q}''_{o,ig} = 1.65$ W/cm^2 and a slope value, $C = 2.3$ (s/mm)$^{1/2}$ (W/cm^2). Figures 15 and 16 show the results of using F(t) based on eq. (16) or eq. (7b), respectively. Both of these functions correlate the data very well. A summary of the flame spread parameters derived

Table 10. Particle Board Flame Spread Test Conditions

Test	Flux to Sample at 50 mm Position (W/cm^2)	Pre-Heat Time (s)	Ignition Time (s)	Plot Symbol
L-1	5.15	0.	41	(1)
L-2	5.2	0.	24	(2)
L-16	5.32	0.	30	(f)
L-6	4.0	40.	57	(6)
L-7	4.01	40.	~ 62	(7)
L-4	2.97	70.	~ 120	(4)
L-5	2.95	80.	116	(5)
L-3	2.99	110.	114	(3)
L-21	2.98	140.	141	(m)
L-20	2.96	150.	151	(k)
L-22	2.98	200.	220	(p)
L-23	2.9	250.	263	(r)
L-9	2.6	120.	137	(9)
L-8	2.57	120.	128	(8)
L-13	2.3	240.	246	(d)
L-12	2.19	180.	183	(c)
L-14	2.26	300.	300	(e)
L-10	2.07	0.	225	(a)
L-11	2.0	0.	240	(b)
L-18	2.1	0.	166	(g) *
L-19	1.7	0.	292	(h) *
L-17	2.0	480.	none	--
D-4	3.0	600.	--	(t)
D-5	3.0	600.	--	(u)
D-6	3.0	600.	--	(v)
D-7	3.0	100.	--	(w)
D-3	3.0	1000.	none	--

* Not pre-conditioned in constant humidity room (sample stored in Building 205 - relative humidity on test date ~ 44%).

NOTE: L = Lateral flame spread test (pilot configuration from Figure 5 was used).
D = Downward flame spread test (contacting pilot was used).
- = Not recorded

from these plots is shown in table 11. The results are reasonably consistent with variations between the various methods, probably equal to the uncertainty in the parameters derived from a given method.

Table 11. Comparison of Flame Spread Parameters by Different Methods for Particle Board

Method	$\dot{q}''_{o,ig}$ W/cm^2	T_{ig} ^oC	C (s/mm)$^{1/2}$(cm^2/W)	$\dot{q}''_{o,f}$ W/cm^2	$T_{s,min}$ ^oC
Ignition test	1.55	395.	--	--	--
Long pre-heat	1.65	409.	2.3	0.45	202.
F(t) of Eq. (7b)	1.55	395.	1.8	0.35	175.
F(t) of Eq. (16)	1.75	422.	2.0	0.45	202.

Based on the correlations in figures 15 and 16 and on examining downward and lateral tests under similar heating conditions, no systematic differences were observed between downward and lateral spread. In both, a well-defined flame front proceeded on the sample. However, in lateral spread the front could be slightly inclined to the vertical, while in downward spread it was horizontal.

PMMA. For downward spread of poly(methyl methacrylate), the flame front was a well defined horizontal line front with some distortion due to dripping which occurred late in the tests. The flame front in lateral spread proceeded in two or three steps with the lead step at the upper region of the sample. The horizontal distance between the steps was less than 5 cm. This step effect may have been due to the manner in which the sample is ignited from above; however, it did not have a significant effect on the flame spread measurements.

Table 12 lists the range of experiments conducted. The raw data are plotted in figure 17 where it should be noted that the downward runs were terminated when dripping became excessive. The velocity measurements plotted against irradiance are shown in figure 18. If these data are examined more closely, it is found that for similar tests (L-8, D-16, 17, 26) there is no difference between downward and lateral results. In fact these same tests were designated as the "long preheating" tests, and neglecting the first few data points at low $V_f^{-1/2}$ in figure 19 yields results for $\dot{q}''_{o,ig}$ and C. Except in experiments where a test was terminated, the flame spread to the end of the sample and the minimum flux $\dot{q}''_{o,f}$ for spread is equal to or less than the lowest flux available in the apparatus, i.e., 0.1 W/cm^2. Good correlations are achieved by operating on the data with either F(t) of eq. (16) or F(t) of eq. (7b) as shown in figures 20 and 21, respectively. A summary of the derived parameters is given in table 13. The long preheat results are more in agreement with using F(t) of eq. (16).

RIGID FOAM. The polyurethane rigid foam material burns with a nearly straight flame front in both lateral and downward spread. Nominally, identical tests were conducted in both modes as shown in table 14. The response of this material is very fast so that a prescribed preheat is not essential. In figure 22, the data of test L-7 with a preheat of 5 s suggest that a thermal equilibration time is about 30 s. That is the time it takes for those data to merge with the other lateral results. Incidentally, the downward and lateral results do not coincide because of the differences in the flux distributions although the initial flux is the same. Hence, except perhaps for test L-7, all the data should yield identical results for velocity as a function of irradiance. The scatter in figure 23 show the inaccuracy in velocity determinations at high speed. Selecting test L-7 as the long preheat case, the flame spread parameters are determined from figure 24. The first two high speed data points are discounted. The use of the F(t) correlating function tends to remove some curvature effects but not the degree of scatter. Those plots are given in figures 25 and 26. The derived parameters from each method are compared in table 15.

Table 12. PMMA Flame Spread Test Conditions

Test	Flux to Sample at 50 mm Position (W/cm^2)	Pre-Heat Time (s)	Ignition Time (s)	Plot Symbol
L-1	2.75	0	97	(1)
L-2	2.84	150	154	(2)
L-3	2.84	200	200	(3)
L-4	2.78	250	250	(4)
L-5	2.77	300	300	(5)
L-6	2.82	400	400	(6)
L-7	2.71	500	500	(7)
L-8	2.71	600	600	(8)
D-16	3.0	600	--	(9)
D-17	3.0	600	--	(a)
D-26	3.0	600	--	(b)
D-29	3.0	100	--	(c)

NOTE: L = Lateral flame spread test (pilot configuration from Figure 5 was used).
D = Downward flame spread test (contacting pilot was used).

Table 13. Comparison of Flame Spread Parameters by Different Methods for PMMA

Method	$\dot{q}''_{o,ig}$ W/cm^2	T_{ig} ^oC	C $(s/min)^{1/2}(cm^2/W)$	$\dot{q}''_{o,f}$ W/cm^2	$T_{s,min}$ ^oC
Ignition test	$\leq$ 1.5	$\leq$ 388.	--	--	--
Long pre-heat	1.57	399.	2.1	< 0.1	< 88.
F(t) of Eq. (7b)	1.25	352.	2.6	< 0.1	< 88.
F(t) of Eq. (16)	1.65	409.	1.9	< 0.1	< 88.

Table 14. Rigid Foam Flame Spread Test Conditions

Test	Flux to Sample at 50 mm Position (W/cm^2)	Pre-Heat Time (s)	Ignition Time (s)	Plot Symbol
L-3	3.03	0	4	(2)
L-2	3.04	0	3	(1)
L-4	3.04	0	2	(3)
L-6	3.05	0	3	(4)
L-7	3.05	5	5	(5)
D-31	3.0	0	-	(6)
D-32	3.0	0	-	(7)
D-33	3.0	0	-	(8)
D-34	3.0	0	-	(9)
D-35	3.0	0	-	(a)
D-36	3.0	0	-	(b)

NOTE: L = Lateral flame spread test (pilot configuration from Figure 5 was used).
D = Downward flame spread test (contacting pilot was used).

Table 15. Comparison of Flame Spread Parameters by Different Methods for Rigid Foam

Method	$\dot{q}''_{o,ig}$ W/cm^2	T_{ig} ^oC	C $(s/mm)^{1/2}(cm^2/W)$	$\dot{q}''_{o,f}$ W/cm^2	$T_{s,min}$ ^oC
Ignition test	2.1	465.	--	--	--
Long pre-heat	1.8	428.	0.60	0.55	225.
F(t) of Eq. (7b)	1.85	434.	0.59	0.54	223.
F(t) of Eq. (16)	2.0	453.	0.55	0.55	225.

FLEXIBLE FOAM. The flexible polyurethane foam burns in a complex manner. In downward spread, significant melting and dripping occurred which appears to promote a more rapid spread. As time increased, flaming drip-channels which preceded the primary flame front, increased in length. The primary horizontal flame front postion was recorded for as long as it was clear. In the lateral spread mode, melting effects did not appear significant; yet, regression of the sample may be an important factor. Behind the flame front, a concave ablated region results due to regression. Approximately 2 cm behind the flame front the sample is completely burned away. Hence, the flame spread phenomenon is promoted by an "edge" flame and external irradiance on that edge as well as by "surface" heating.

The tests conducted are described in table 16. The flame position results are shown in figure 27 where tests L-2 and L-4 constitute the long preheating tests. The velocity results in figure 28 tend to show the more rapid and uneven spread for downward burning as compared to lateral spread. A straight line fit to the "long preheat" data of tests L-2 and L-5 in figure 29 yield $\dot{q}''_{o,ig} = 1.4\ W/cm^2$ and $C = 0.89\ (s/mm)^{1/2}\ (W/cm^2)$. Figures 30 and 31 are used to derive these same parameters. There the more obvious data points affected by downward dripping were ignored. A summary of these parameters are tabulated in table 17. There is a fair degree of consistency among the results, despite the complex burning behavior of this material.

CARPET. In flame spread tests for the wool/nylon carpet, a distinct flame front was not observed. Indeed, the spread phenomenon followed the discrete ignition behavior observed to occur at irradiance levels of below 3.5 W/cm^2. This was observed in both downward and lateral tests. The most significant spread was noted for a lateral spread test (L-3) in which the initial irradiance was 5.1 W/cm^2. Even in that test the progression of the flame front was erratic, advancing by 10 to 50 mm steps and sometimes receding before advancing again. In general this progression could be described by a series of discrete ignitions advancing with decreasing speed. A summary of most of the tests conducted is shown in table 18, and the advance in flame spread is plotted with time in figure 32. An interesting result follows if the external irradiance corresponding to the flame position is plotted against time measured from the commencement of the test. These data are plotted in

Table 16. Flexible Foam Flame Spread Test Conditions

Test	Flux to Sample at 50 mm Position (W/cm^2)	Pre-Heat Time (s)	Ignition Time (s)	Plot Symbol
L-1	2.2	0	-	(1)
L-2	2.15	100	-	(2)
L-4	2.15	50	-	(3)
L-5	2.19	100	-	(4)
L-6	2.2	0	-	(5)
D-37	3.0	0	-	(6)
D-38	3.0	0	-	(7)
D-40	3.0	0	-	(8)
D-41	3.0	0	-	(9)
D-42	3.0	0	-	(a)
D-46	3.0	0	-	(b)

NOTE: L = Lateral flame spread test (pilot configuration from Figure 5 was used).
D = Downward flame spread test (contacting pilot was used).

Table 17. Comparison of Flame Spread Parameters by Different Methods for Flexible Foam

Method	$\dot{q}''_{o,ig}$ W/cm^2	T_{ig} ^oC	C $(s/mm)^{1/2}(cm^2/W)$	$\dot{q}''_{o,f}$ W/cm^2	$T_{s,min}$ ^oC
Ignition test	$\leq$ 1.6	$\leq$ 402.	--	--	--
Long pre-heat	1.4	374.	0.89	0.22	135.
F(t) of Eq. (7b)	1.15	337.	1.1	0.22	135.
F(t) of Eq. (16)	1.25	352.	1.06	0.22	135.

figure 33 along with the ignition data, taken under uniform irradiance conditions, from table 18. Except for times greater than 200 s, all of the "flame spread" data generally coincide with the ignition results. This suggests that the spread of flame, at least for heat fluxes greater than $\dot{q}''_{o,ig} = 1.55\ W/cm^2$, is essentially an ignition phenomenon. The time for the flame to advance to the new position at a lower external irradiance is equal to the time for piloted ignition at that irradiance level. The flame at the preceding location appears to act as the pilot flame. In test L-3 the spread advanced beyond $1.55\ W/cm^2$ so that flame spread in the sense of this analysis is possible, but does not always occur. The last three data points ($t > 250$ s) were analyzed for test L-3, taking them to represent long preheat data in order to determine C and $\dot{q}''_{o,f}$. It was felt that these data were too scant to report results using the F(t) correlations, but they were consistent with the values shown in table 19.

Table 18. Carpet Flame Spread Test Conditions

Test	Flux to Sample at 50 mm Position (W/cm^2)	Pre-Heat Time (s)	Ignition Time (s)	Plot Symbol
L-3	5.1	0	37	(1)
D-19	3.0	120	212	(2)
D-24	5.0	0	110	(3)
D-25	5.0	0	11-192	(4)
D-27	5.0	0	45-207	(5)
D-28	5.0	0	31	(6)

NOTE: L = Lateral flame spread test (pilot configuration from Figure 5 was used).
D = Downward flame spread test (contacting pilot was used).

Table 19. Flame Spread Parameters for Carpet Material

Method	$\dot{q}''_{o,ig}$ W/cm^2	T_{ig} ^oC	C $(s/mm)^{1/2}(cm^2/W)$	$\dot{q}''_{o,f}$ W/cm^2	$T_{s,min}$ ^oC
Ignition test	1.55	395.	--	--	--
Long pre-heat	1.8	432.	1.7	0.82	280.

AIRCRAFT PANEL. The aircraft interior panel behaved similarly to that observed in the ignition tests. However, no substantial flame spread was observed on the material beyond the critical flux determined from the ignition data. Some of the tests conducted are shown in table 20. Typically, following ignition of the fiberite face sheets, a stationary flame front would follow and flames would persist for approximately 15 s. The tests on this material did not yield sufficient data for analysis and by all indications flame spread does not occur in the normal sense. By this, it is meant that there is not sufficient forward flame heat transfer so that eq. (12) can not be satisfied for $\dot{q}''_e < 2.7$ W/cm^2.

Table 20. Aircraft Panel Flame Spread Test Conditions

Test	Flux to Sample at 50 mm Position (W/cm^2)	Pre-Heat Time (s)	Ignition Time (s)
L-1	5.05	0	19
D-43	3.07	0	36
D-44	3.31	0	30
D-45	3.19	0	30

NOTE: L = Lateral flame spread test (pilot configuration from Figure 5 was used).
D = Downward flame spread test (contacting pilot was used).

FLAME SPREAD AS A FUNCTION OF TEMPERATURE. Having derived these results, it is now possible to express flame spread velocity as a function of surface temperature. The form of this result is given by eq. (13) in which the heat transfer coefficient (h) is evaluated at the ignition temperature (T_{ig}). Thus the surface heat loss coefficient was assumed constant. The minimum temperature for flame spread ($T_{s,min}$) is, however, computed using a h value based on that temperature. In this manner these nonlinear heat loss effects were linearized. These calculations were performed for each material using the "long preheat" results since they were reasonably consistent with the other

methods. A summary of those calculations is shown in table 21. The parameter Φ of eq. (1) was also computed. This parameter displays the potential for the flame to transfer heat and increase the surface temperature. The ignition temperature gives the requirements for temperature rise. V_f increases with ϕ but decreases with an increase of T_{ig}. The minimum temperature ($T_{s,min}$) expresses the ease with which flame spread can be initiated. The accuracy of these results will now be examined.

In several of the downward flame spread tests, surface temperatures were measured so that velocity measurements could be correlated with them. The predicted results using the parameters of table 21 are compared to those measured values in figure 35. For the four materials in which temperature measurements were recorded, the predicted curves are in fair agreement with the data.

Table 21. Flame Spread Parameters Based on Temperature $V_f = \Phi/(T_{ig} - T_s)^2$

Material	$T_{s,min}$ (^oC)	T_{ig} (^oC)	Ch $10^{-2}(s/m)^{1/2}K^{-1}$	$\Phi = (Ch)^{-2}$ (10^4 mm/s·K^2)
Particle Board	202.	409.	0.99	1.02
PMMA	< 88.	399.	0.92	1.17
Rigid Foam	225.	428.	0.27	13.7
Flexible Foam	135.	374.	0.33	9.2
Carpet	280.	432.	0.71	2.0
Aircraft Panel	536.	536.	∞	0.

The form of the results in figure 34 offers an overall view of the flame spread and ignition characteristics of a material. This can be illustrated by considering fire development in a compartment involving a vertical wall of a material of interest. For that material to become involved it must be exposed to heating conditions sufficient to have its surface attain T_{ig}. This might be initiated by an igniting flame. Adjacent wall material must achieve a

surface temperature of $T_{s,min}$ in order for lateral (or downward) spread to begin. If sufficient energy is released in the compartment, the wall surface temperatures will increase. As they increase beyond $T_{s,min}$ and approach T_{ig}, very rapid spread would occur; and provided sufficient wall material was present, it would be responsible for flashover of the compartment. Of course, other significant measurement, such as the energy release rate of the material, must be considered in assessing this fire growth process.

RESULTS ON SURFACE TEMPERATURE.

Some further considerations on surface temperature results will be presented. These bear on the prescribed time used in preheating before the initiation of spread, and on the accuracy of the F(t)-functions used to predict the surface temperature rise in the flame spread correlations.

Temperature data were recorded every 0.4 seconds using 0.005 inch chromel-alumel thermocouple threaded through two holes spaced one inch apart on the horizontal and then secured at the back of the sample. The bead was centered on the sample and half of it pressed into the surface. For PMMA, the bead was heated prior to being pressed into the sample. The vertical location was selected such that thermocouples spanned the area of flame spread measurement. The thermocouples were located at 50 mm increments which were points of known external heat flux. Figures 35 to 39 display the measured surface temperature rise as a function of irradiance for each material except the carpet. Because of the melting and shrinking away of the pile fibers, it was not very practical to measure the surface temperature of the carpet. In some cases, these measurements were taken without flame spread affecting the results; in other cases, an abrupt termination of a curve implies flame spread or ignition of the material near the thermocouple. Also the difficulty of this measurement surely affects the accuracy of the results. Nevertheless, some conclusions can be drawn from the measurements.

The measurements on the particle board in figure 35 suggest that surface charring may be reducing the conductivity of the wood at temperatures above 250°C. A pilot flame was not present for these measurements, yet the maximum surface temperature reached at 1.68 W/cm^2 is similar to the T_{ig} values

estimated for the critical flux, $\dot{q}''_{o,ig} \sim 1.6$ W/cm^2. At a lower flux (0.97 W/cm^2), the rate of temperature rise slows significantly after 400 s, but equilibrium does not appear to be achieved at 1000 s. The temperature rise for PMMA also appears to take a considerable time to reach equilibrium, although the remaining results suggest the equilibration time for the flexible and rigid foams and the aircraft panel are less than one to two minutes.

From eq. (7a) the surface temperature should be predicted by using either of the F(t) functions. Since the parameters used for the F(t) functions were derived from the ignition data, such a comparison would suggest the accuracy of their use and in correlating the flame spread data. It was decided that a way to weigh this comparison was to derive a corresponding F(t) function from the surface temperature measurements. This can be regarded as a dimensionless temperature given by

$$F(t) = \frac{h\left(T_s - T_i\right)}{\dot{q}''_e}$$

where h was evaluated at the ignition temperature to be consistent with the analysis in the previous section. More temperature data were included in this analysis than shown previously, and consequently a range of results are presented in figures 40 to 44. This band of results can be attributed to nonlinear effects in part. The F(t) functions corresponding to eq. (16) and eq. (7b) are also plotted. Eq. (16) tends to agree with the data better than eq. (7b) and this is consistent with the ignition correlations as well. The results for the foam materials are poor and this is not easily explainable in terms of the simple theory. Consequently those F(t) functions are not expected to be capable of accurately predicting surface temperature rise before ignition.

It is interesting to observe from these results that the density of the material is a good indicator of the thermal response time of the material. This could have some advantages in setting preheating times so that a material will be nearly in thermal equilibrium during a flame spread test. In table 22, the bulk density of the materials tested are compared to several parameters characteristic of the time to reach equilibrium. Also, there is consistent agreement among the three "equilibrium" times shown. Moreover, the

Table 22. Characteristic Thermal Equilibration Times

Material	Bulk Density (kg/m^3)	Times: 1/a Corresponds to F = 0.57 (s)	Times: t_m Corresponds to F = 1 (s)	Times: t at F = 0.8 From Temperature Measurements * (s)
Rigid Foam GM-31	35	1.4	10	13
Flexible Foam	36	14.3	81	12
Aircraft Panel	126	20.	57	50
Carpet	365	66.7	243	--
Particle Board	655	222	393	400
PMMA	1080	250	456	450

* Estimated average values

times to achieve F = 0.8 for the measured results are less than the ignition time, t_m, used in the "long preheat" flame spread analyses. Hence, those analyses should correspond to nearly equilibrium conditions. The $F(t) \sim \sqrt{t}$ derived from ignition data may not be sufficiently accurate to estimate surface temperature, but the equilibrium time (t_m) from ignition data appears to be a good indicator to insure spread data under thermal equilibrium. The conversion of those data to surface temperature primarily relies on the surface heat loss coefficient (h) for non-conduction.

CONCLUSIONS

It has been demonstrated that physically meaningful parameters can be derived from test data to characterize flame spread on materials. Furthermore, it has been shown this could be done, with reasonable success, for complex materials as well as homogenous materials. However, for complex materials, the burning behavior can present effects that are not taken into account by the theoretical basis for the data analysis. In this case, more effort may be required to

derive the flame spread parameters, and these parameters would more represent correlating factors rather than true material properties. The flexible polyurethane foam represents a complex material in which the melting and regressing effects are not represented by the simple theory. Yet the flame spread parameters derived serve to correlate the data, and yield results consistent with ignition data. The aircraft panel material did not appear to sustain flame spread at all, so that results from the ignition tests were needed in analyzing the flame spread data.

Reasonable consistency has been demonstrated for the derived data. This has been shown by demonstrating the complementary aspects of flame spread and ignition at the critical flux $\dot{q}''_{o,ig}$. Tables 11, 13, 15, 17, and 19 show that $\dot{q}''_{o,ig}$, the upper limit for spread and the lower limit for ignition, are generally consistent for each material. Also by accounting for transient heating effects, most of the flame spread results can be correlated so that the parameter C is invariant for a given specimen. Finally, measured results for flame spread rate as a function of surface temperature tend to be in good agreement with predicted results based on the parameters determined for each material.

The specific results for each material are shown in tables 9 and 21 for ignition and flame spread, respectively. Although the ignition temperatures cited are modeling parameters and not necessarily true surface temperatures, their values do reflect the energy necessary for ignition. This reflects the point of sufficient decomposition to provide a flammable mixture; it does not reflect the time to reach that limit. That is represented roughly by the thermal properties of the material, e.g. a, b and E_m. Hence, the aircraft paneling has the highest ignition temperature. At an irradiance level of 2.5 W/cm^2 it would not sustain ignition, yet the other materials tested all would. But at 3 W/cm^2 the ignition times were approximately as follows:

Particle board	100 s
PMMA	50 s
Rigid foam	3 s
Flexible foam	20 s
Carpeting	50 s
Aircraft paneling	50 s

In considering flame spread under external heating conditions which lead to surface temperatures less than the ignition temperature, the parameter ϕ least reflects spread rate. The aircraft does not appear to exhibit spread (it will only ignite). The foam materials both exhibit spread rates of roughly five to ten times that of the wood, PMMA and carpeting samples tested.

Although quantitative and consistent results have been derived, various techniques have been used. A single test procedure has not been specified to routinely measure these flame spread parameters for materials. The approach of conducting a flame spread test with arbitrary preheating and then applying F(t) by eq. (16) to correct for transient effects is attractive. Although this appears to work well, at least for simple materials, it is empirical and may not be general enough. It would appear that an attempt to conduct a "long preheat" test is best. This could be done in several ways. A preheating time could be estimated from table 22 by determining a bulk density of the material. Several flame spread tests could then be run at this preheating time and longer times. The sufficiency of the preheating time could be decided by the manner in which the data fall on plotting $V_f^{-1/2}$ versus $\dot{q}_e''$. Data which coalesce to the left, on such a plot, would indicate sufficient heat times. Alternatively, an optical pyrometer could be used to measure the surface temperature response to radiant heating in the flame spread apparatus. An equilibration time could then be determined. Subsequently, a flame spread test could be run with the appropriate preheating time. Although this latter technique was not attempted in this study, it is something that will be tried in the future.

Finally, it should be noted that downward and lateral spread rates were essentially identical except where substantial melting and dripping occurred. But even for those materials that melted, it took some time for dripping

effects to have a profound influence on the downward flame spread rate. Also it was interesting to find that a $\sqrt{t}$ relationship was adequate for correlating the ignition behavior for most of these materials. This may prove to be a useful empirical result.

The form of results presented provide a means of predicting aspects of ignition and flame spread. They do not in themselves provide indications of general flammability. Where these phenomena are relevant, a knowledge of the level and duration of the thermal exposure must be determined. This can be derived from realistic fire tests or from mathematical models of fire growth. Indeed, the form of the results presented here should be amenable to current mathematical models of fire growth.

REFERENCES

1. Quintiere, J. and Huggett, C., "An Evaluation of Flame Spread Test Methods for Floor Covering Materials", Fire Safety Research, NBS Spec. Pub. 411, National Bureau of Standards, Nov. 1974.

2. Tustin, E.A., "Development of Fire Test Methods for Airplane Interior Materials", NASA-CR-14568, Boeing Commercial Airplane Co., 1979.

3. Nicholas, E.B., "Evaluation of Existing Flammability Test Methods by Comparison of Flammability Characteristics of Interior Materials", Federal Aviation Administration Report No. FAA-NA-79-46, March 1980.

4. Quintiere, J., "An Assessment of Correlations Between Laboratory and Full-Scale Experiments for the FAA Aircraft Fire Safety Program, Part 4: Flammability Tests", NBSIR 82-2525, National Bureau of Standards, July 1982.

5. Magee, R.S. and McAlevy, R.F., "The Mechanism of Flame Spread", J. Fire Flammability, Vol. 2, Oct. 1971.

6. deRis, J., "Spread of a Laminar Diffusion Flame", Twelfth International Symposium on Combustion, The Combustion Institute, 1969.

7. Fernandez-Pello, A.C., Ray, S.R. and Glassman, I., "Flame Spread in an Opposed Forced Flow: The Effect of Ambient Oxygen Concentration", Eighteenth Int. Symposium on Combustion, The Combustion Institute, 1981.

8. Frey, A.E. and Tien, J.J., "A Theory of Flame Spread Over a Solid Fuel Including Finite Chemical Kinetics", Combustion and Flame, Vol. 36, 1979.

9. Fernandez-Pello, A.C. and Santoro, R.J., "On the Dominant Mode of Heat Transfer in Downward Flame Spread", Seventeenth International Symposium on Combustion, The Combustion Institute, 1978.

10. Borgeson, R.A., "Flame Spread and Spread Limits", NBS-GCR-82-396, National Bureau of Standards, July 1982.

11. Quintiere, J., "A Simplified Theory for Generalizing Results from a Radiant Panel Rate of Flame Spread Apparatus", Fire and Materials, Vol. 5, June 1981.

12. Fernandez-Pello, A.C., "Downward Flame Spread Under the Influence of Externally Applied Thermal Radiation", Combustion Science and Technology, Vol. 17, 1977.

13. Kreith, F., Principles of Heat Transfer, Nat. Ed., International Text Book Co., Scanton, PA, 1967.

14. Quintiere, J., Harkleroad, M. and Walton, W., "Measurement of Material Flame Spread Properties", NBSIR 82-2557, National Bureau of Standards, August 1982.

15. Robertson, A.F., "A Flammability Test Based on Proposed ISO Spread of Flame Test", Third Progress Report, Intergovernmental Maritime Consultative Organization, IMCO FP/215, 1979.

16. Simms, D.L., "On the Pilot Ignition of Wood by Radiation", Combustion and Flame, Vol. 7, Sept. 1973.

17. Kashiwagi, T., Private Communication, Nat. Bur. Stand., 1982.

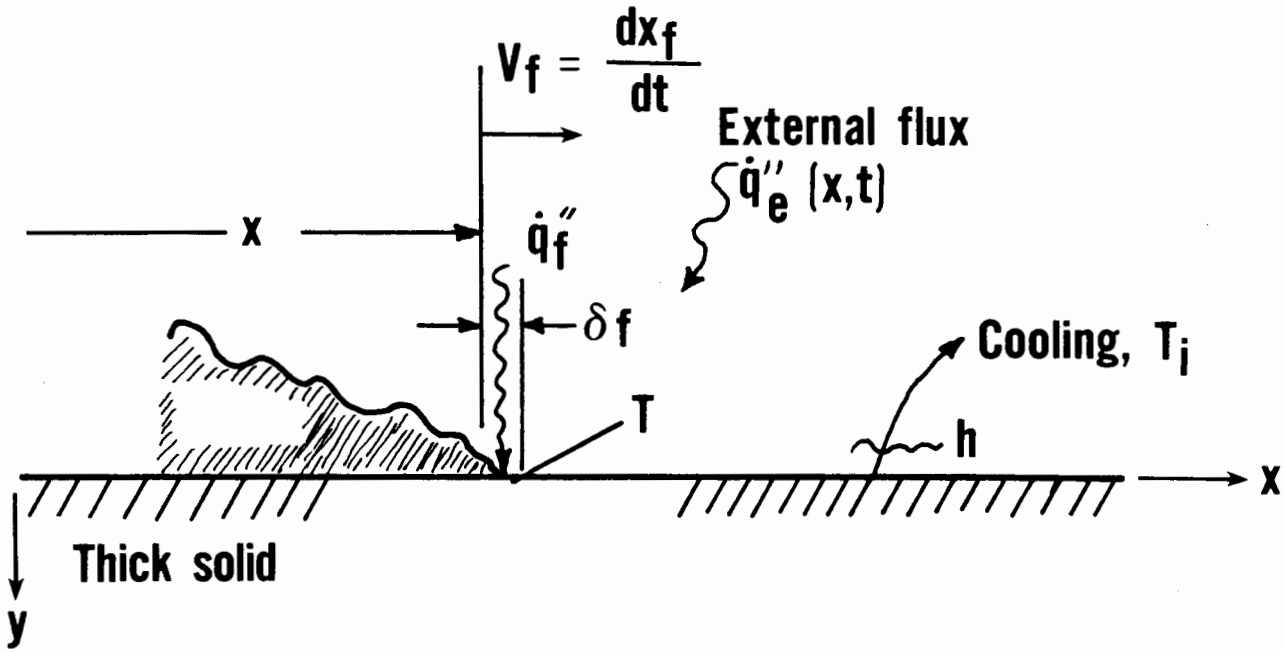

FIGURE 1. COMPONENTS OF FLAME SPREAD MODEL

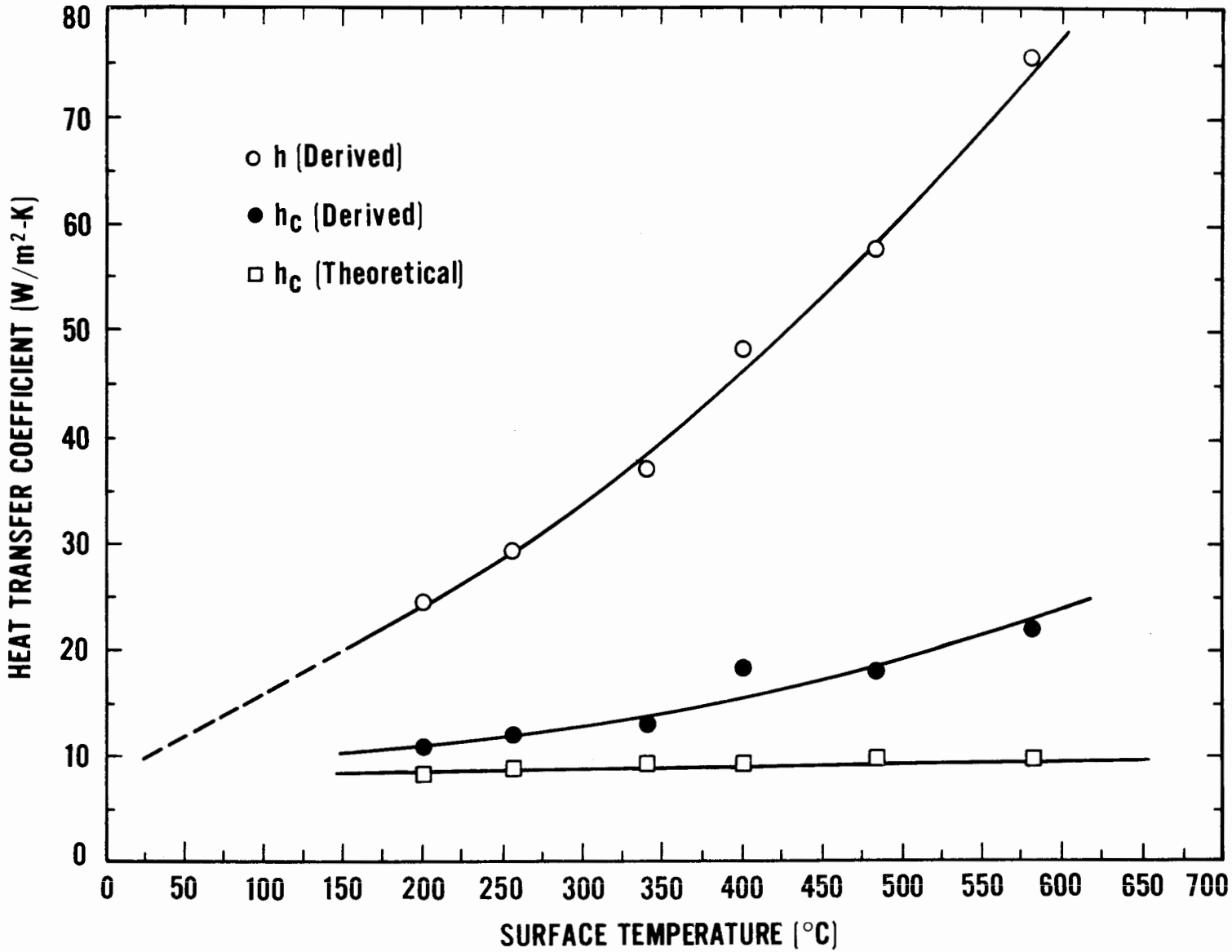

FIGURE 2. HEAT TRANSFER COEFFICIENT

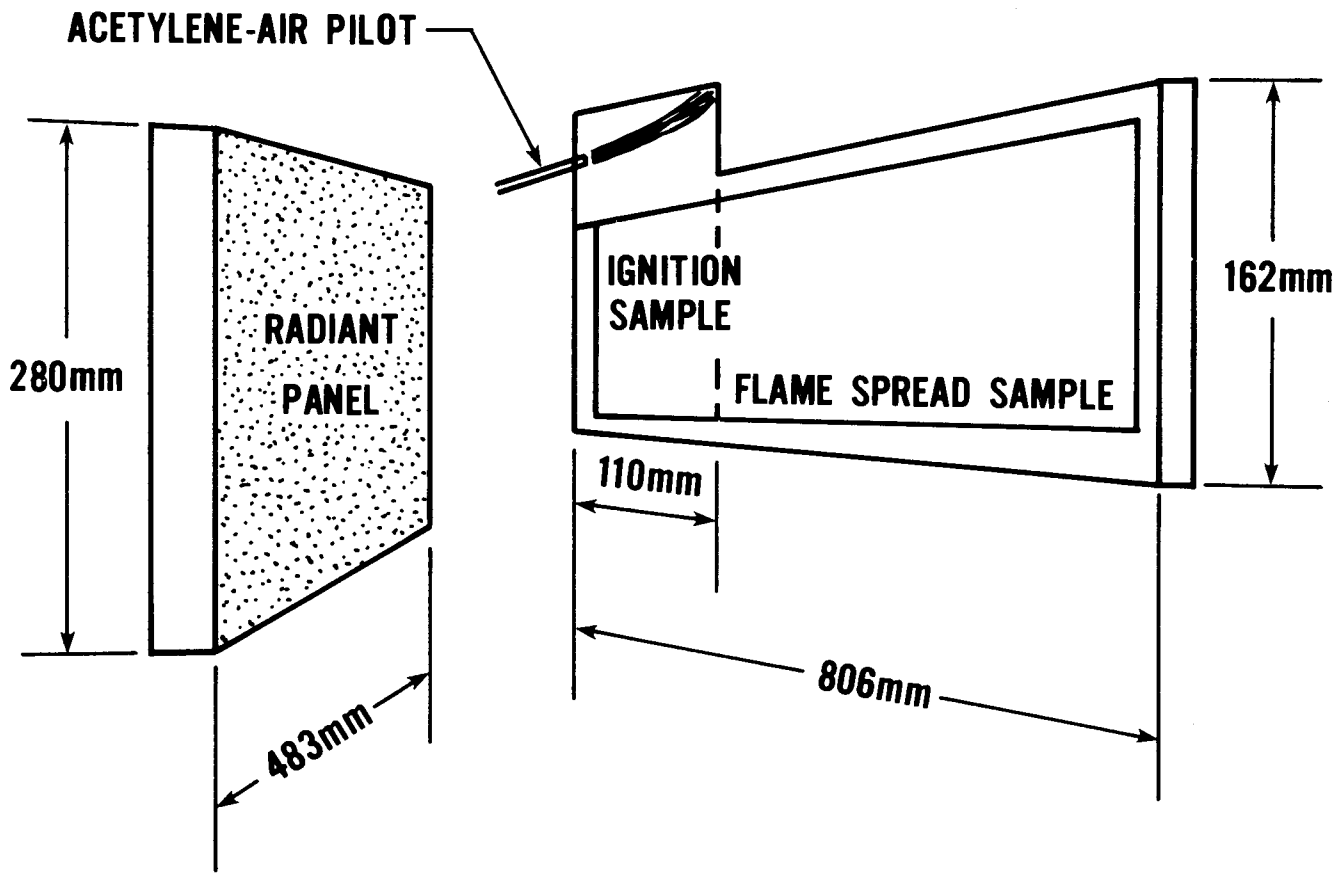

FIGURE 3. SCHEMATIC OF EXPERIMENTAL APPARATUS

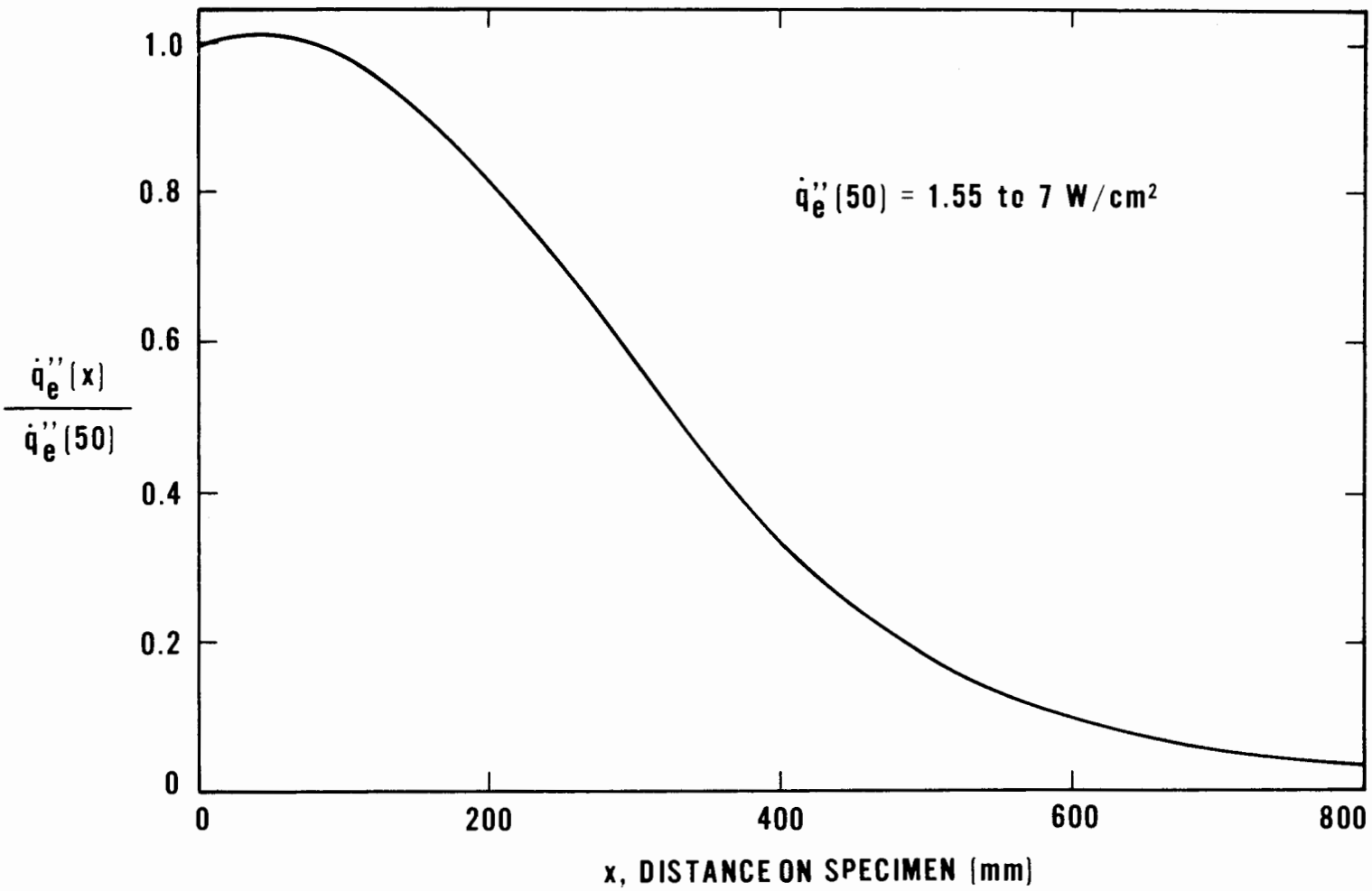

FIGURE 4. NORMALIZED RADIANT FLUX DISTRIBUTION

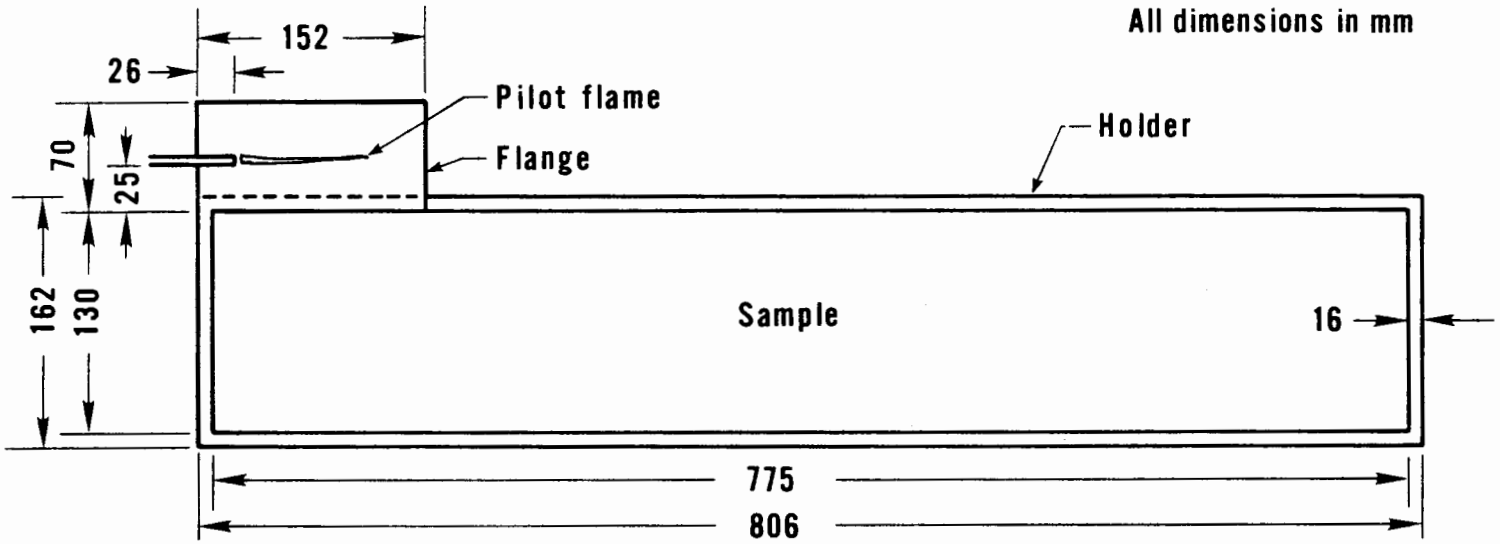

FIGURE 5. PILOT FLAME CONFIGURATION

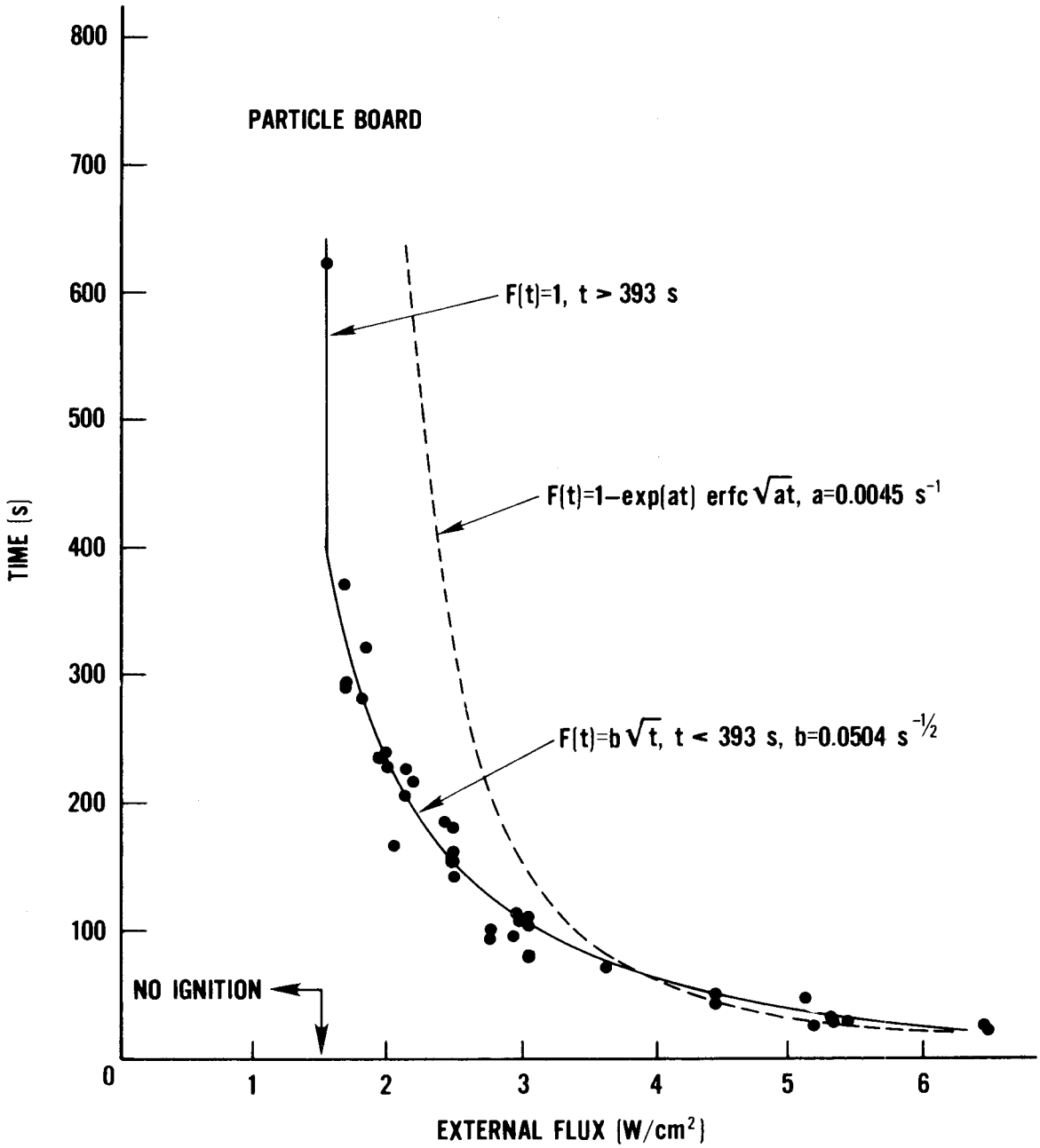

FIGURE 6. TIME TO IGNITE FOR PARTICLE BOARD

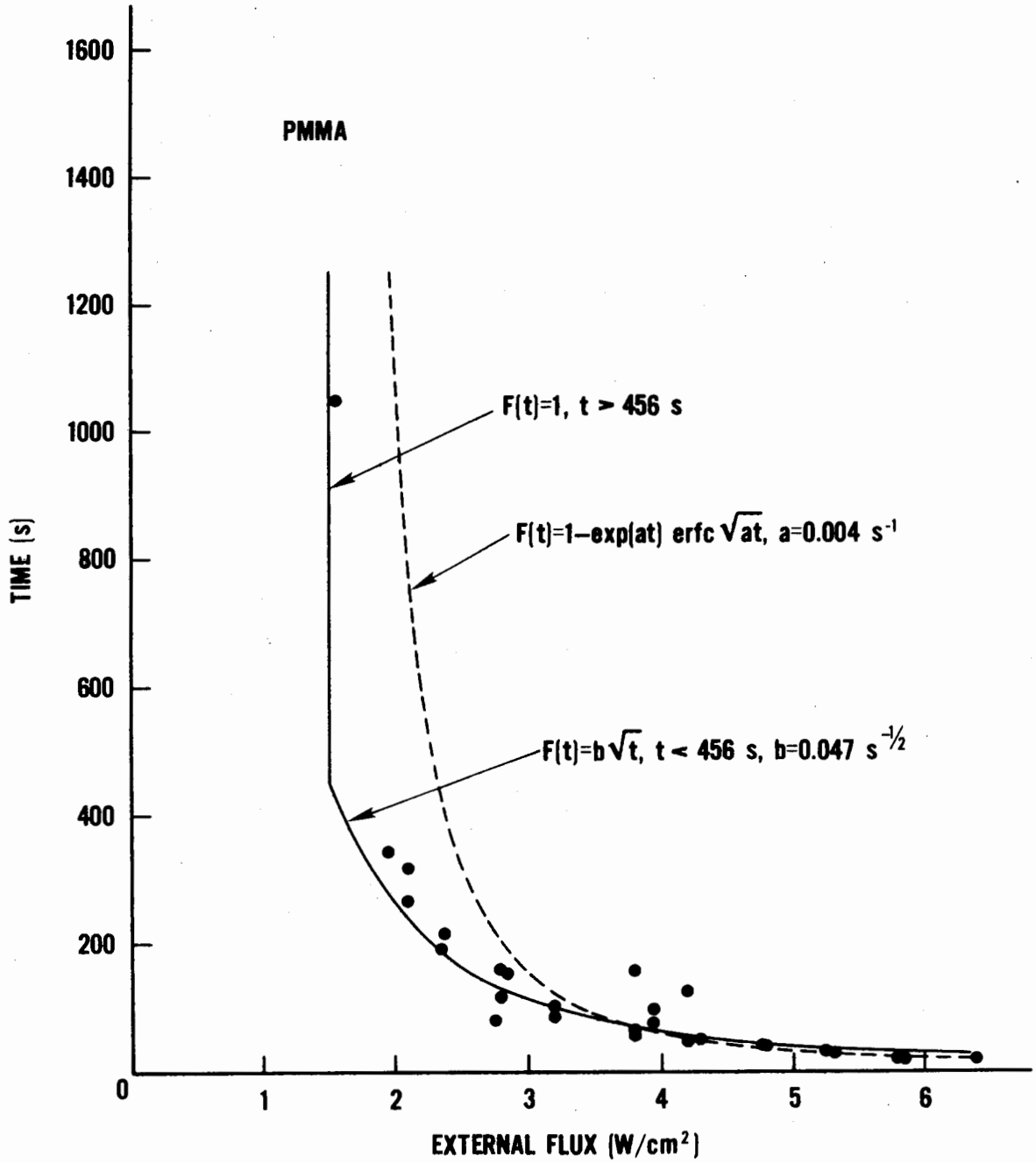

FIGURE 7. TIME TO IGNITE FOR PMMA

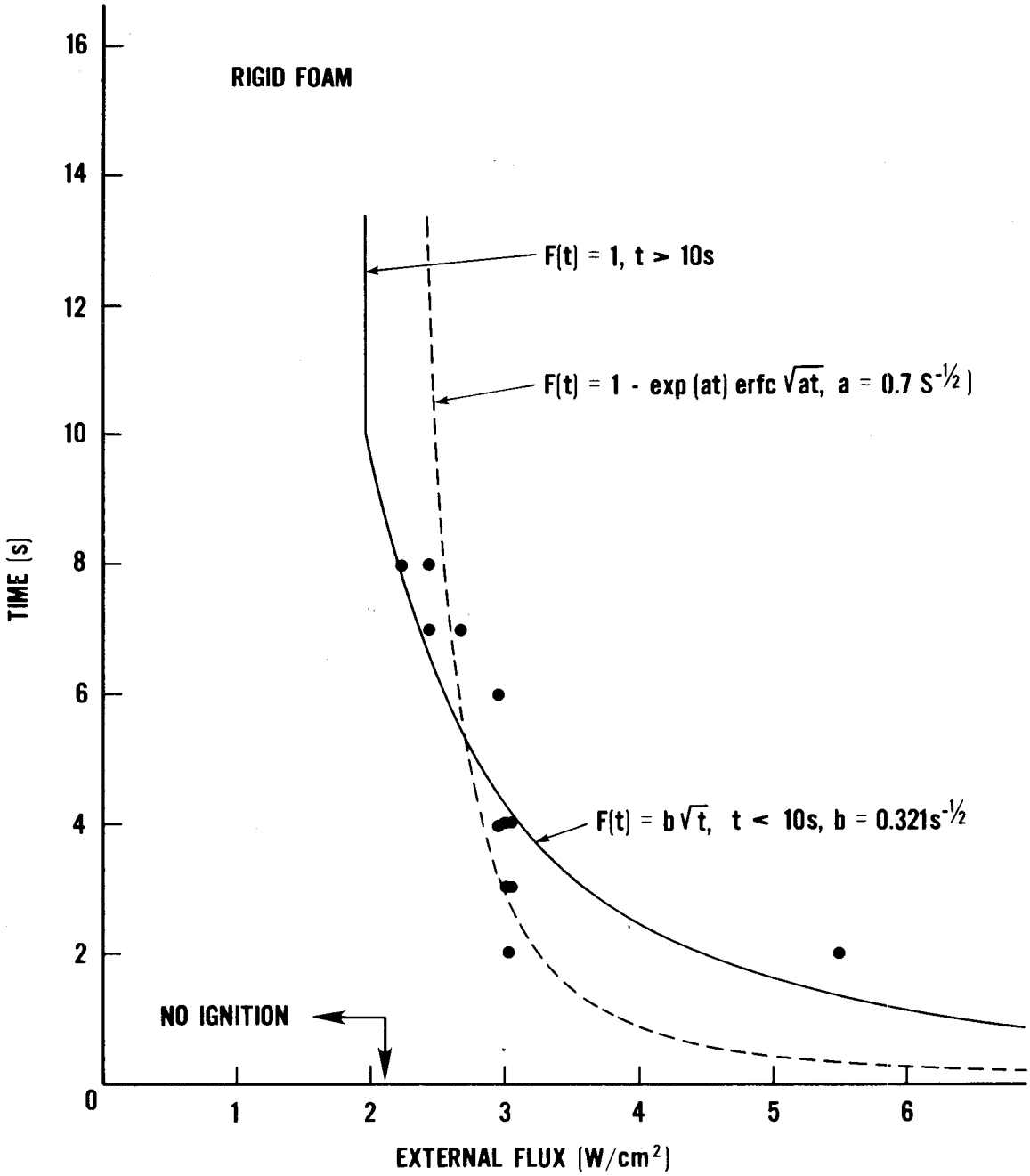

FIGURE 8. TIME TO IGNITE FOR RIGID FOAM

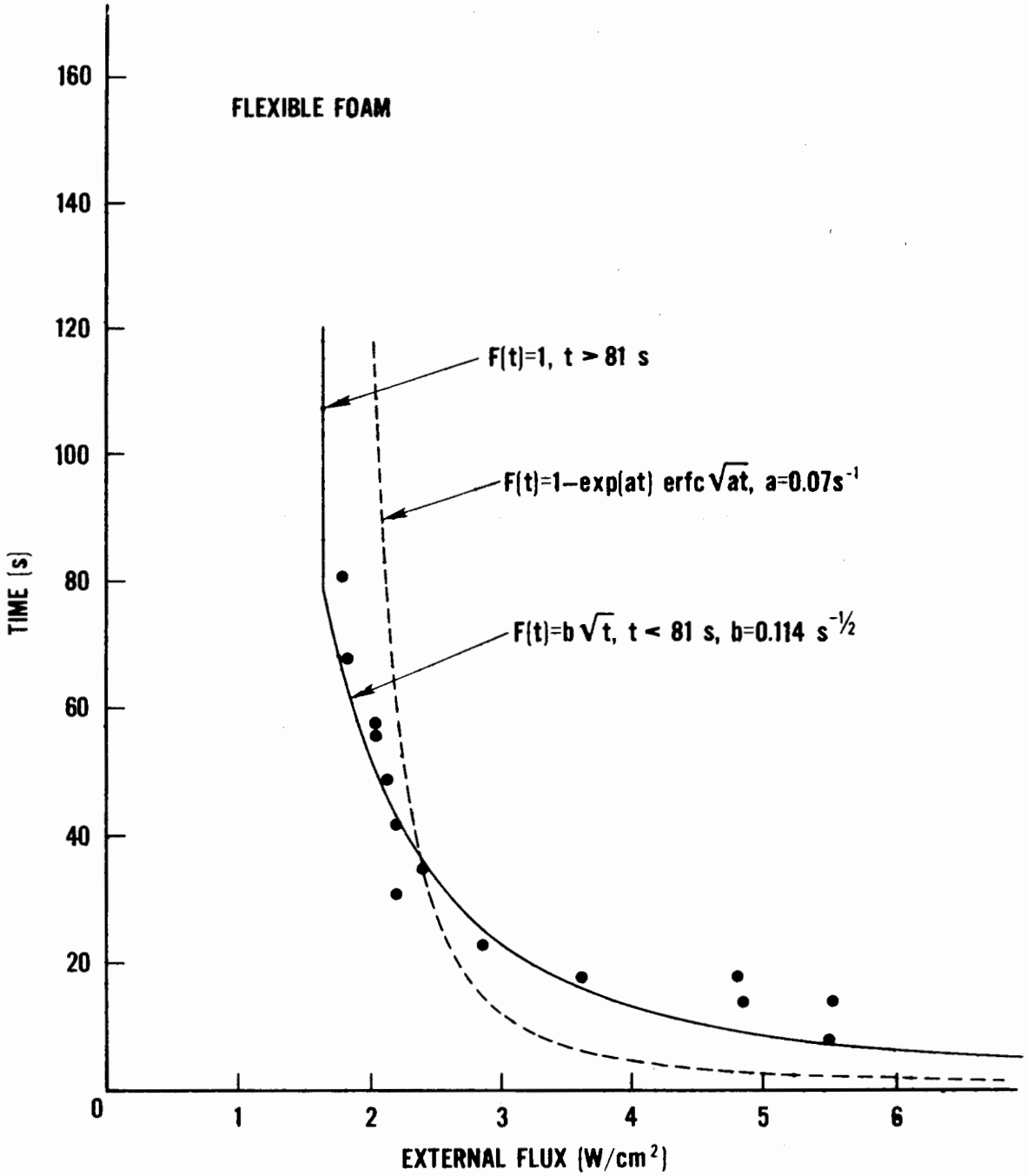

FIGURE 9. TIME TO IGNITE FOR FLEXIBLE FOAM

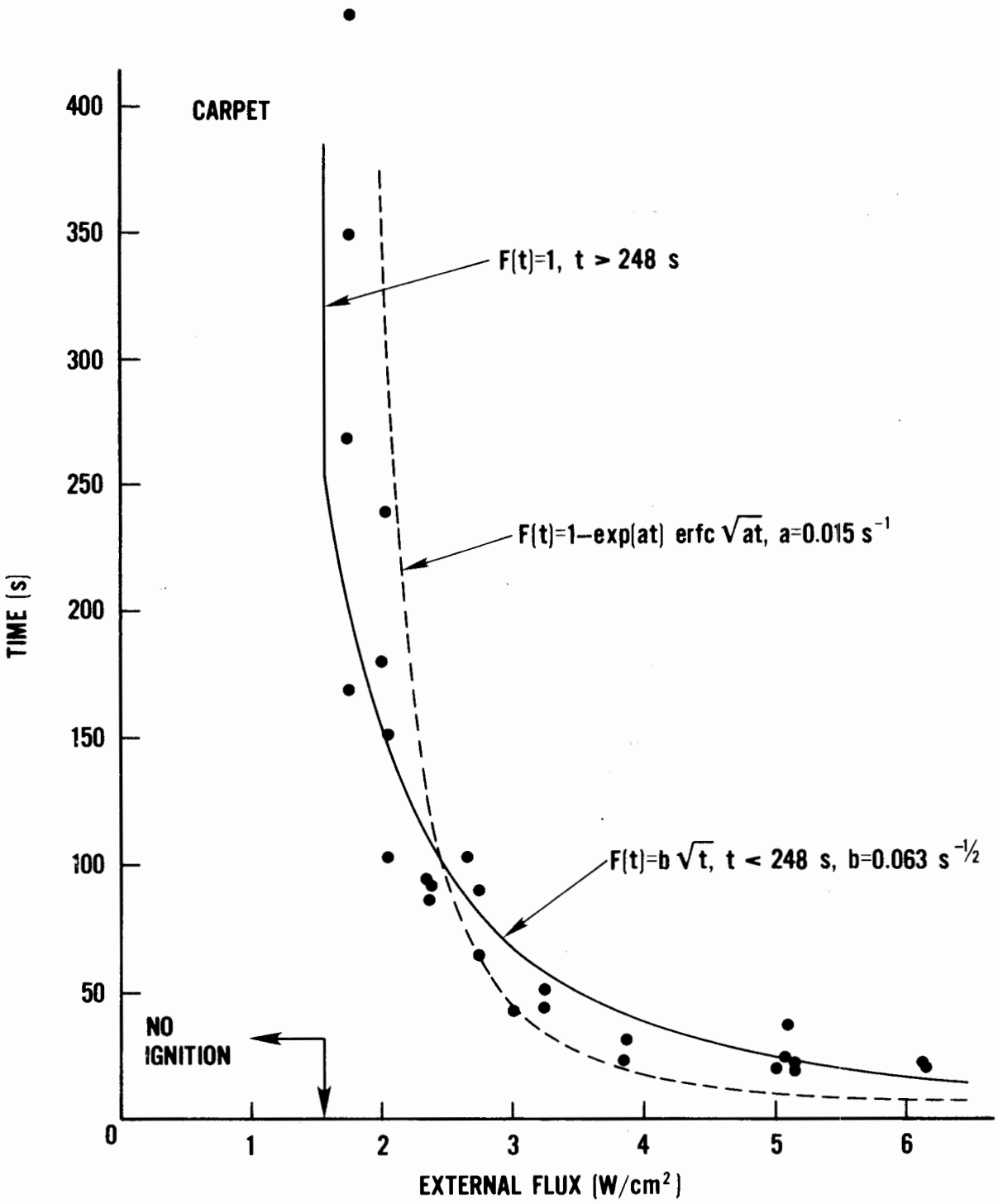

FIGURE 10. TIME TO IGNITE FOR CARPET

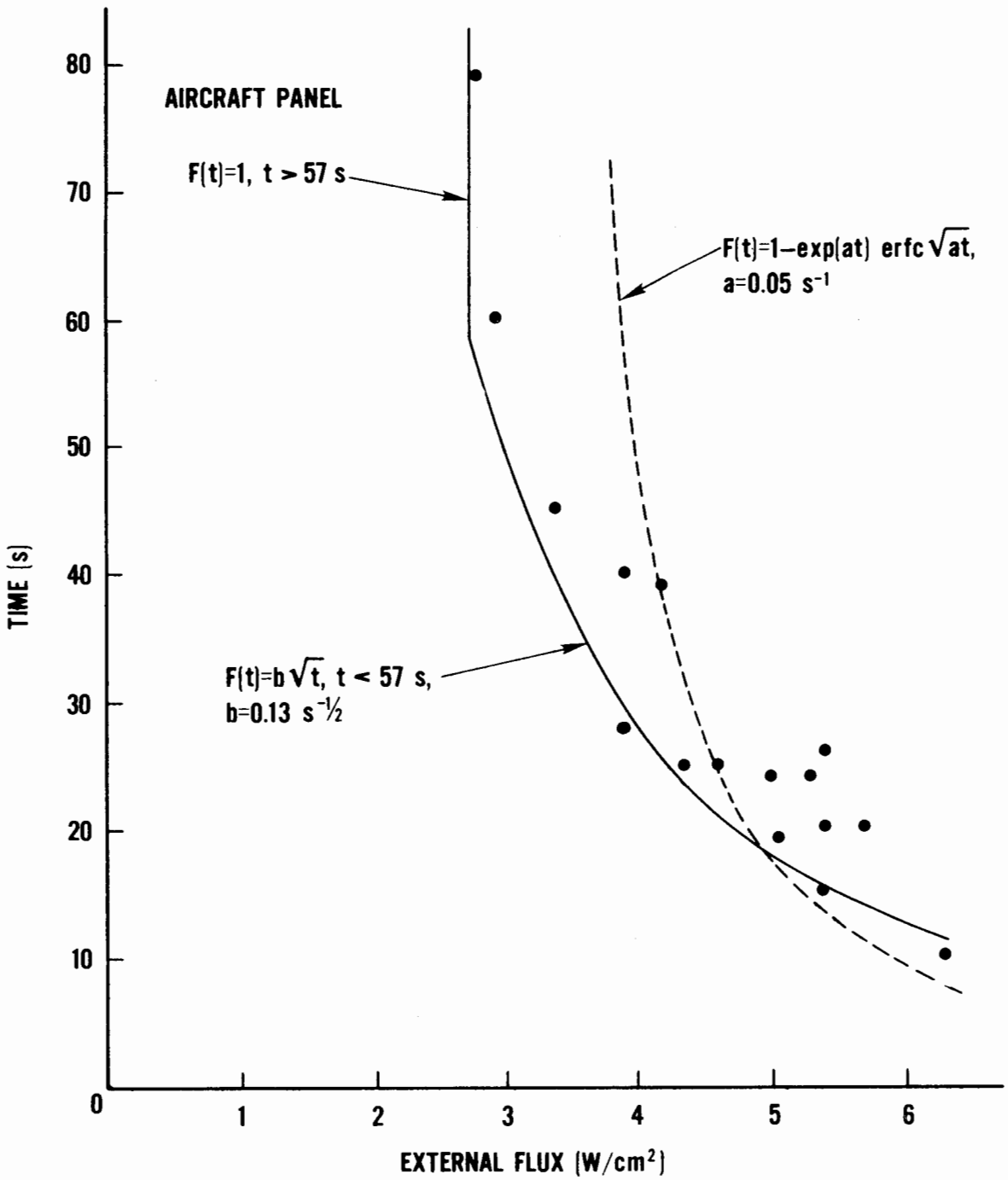

FIGURE 11. TIME TO IGNITE FOR AIRCRAFT PANEL

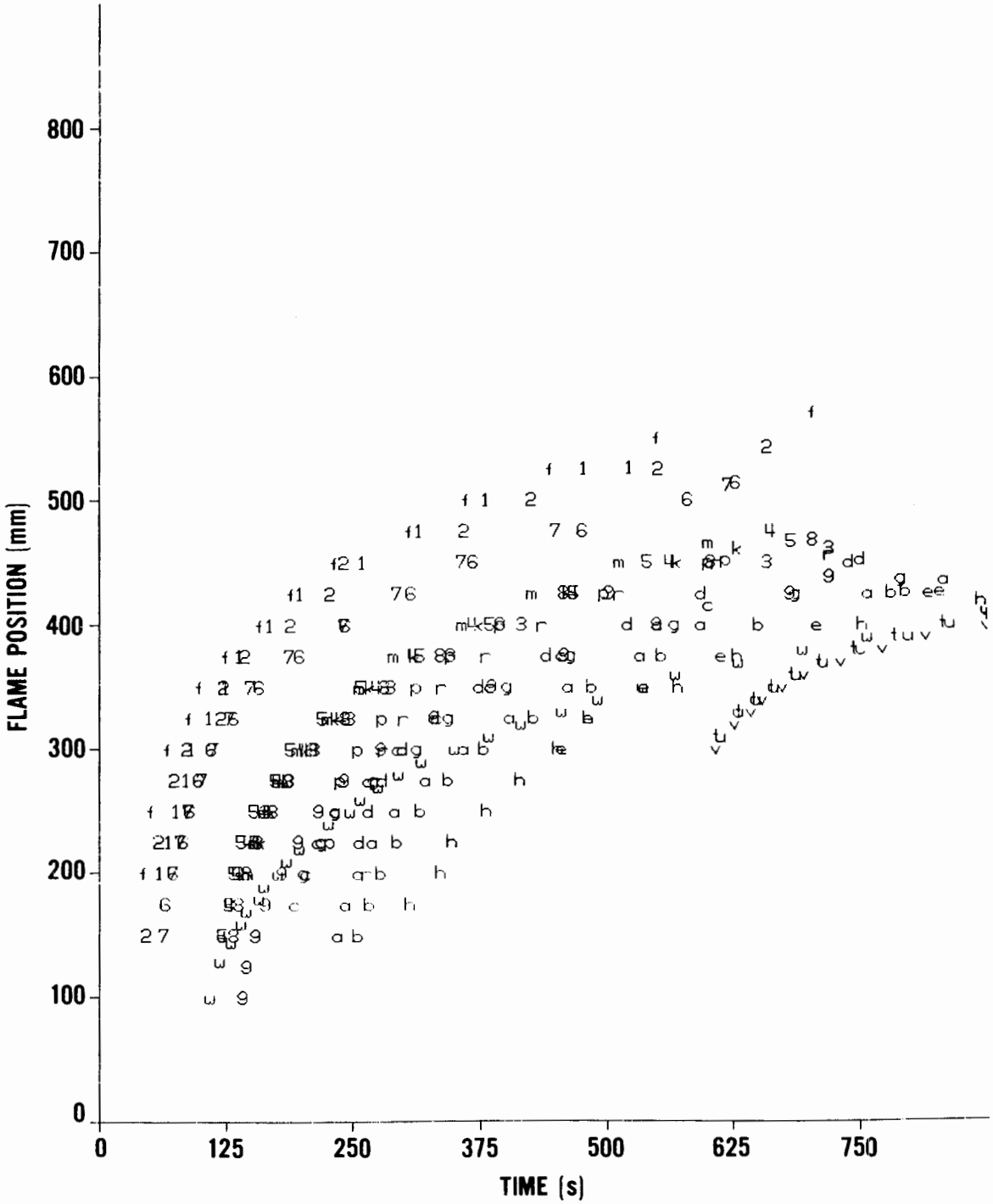

FIGURE 12. FLAME FRONT MOVEMENT FOR PARTICLE BOARD TESTS

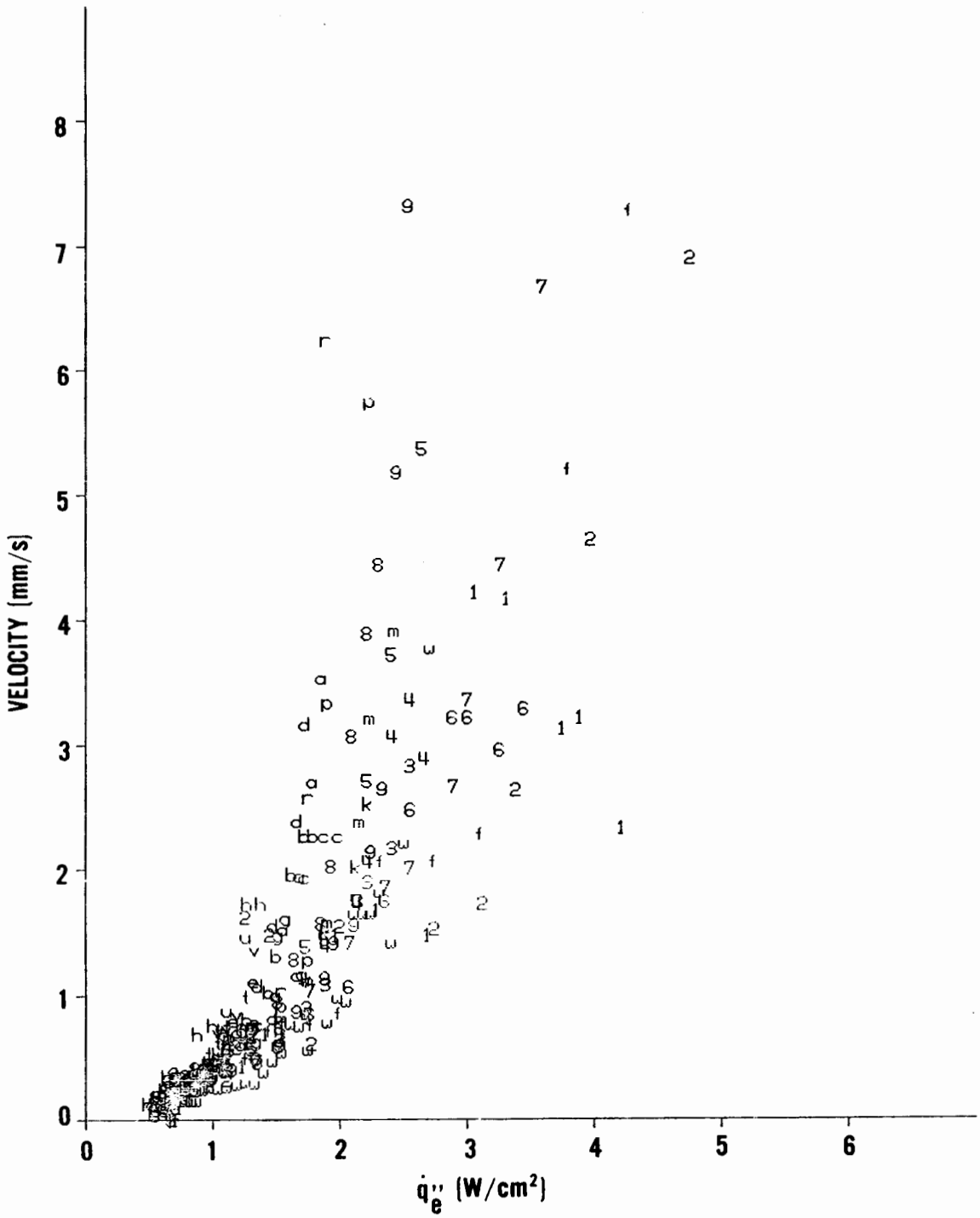

FIGURE 13. FLAME SPREAD VELOCITY FOR PARTICLE BOARD TESTS

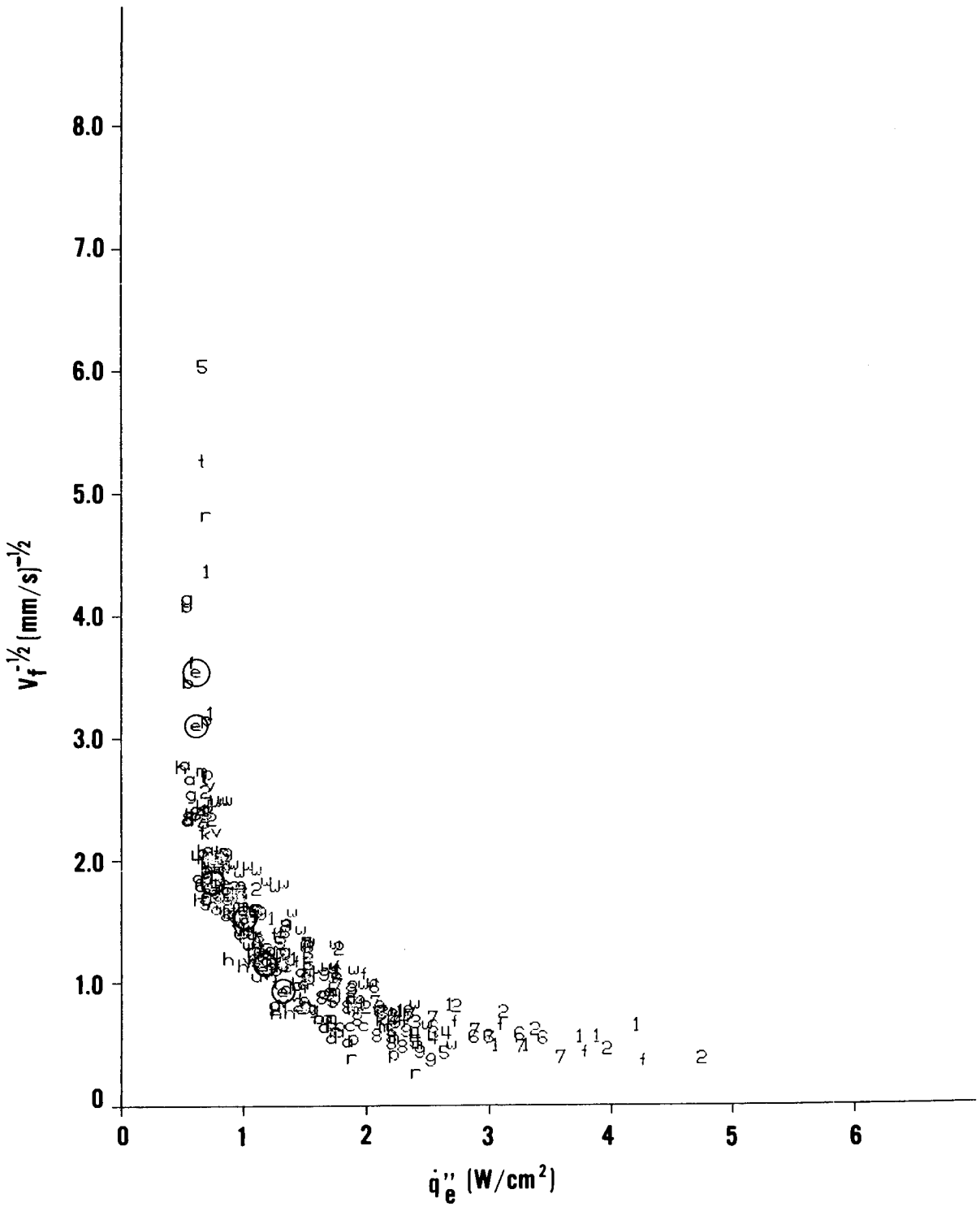

FIGURE 14. CORRELATION FOR PARTICLE BOARD FLAME SPREAD WITH FLUX
(ⓔ INDICATES LONG PREHEAT TEST)

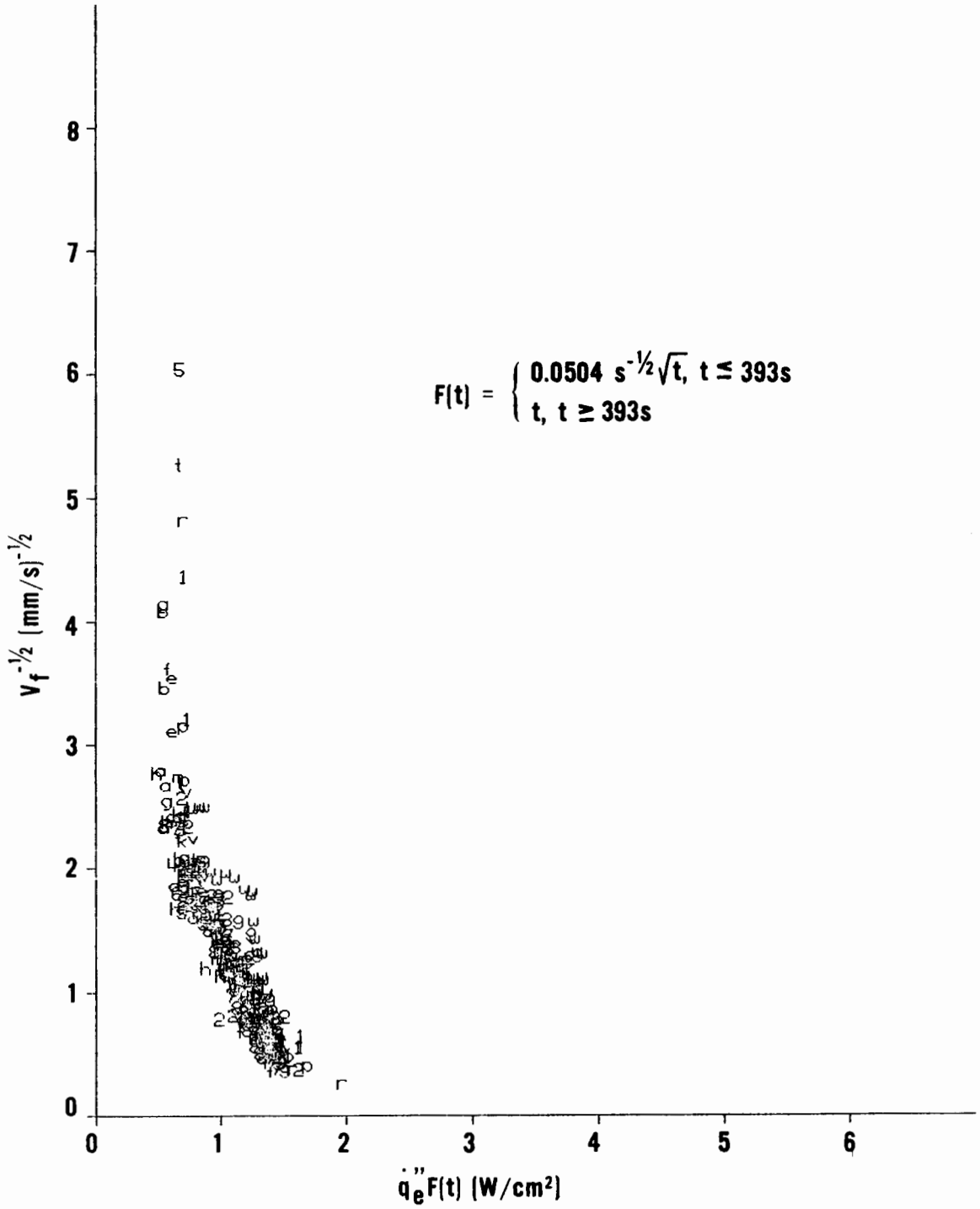

FIGURE 15. CORRELATION FOR PARTICLE BOARD FLAME SPREAD, F(t) BY EQ. (16)

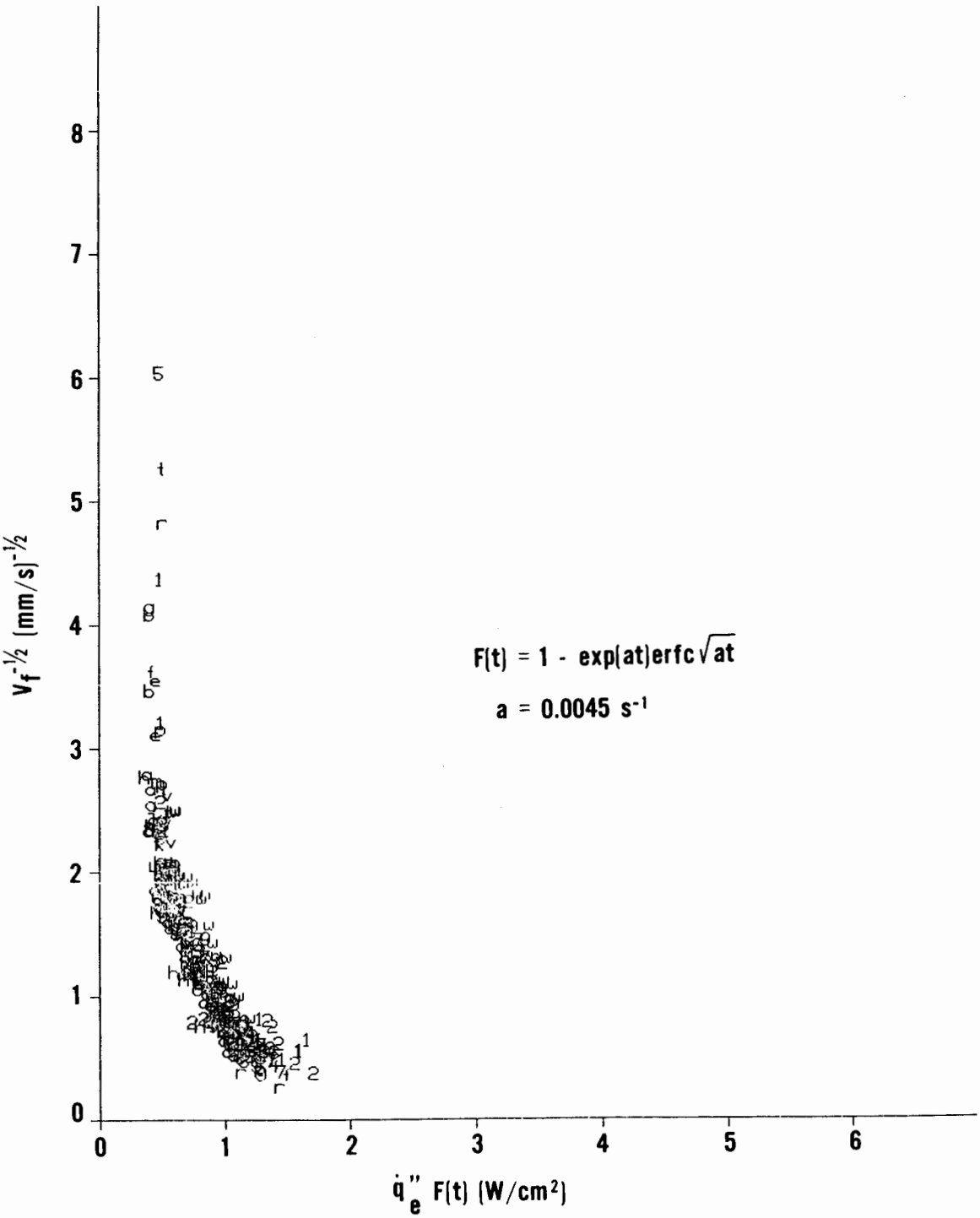

FIGURE 16. CORRELATION FOR PARTICLE BOARD FLAME SPREAD, F(t) BY EQ. (7b)

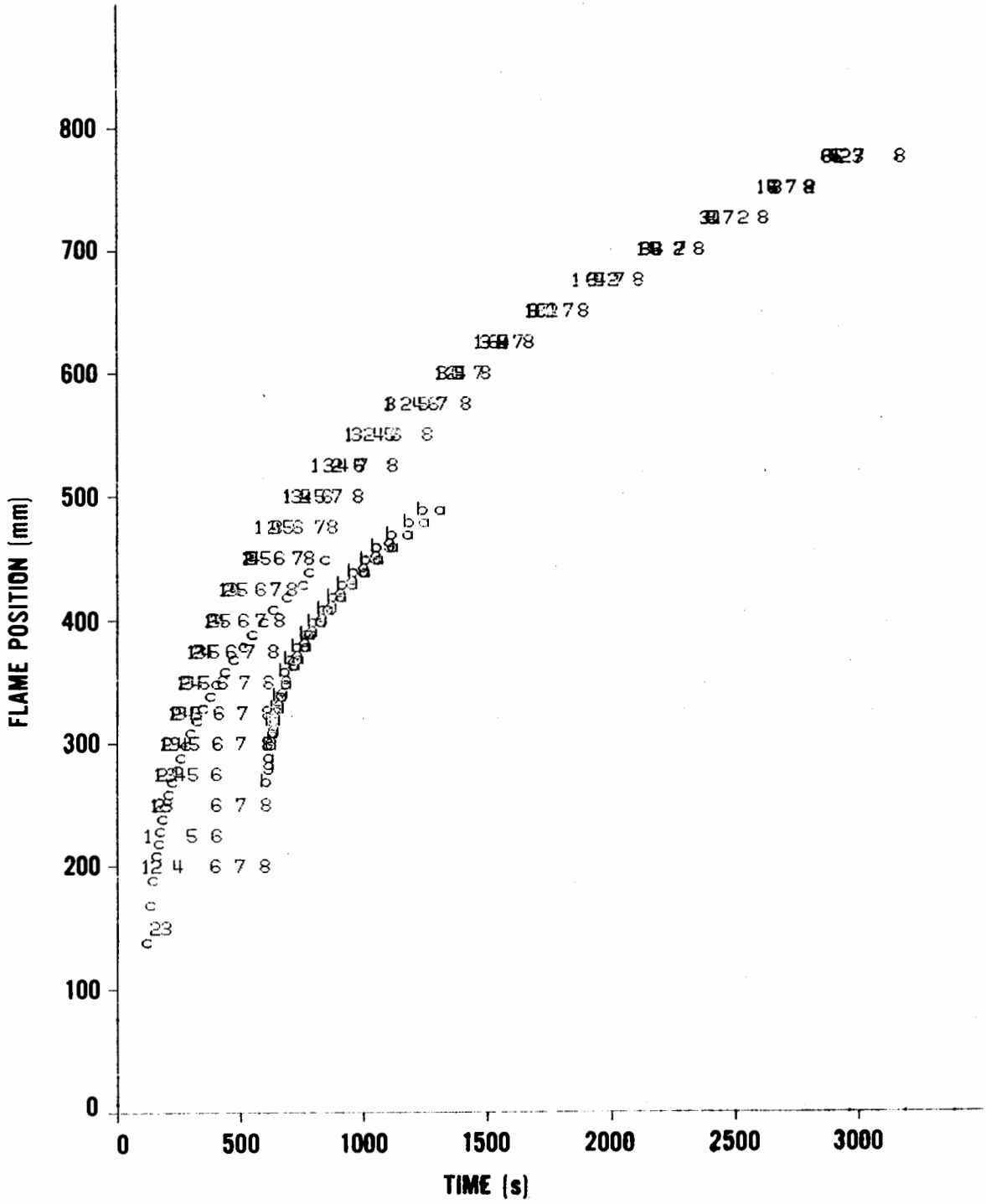

FIGURE 17. FLAME FRONT MOVEMENT FOR PMMA TESTS

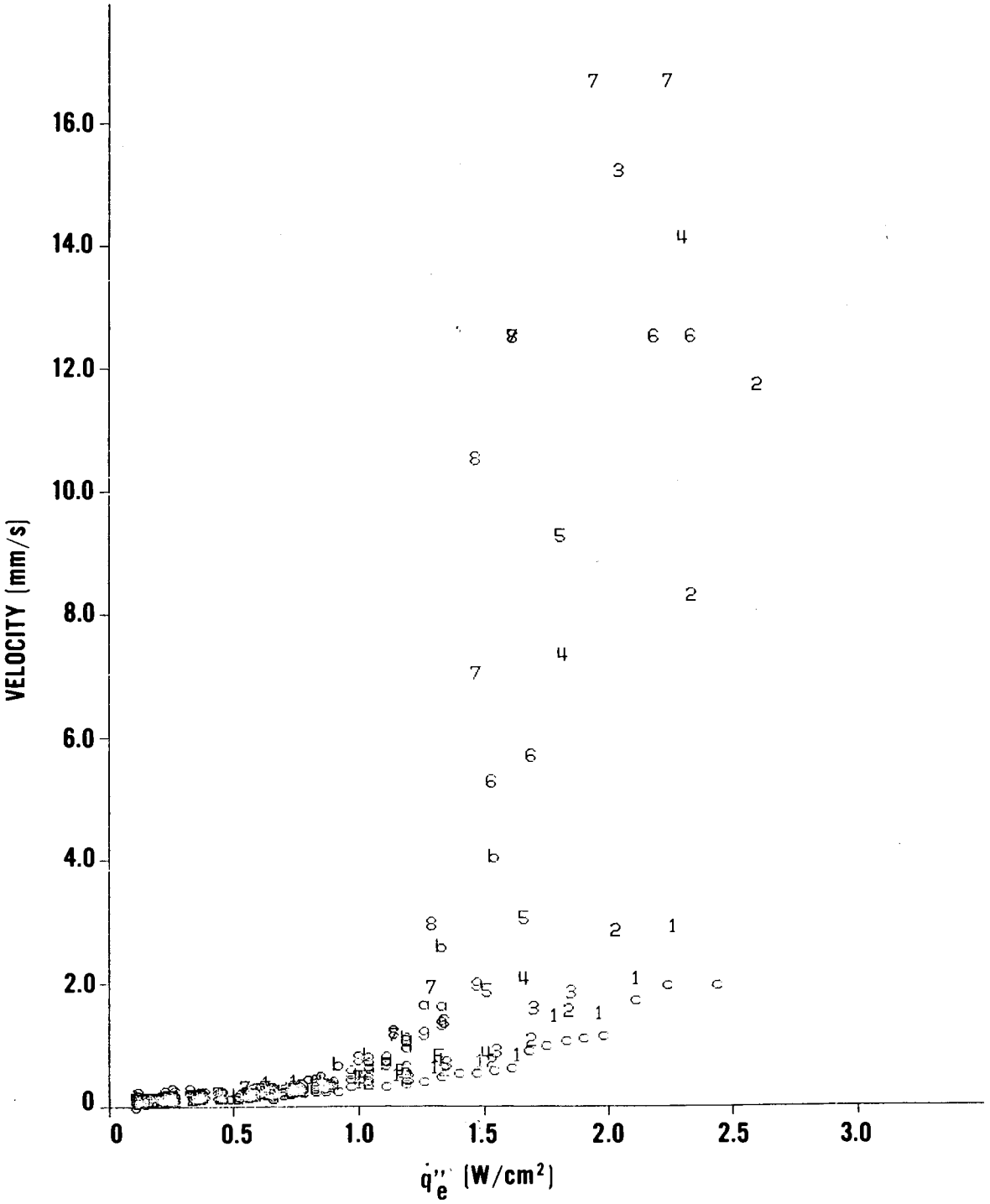

FIGURE 18. FLAME SPREAD VELOCITY FOR PMMA TESTS

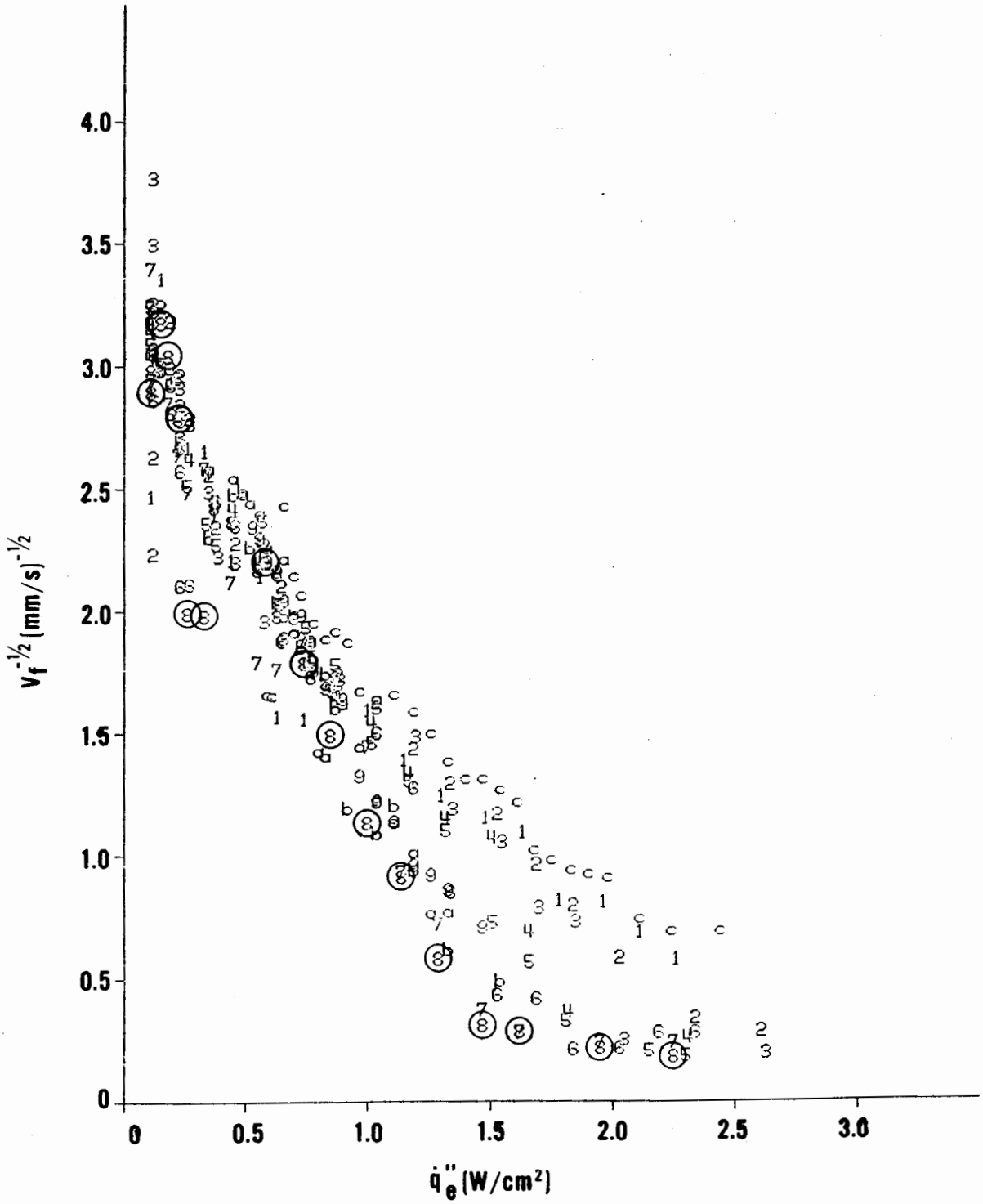

FIGURE 19. CORRELATION FOR PMMA FLAME SPREAD WITH FLUX
(8 INDICATES LONG PREHEAT TEST)

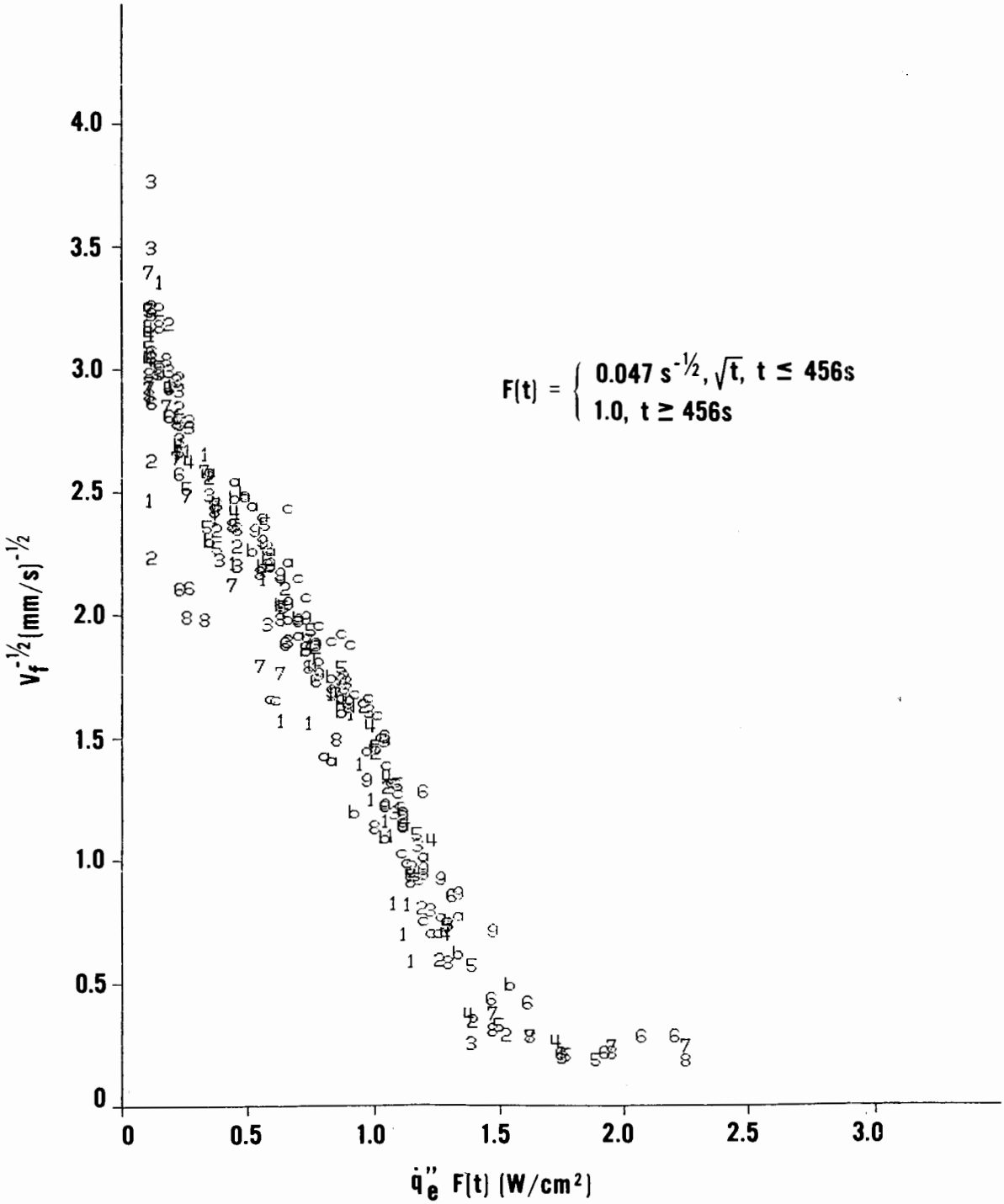

FIGURE 20. CORRELATION FOR PMMA FLAME SPREAD, F(t) BY EQ. (16)

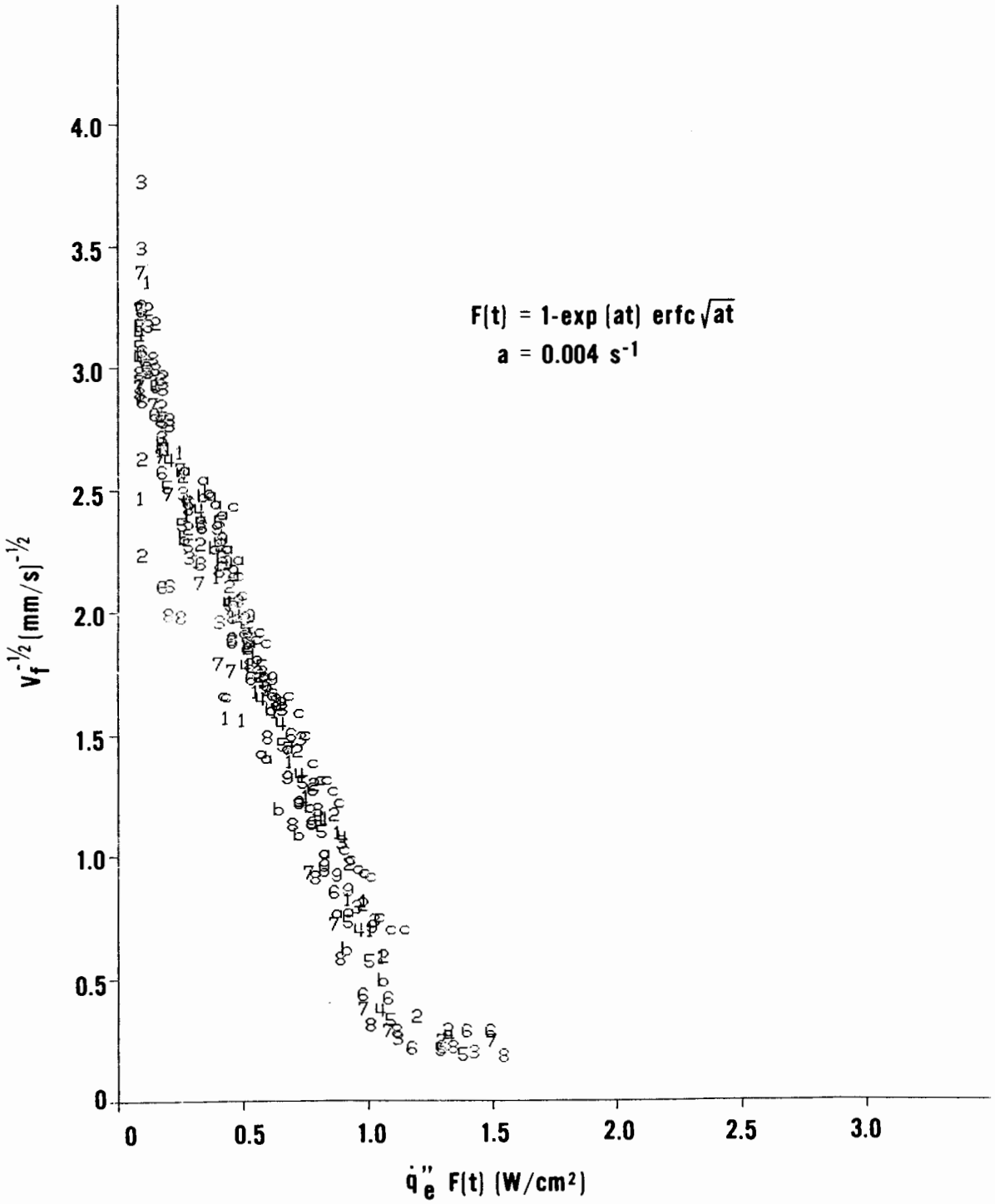

FIGURE 21. CORRELATION FOR PMMA FLAME SPREAD F(t) BY EQ. (7b)

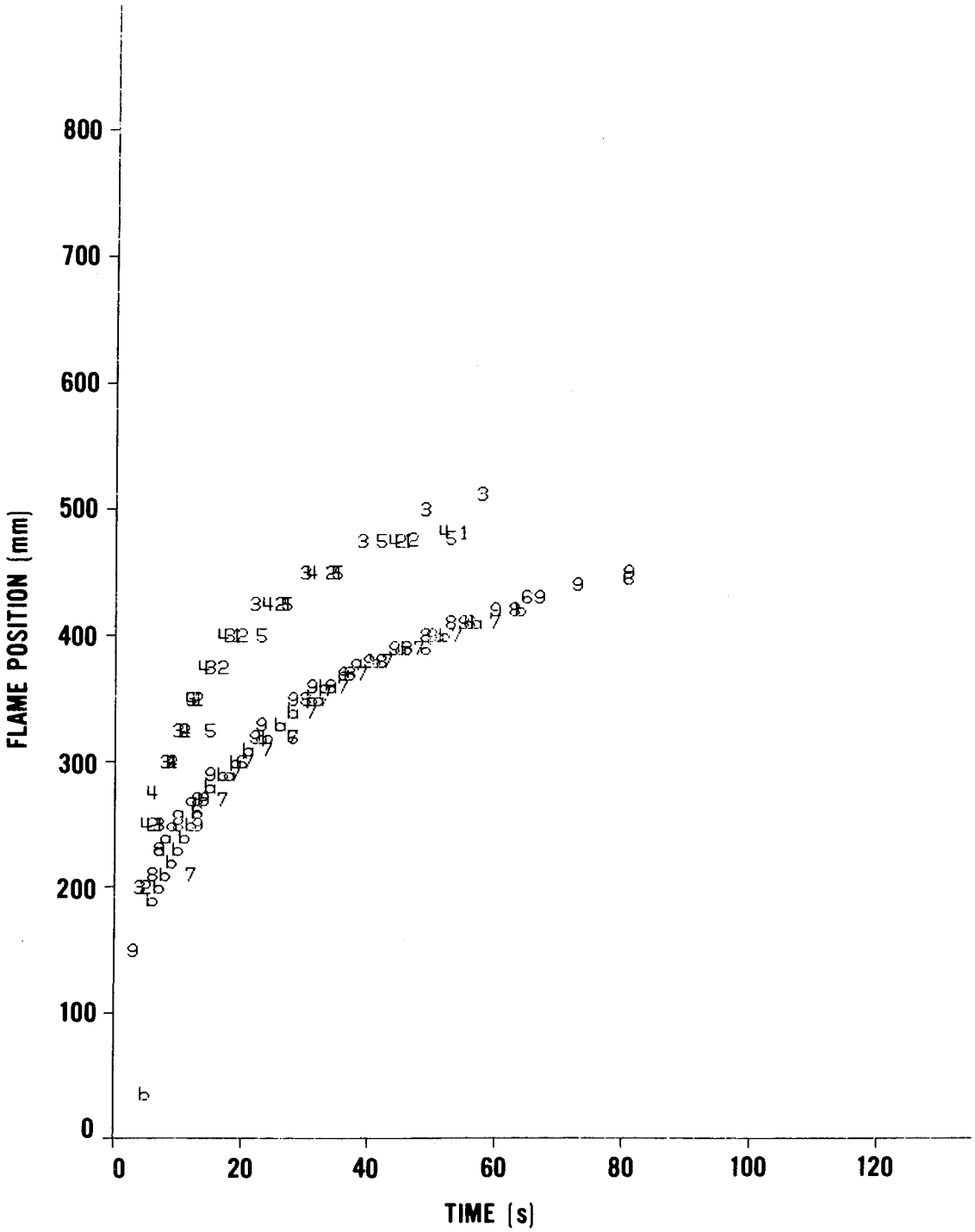

FIGURE 22. FLAME FRONT MOVEMENT FOR RIGID FOAM

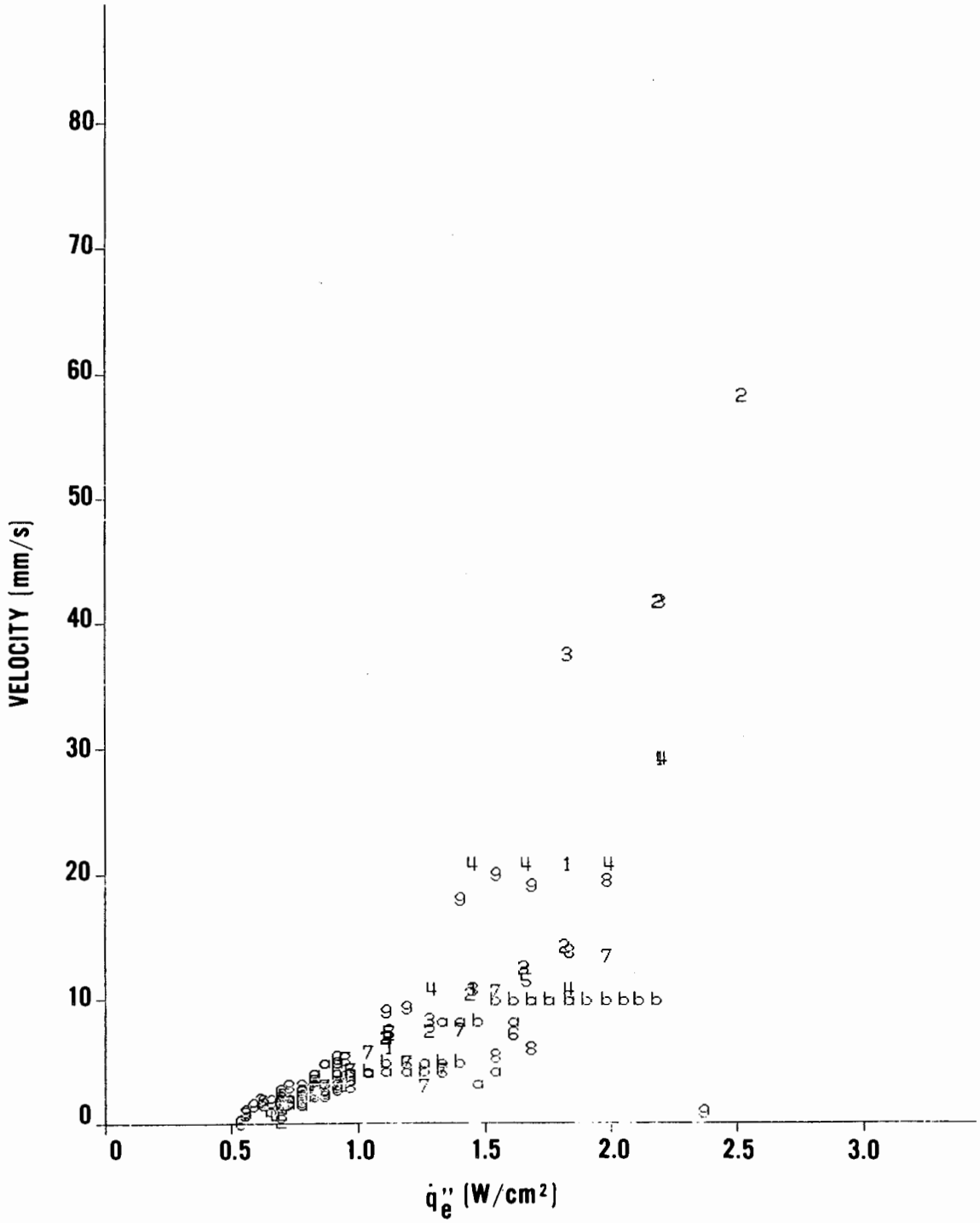

FIGURE 23. FLAME SPREAD VELOCITY FOR RIGID FOAM

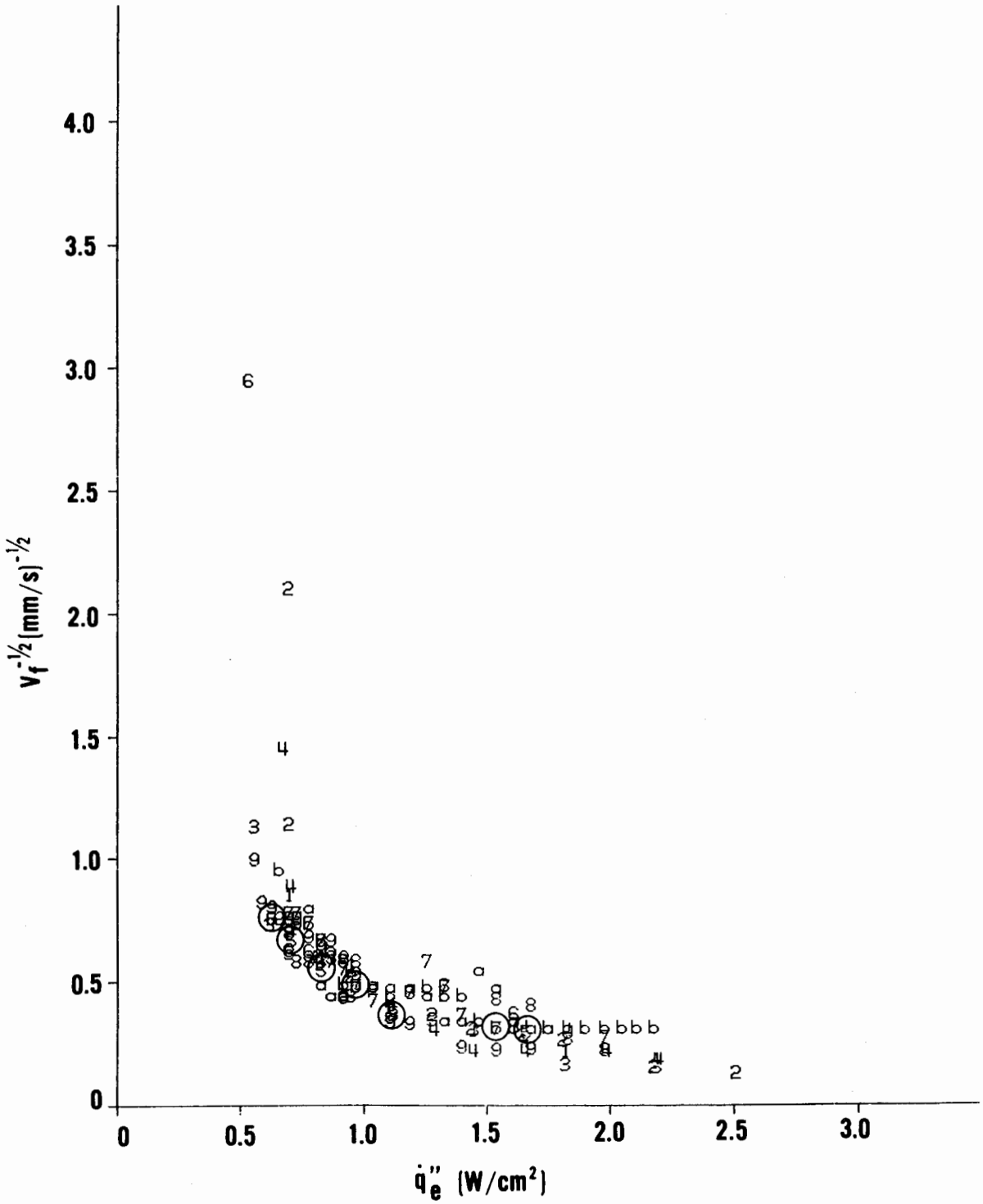

FIGURE 24. CORRELATION FOR RIGID FOAM FLAME SPREAD WITH FLUX
(5 INDICATES LONG PEREHEAT TEST)

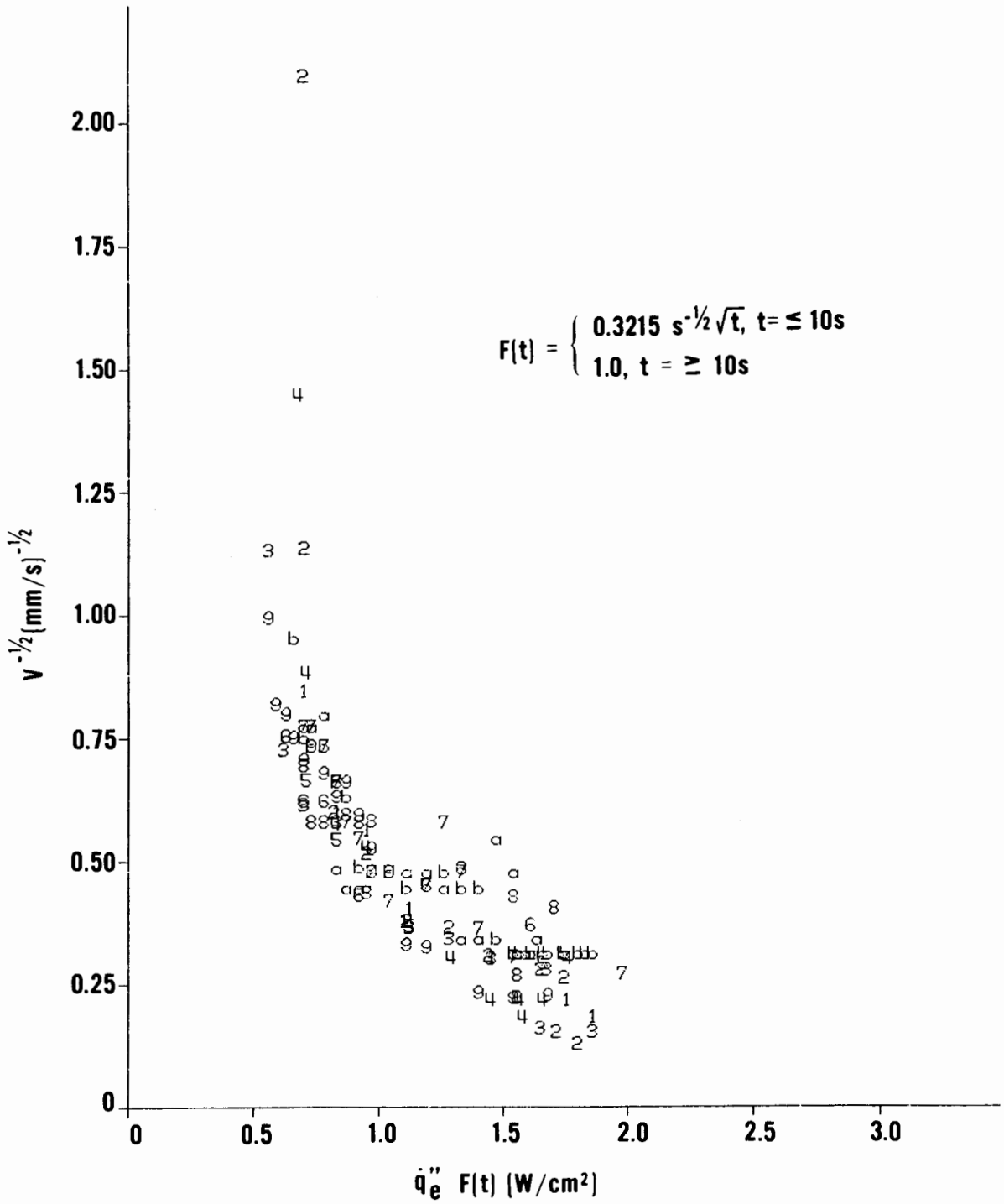

FIGURE 25. CORRELATION FOR RIGID FOAM FLAME SPREAD, F(t) BY EQ. (16)

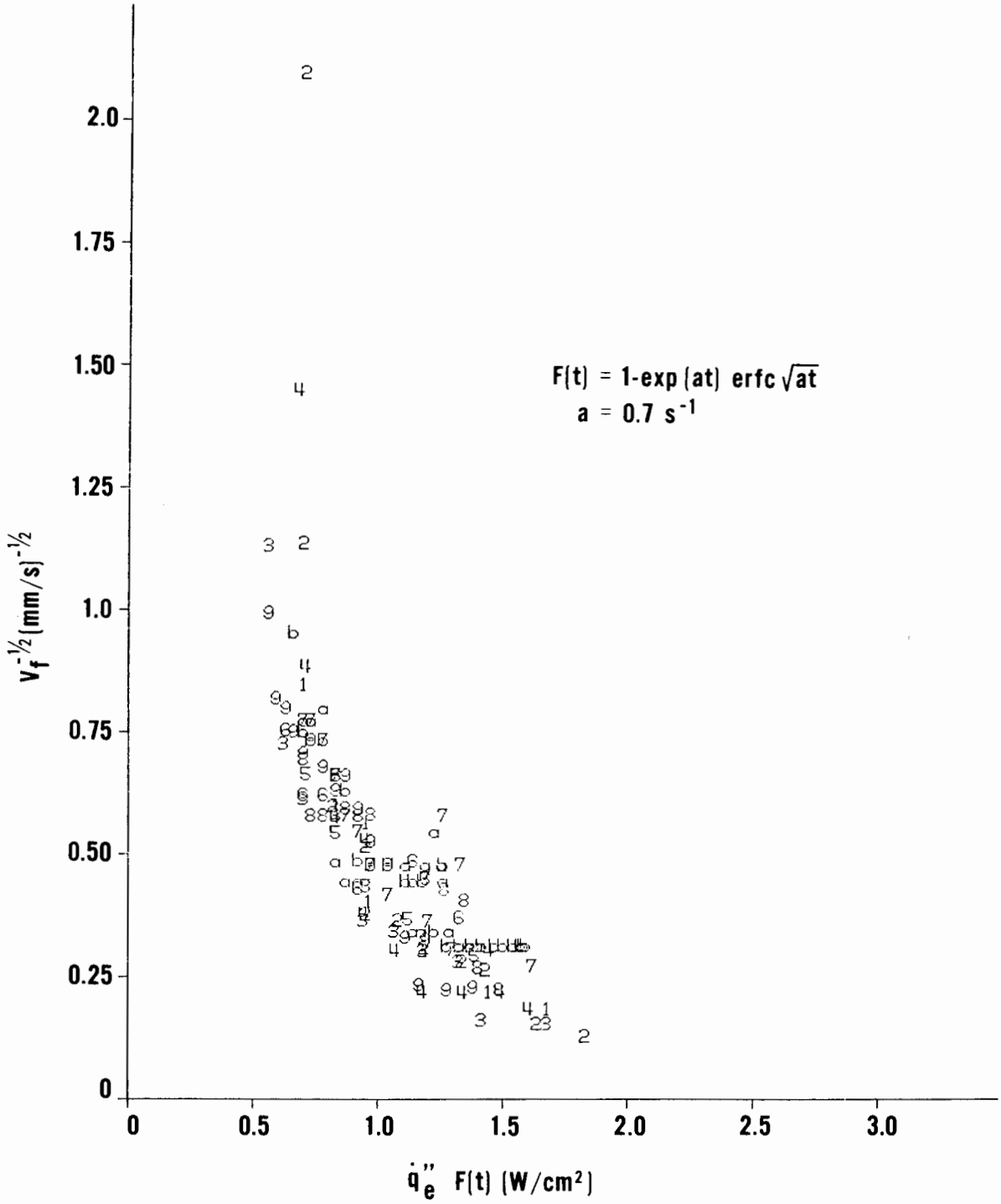

FIGURE 26. CORRELATION FOR RIGID FOAM FLAME SPREAD, F(t) BY EQ. (7b)

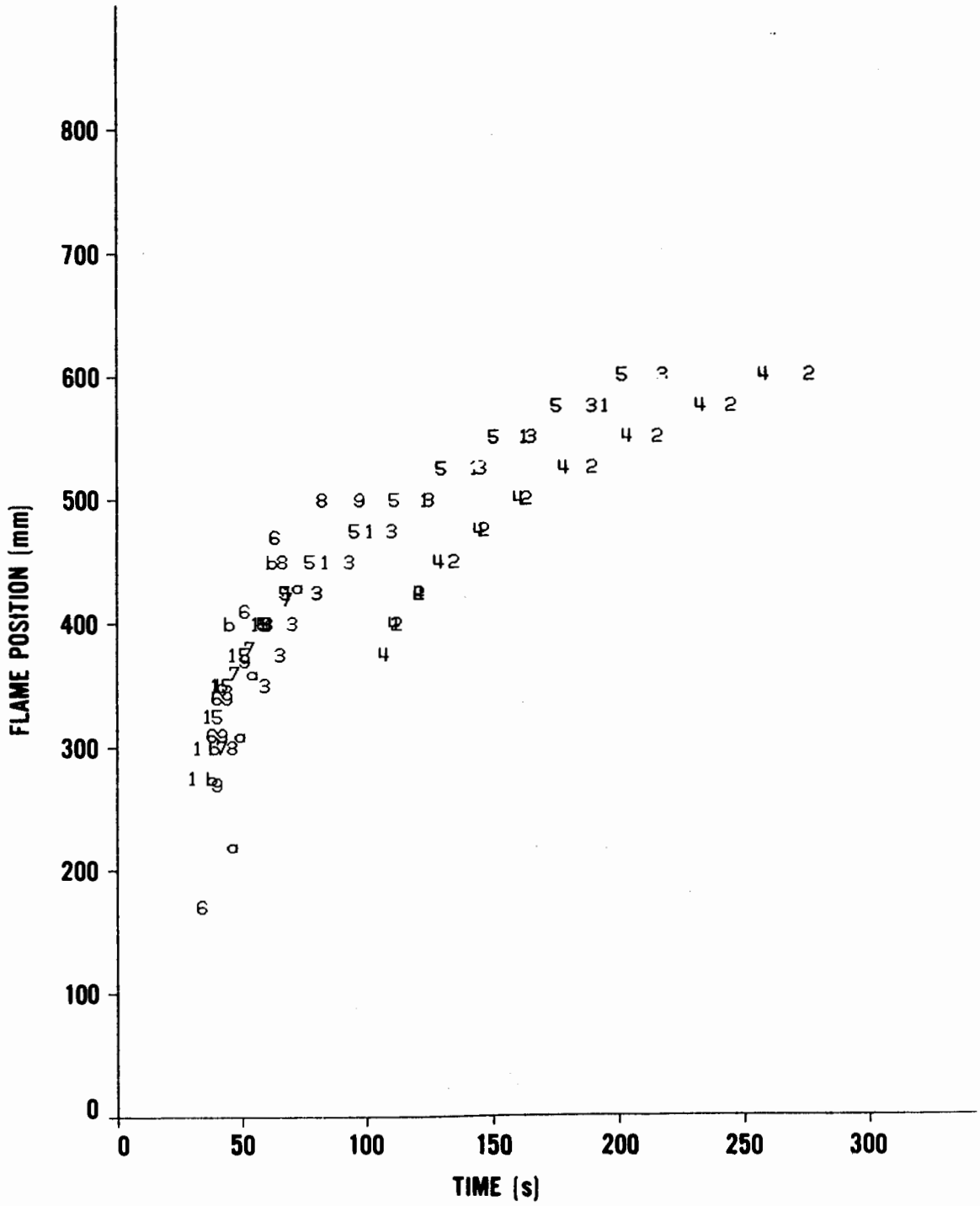

FIGURE 27. FLAME FRONT MOVEMENT FOR FLEXIBLE FOAM

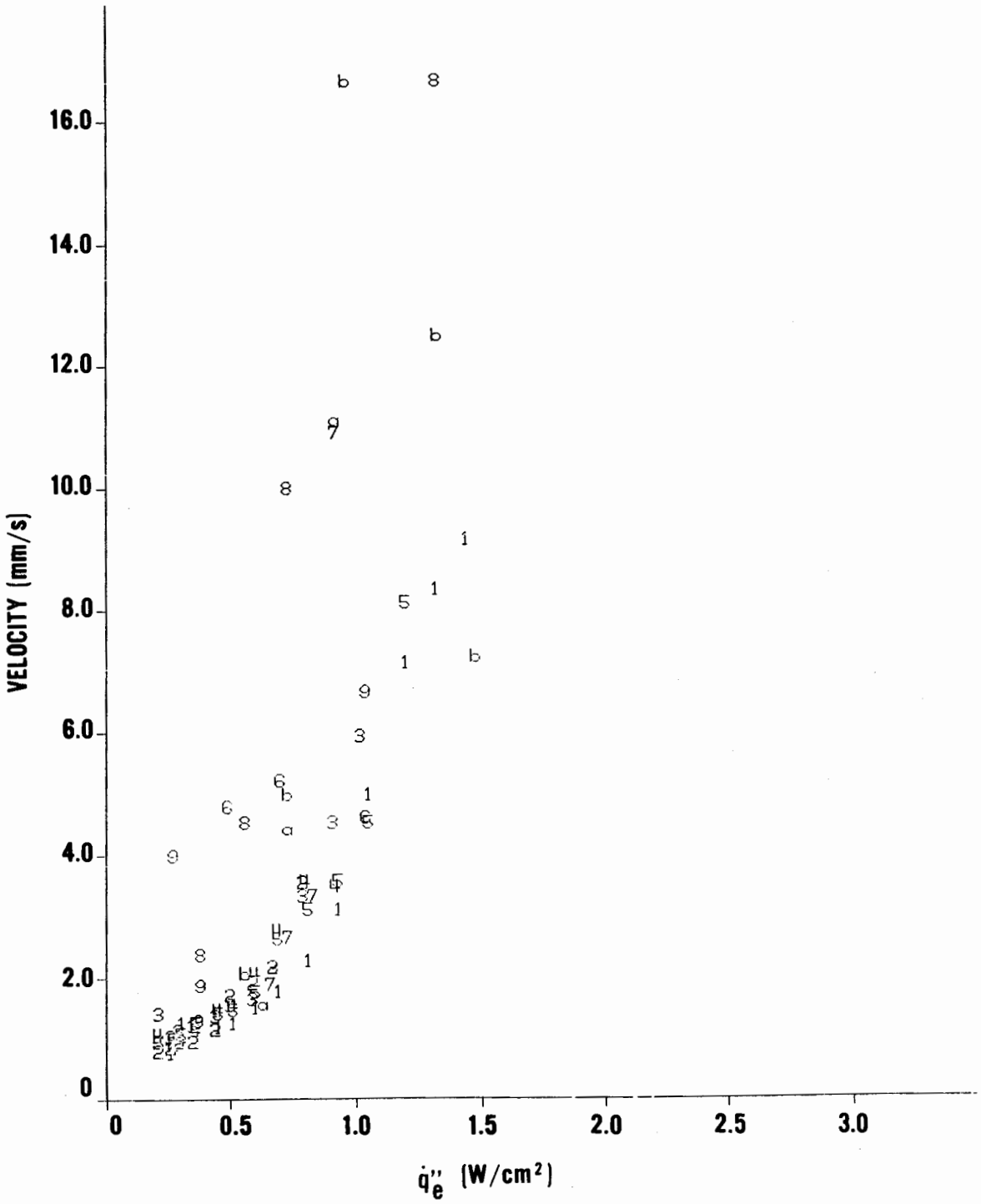

FIGURE 28. FLAME SPREAD VELOCITY FOR FLEXIBLE FOAM

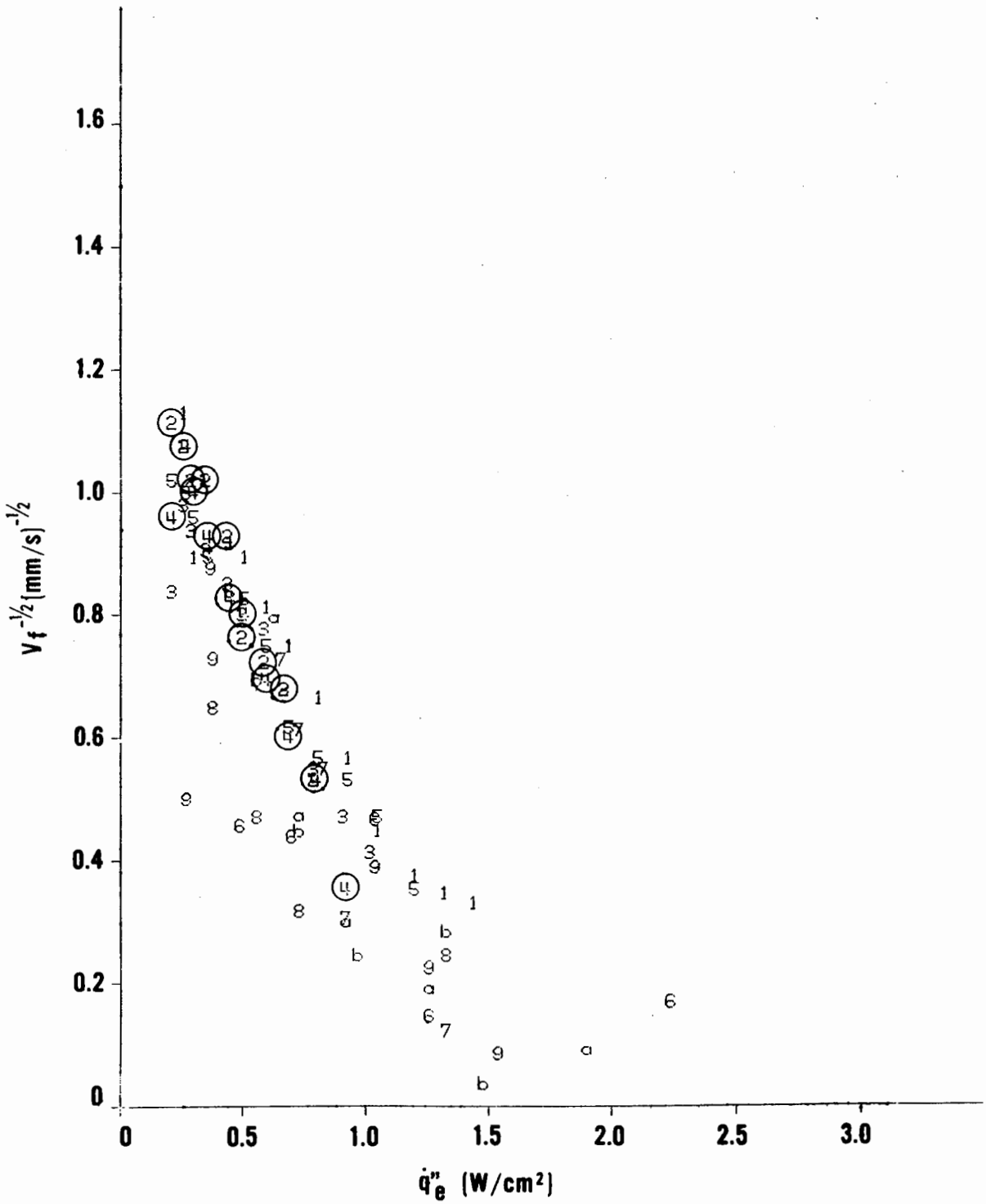

FIGURE 29. CORRELATION FOR FLEXIBLE FOAM FLAME SPREAD WITH FLUX (2 AND 4 INDICATES LONG PREHEAT TEST)

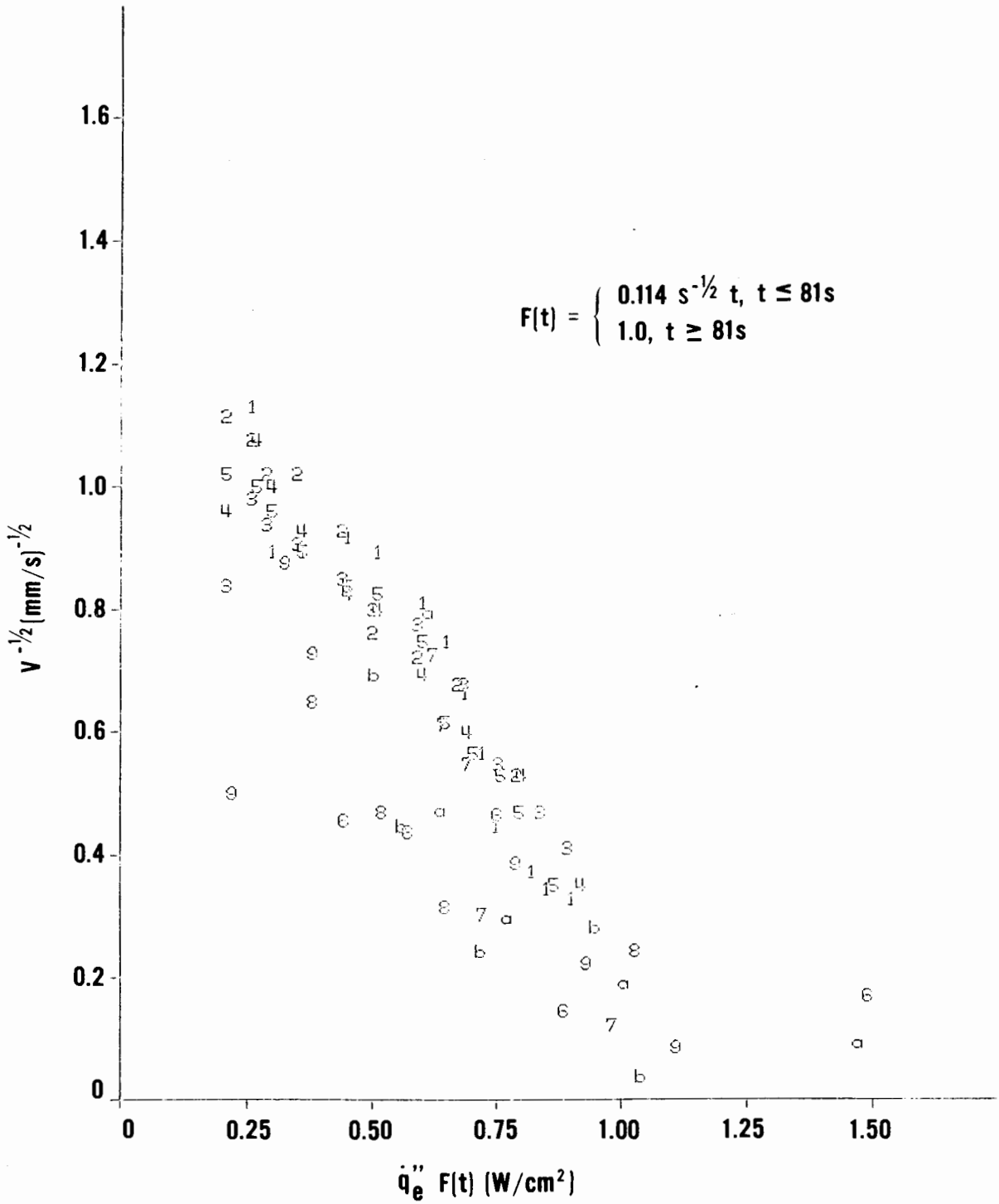

FIGURE 30. CORRELATION FOR FLEXIBLE FOAM FLAME SPREAD, F(t) BY EQ. (16)

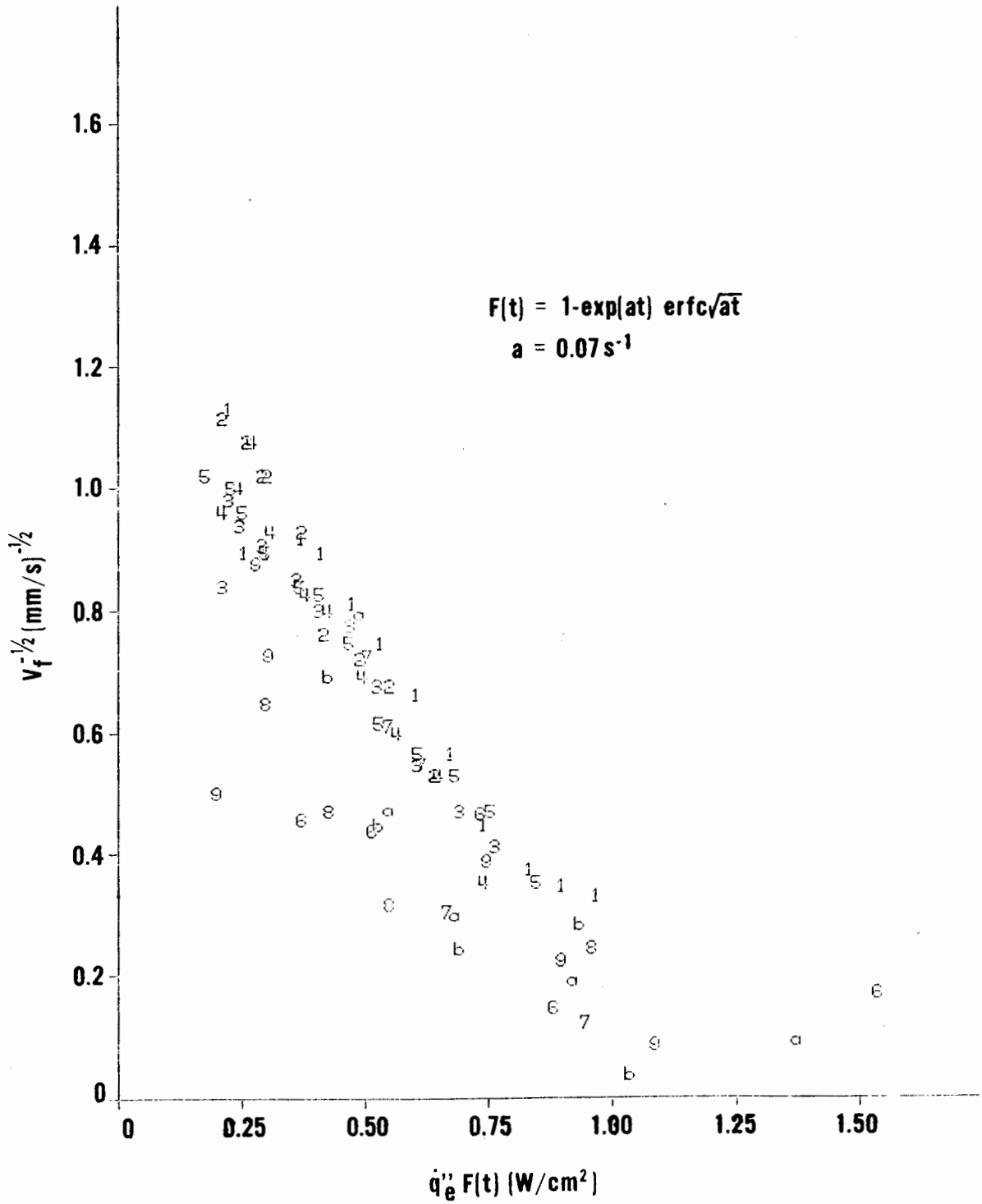

FIGURE 31. CORRELATION FOR FLEXIBLE FOAM FLAME SPREAD, F(t) BY EQ. (7b)

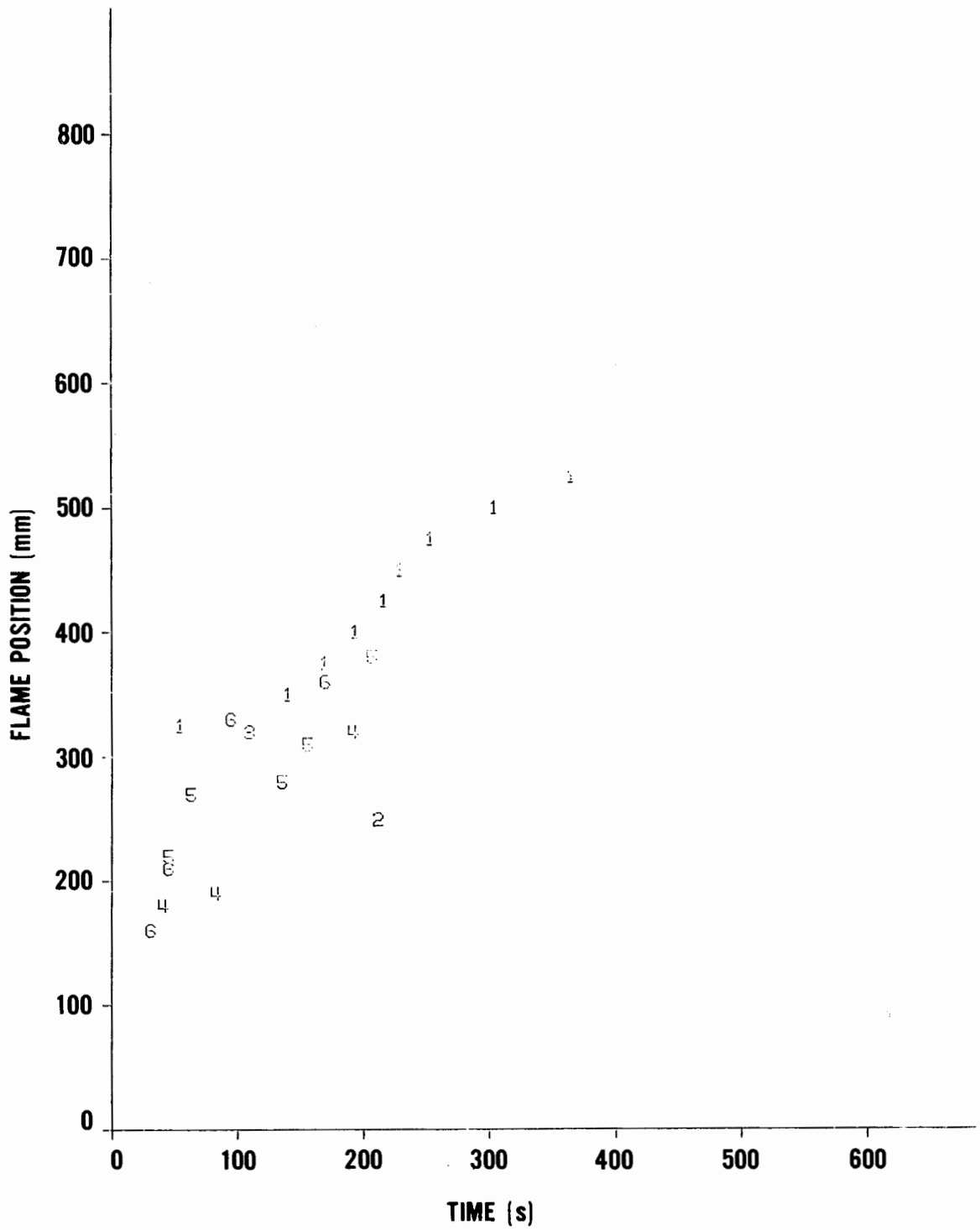

FIGURE 32. FLAME FRONT MOVEMENT FOR CARPET

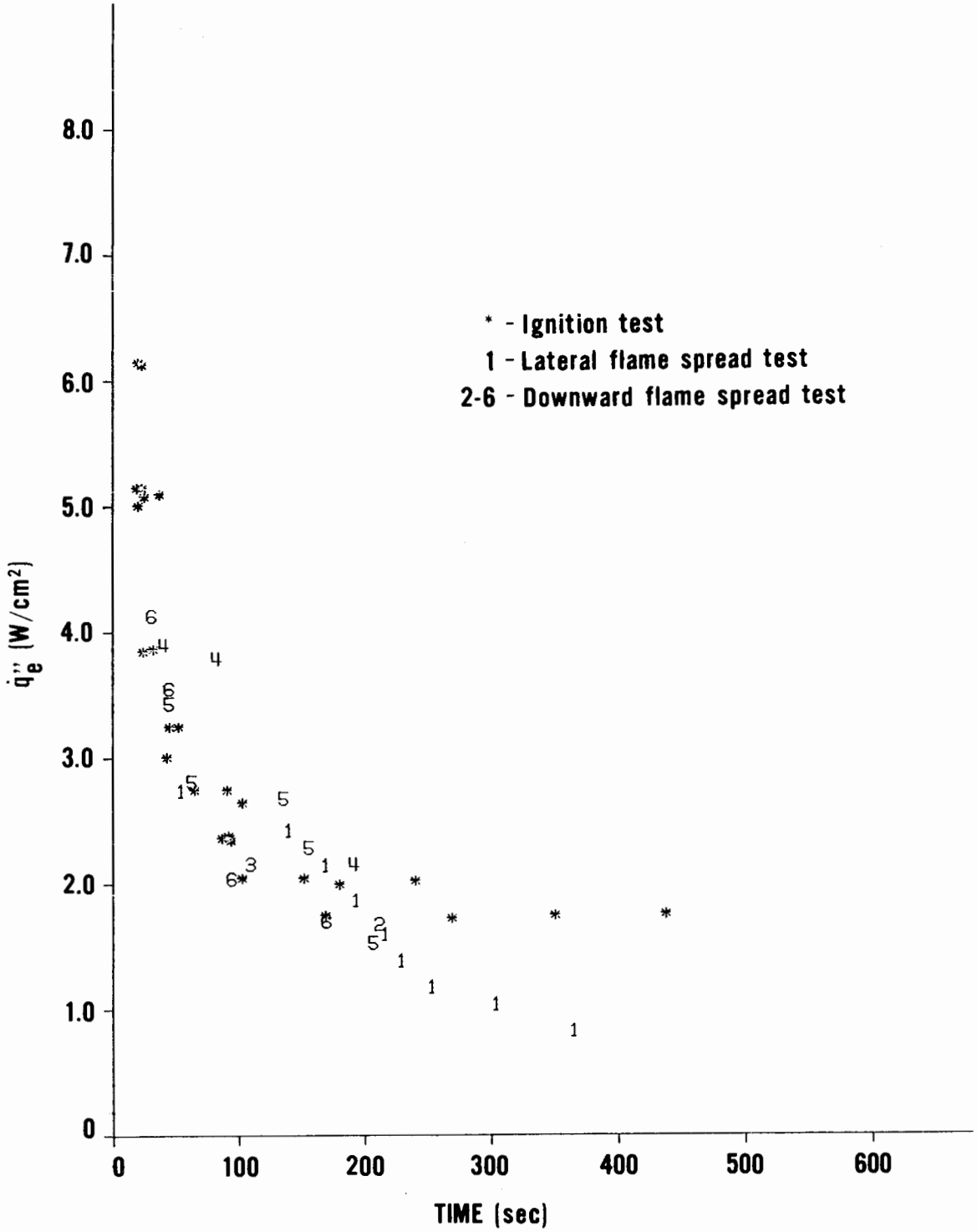

FIGURE 33. COMPARISON OF EXTERNAL FLUX WITH TIME FOR CARPET IGNITION AND FLAME SPREAD TESTS

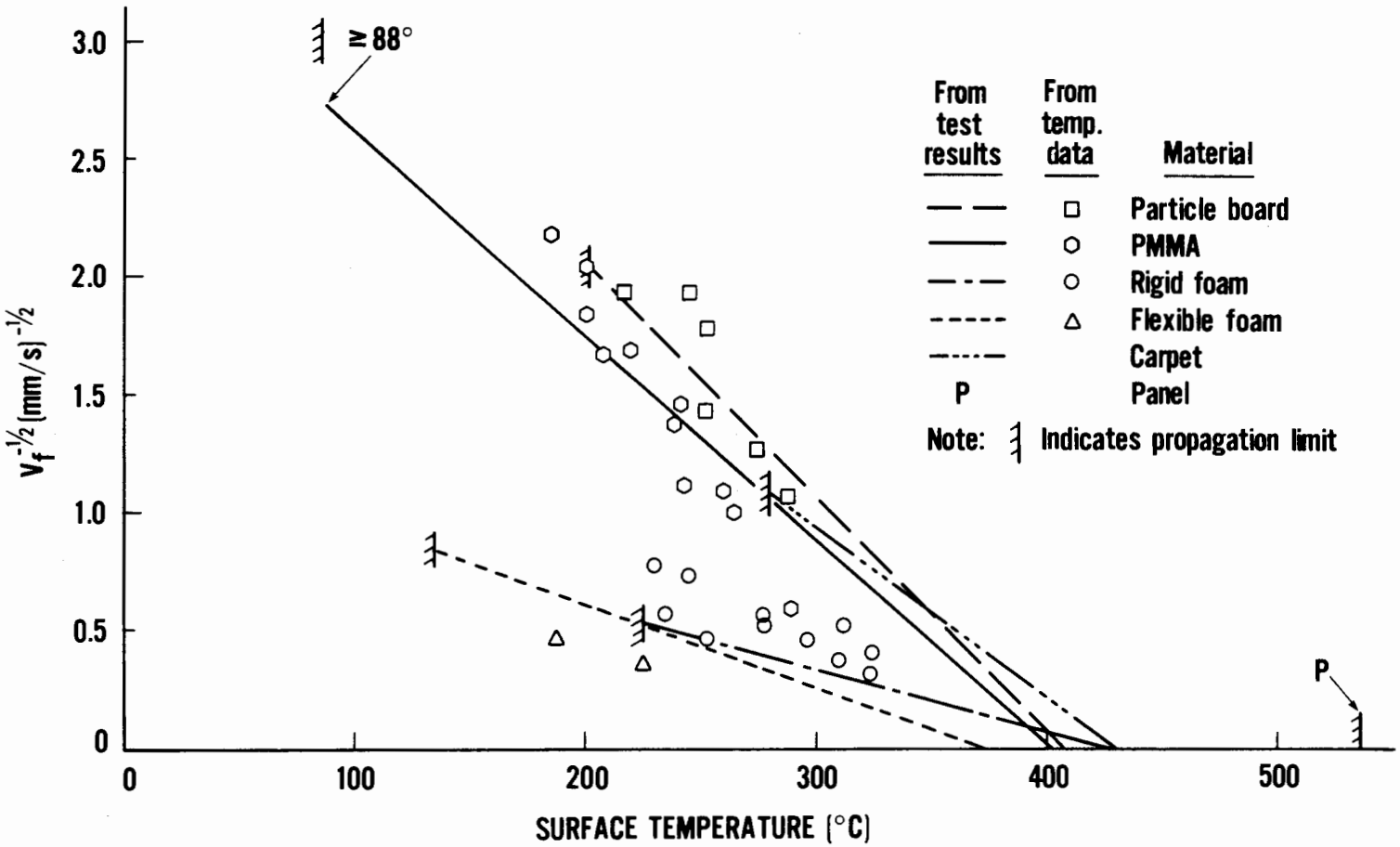

FIGURE 34. FLAME SPREAD VELOCITY IN TERMS OF SURFACE TEMPERATURE

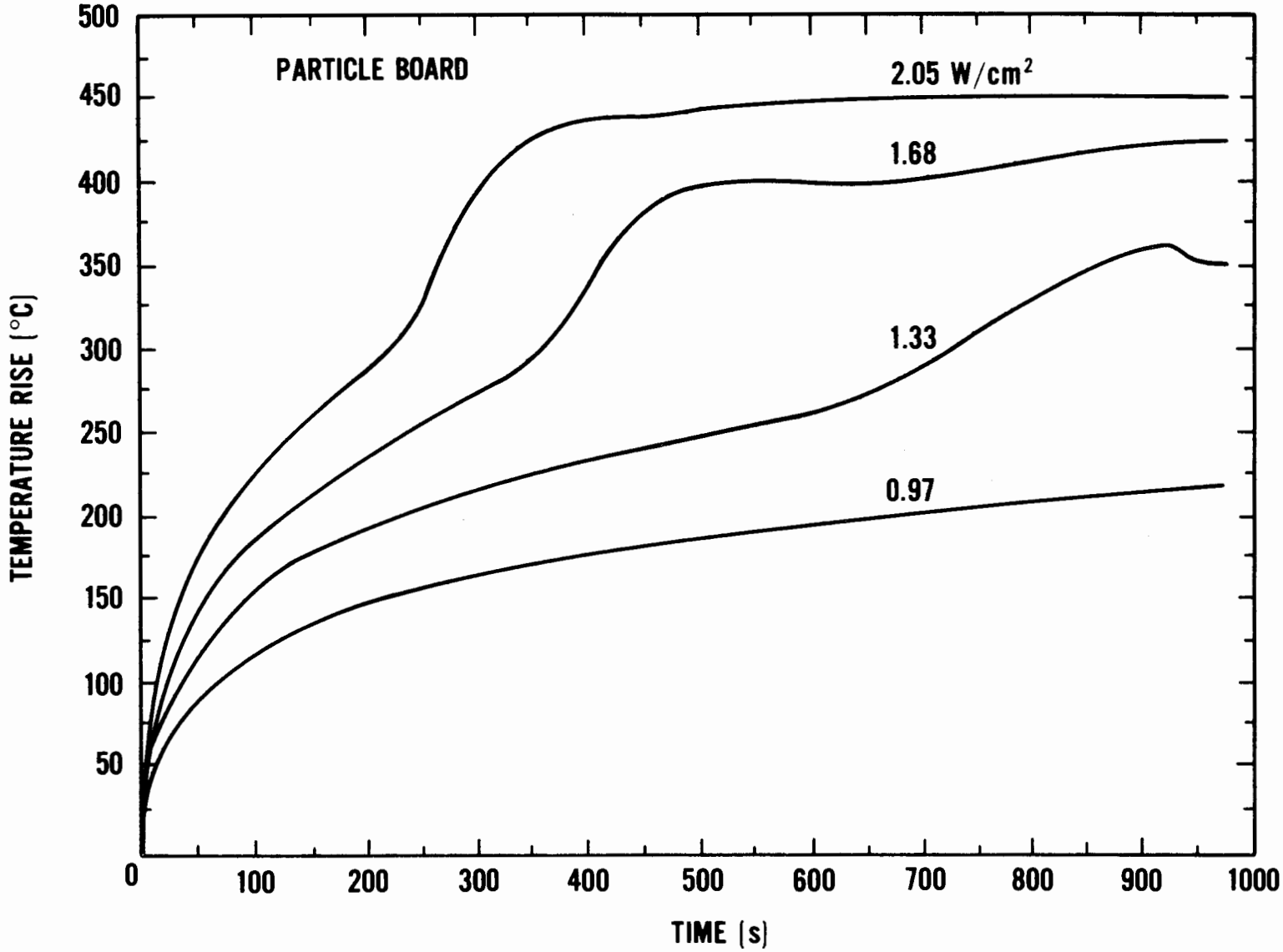

FIGURE 35. SURFACE TEMPERATURE RISE FOR PARTICLE BOARD

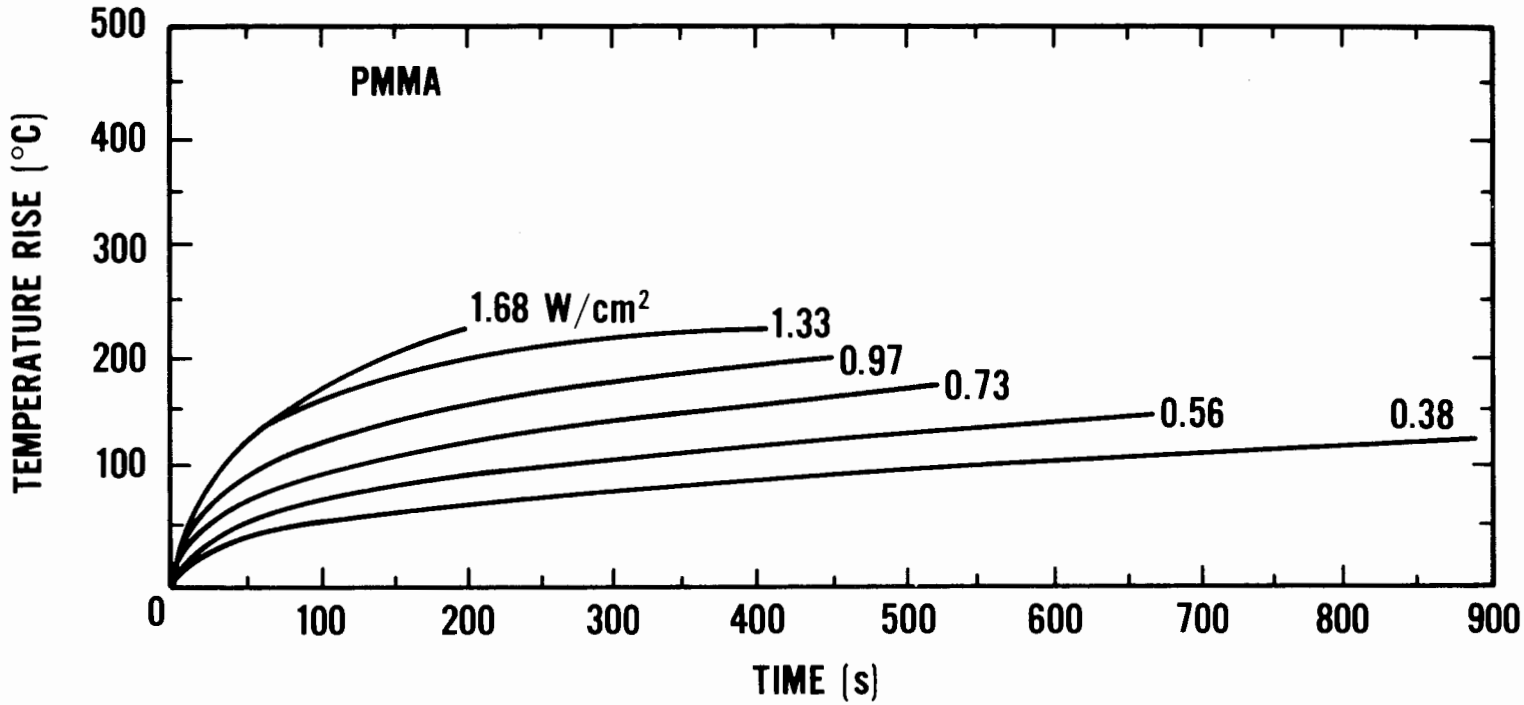

FIGURE 36. SURFACE TEMPERATURE RISE FOR PMMA

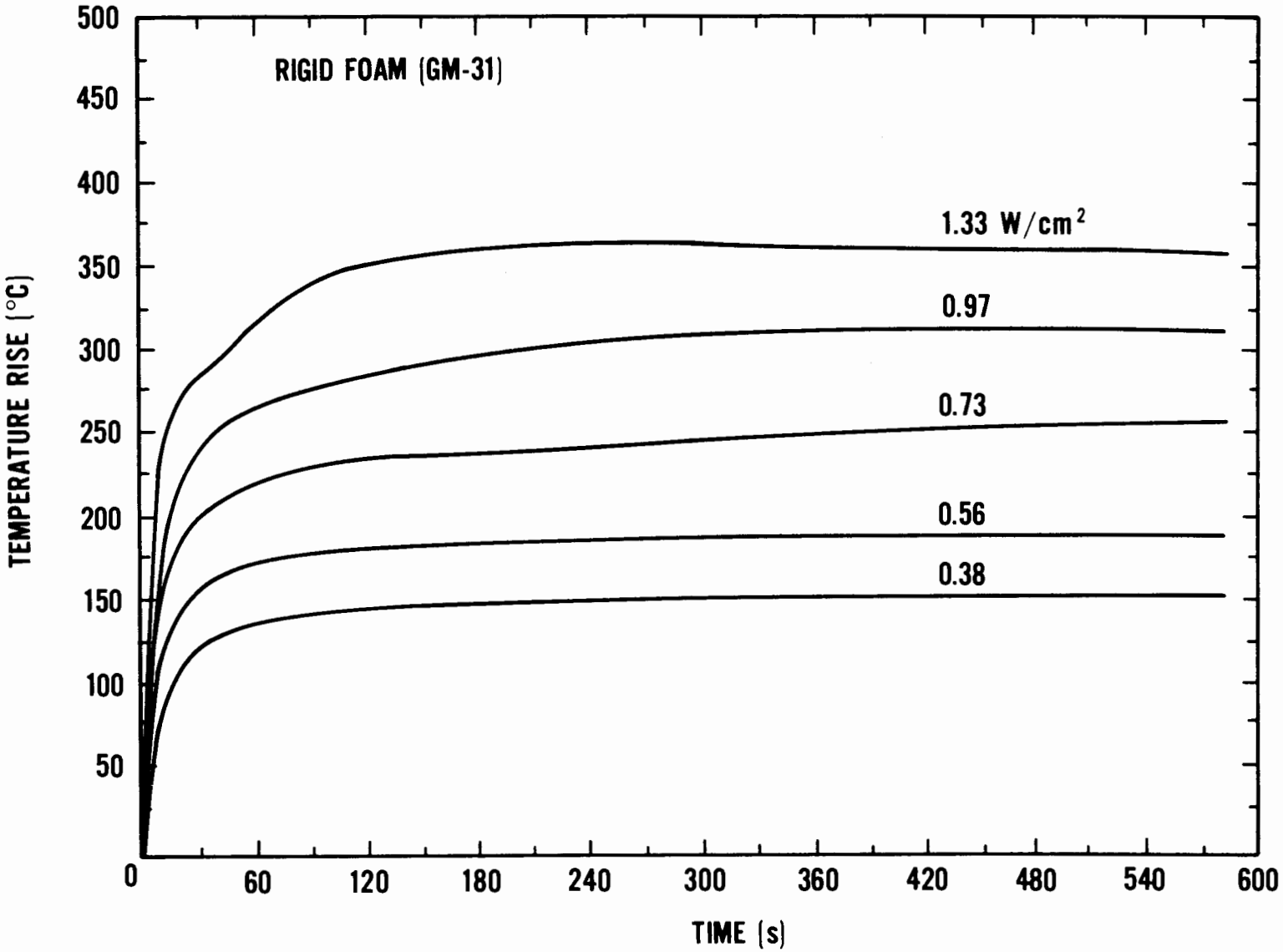

FIGURE 37. SURFACE TEMPERATURE RISE FOR RIGID FOAM

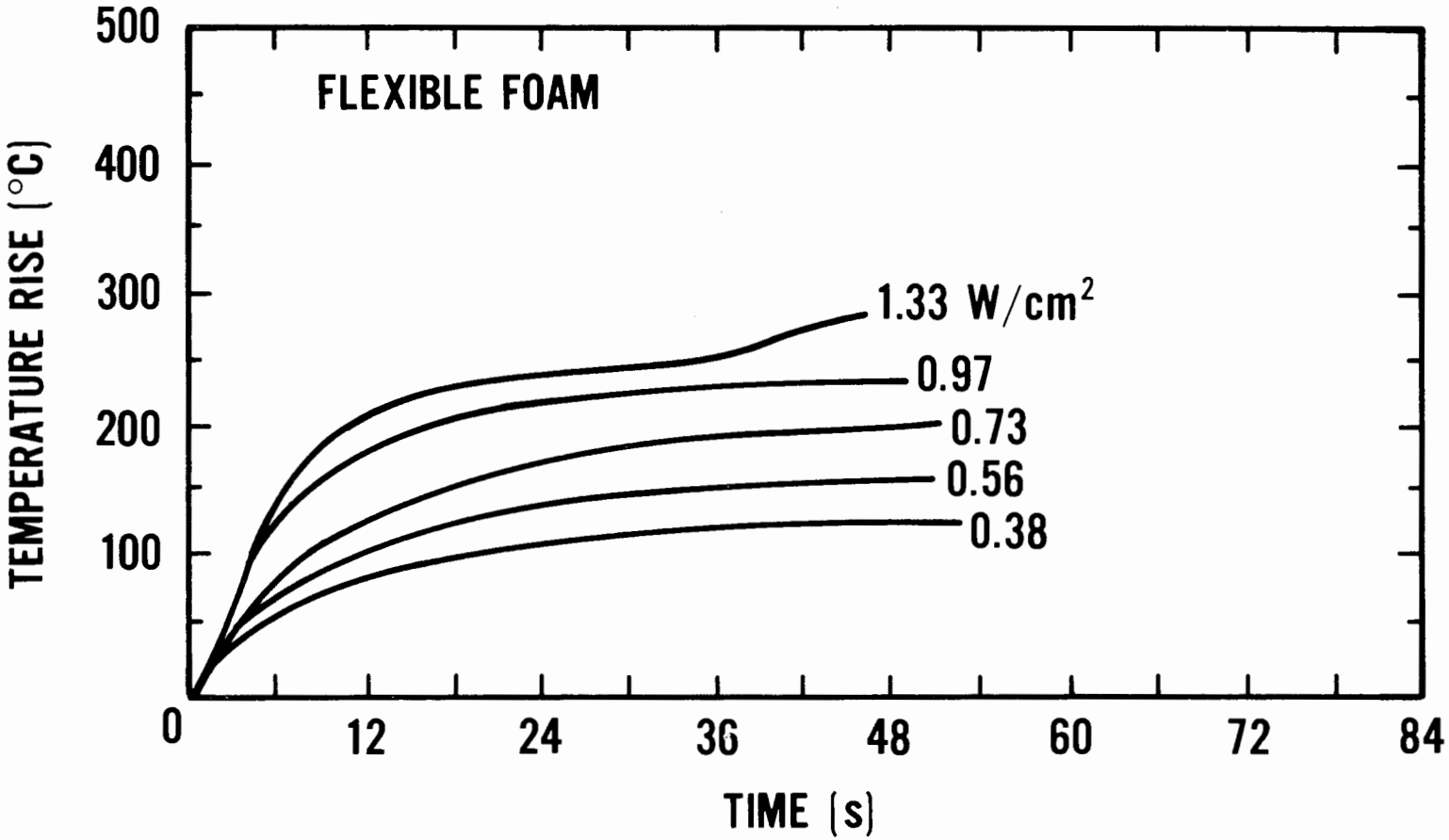

FIGURE 38. SURFACE TEMPERATURE RISE FOR FLEXIBLE FOAM

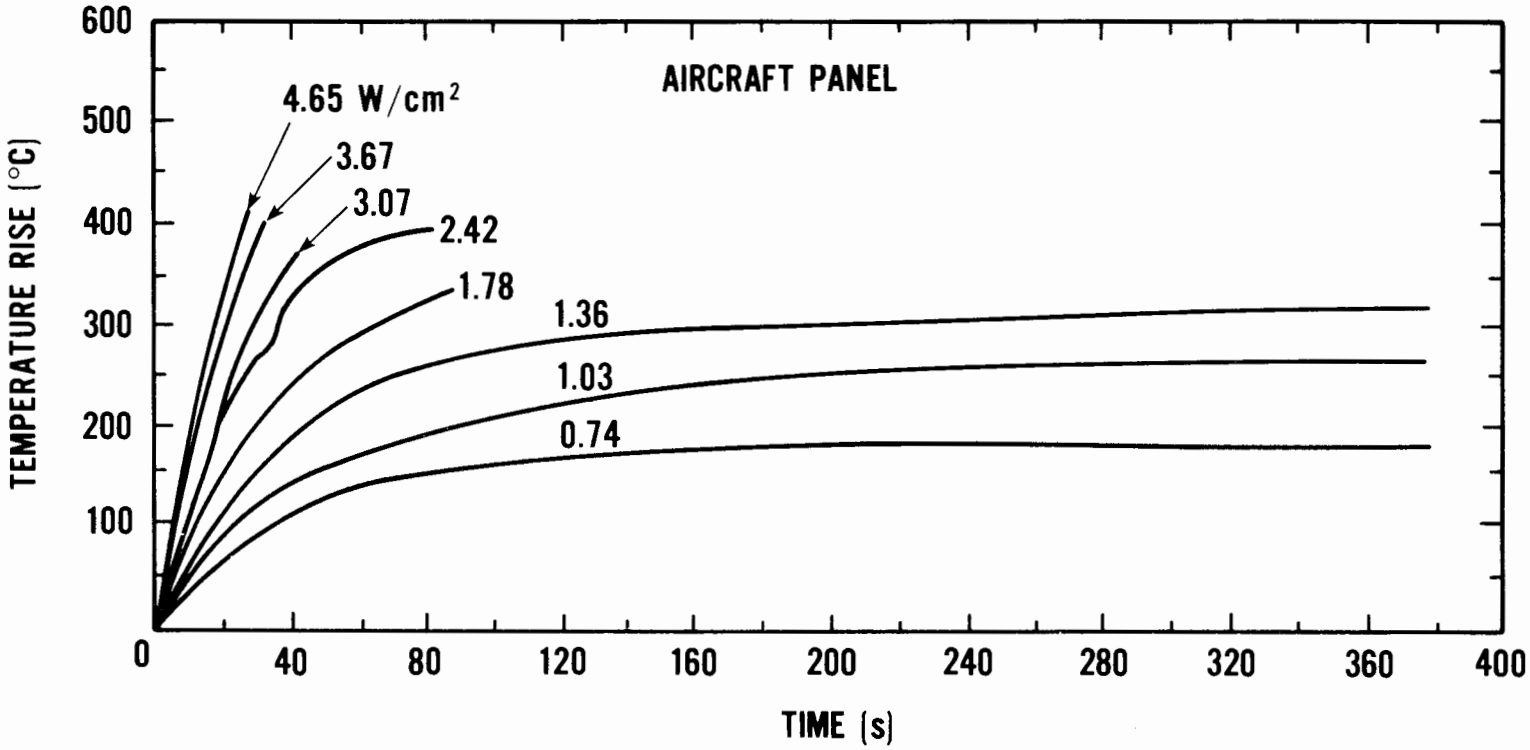

FIGURE 39. SURFACE TEMPERATURE RISE FOR AIRCRAFT PANEL

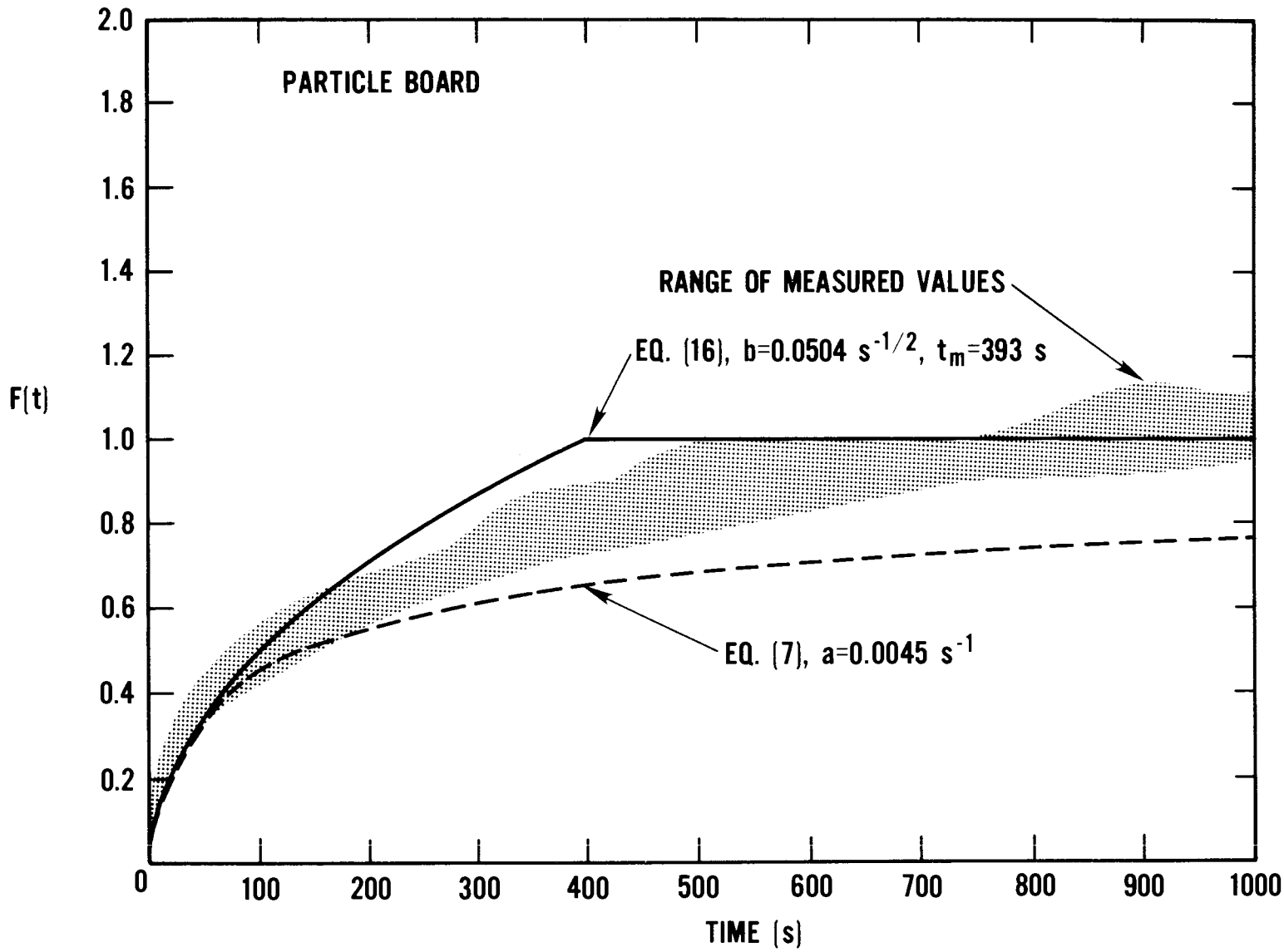

FIGURE 40. SURFACE TEMPERATURE PREDICTION FROM F(t) FOR PARTICLE BOARD

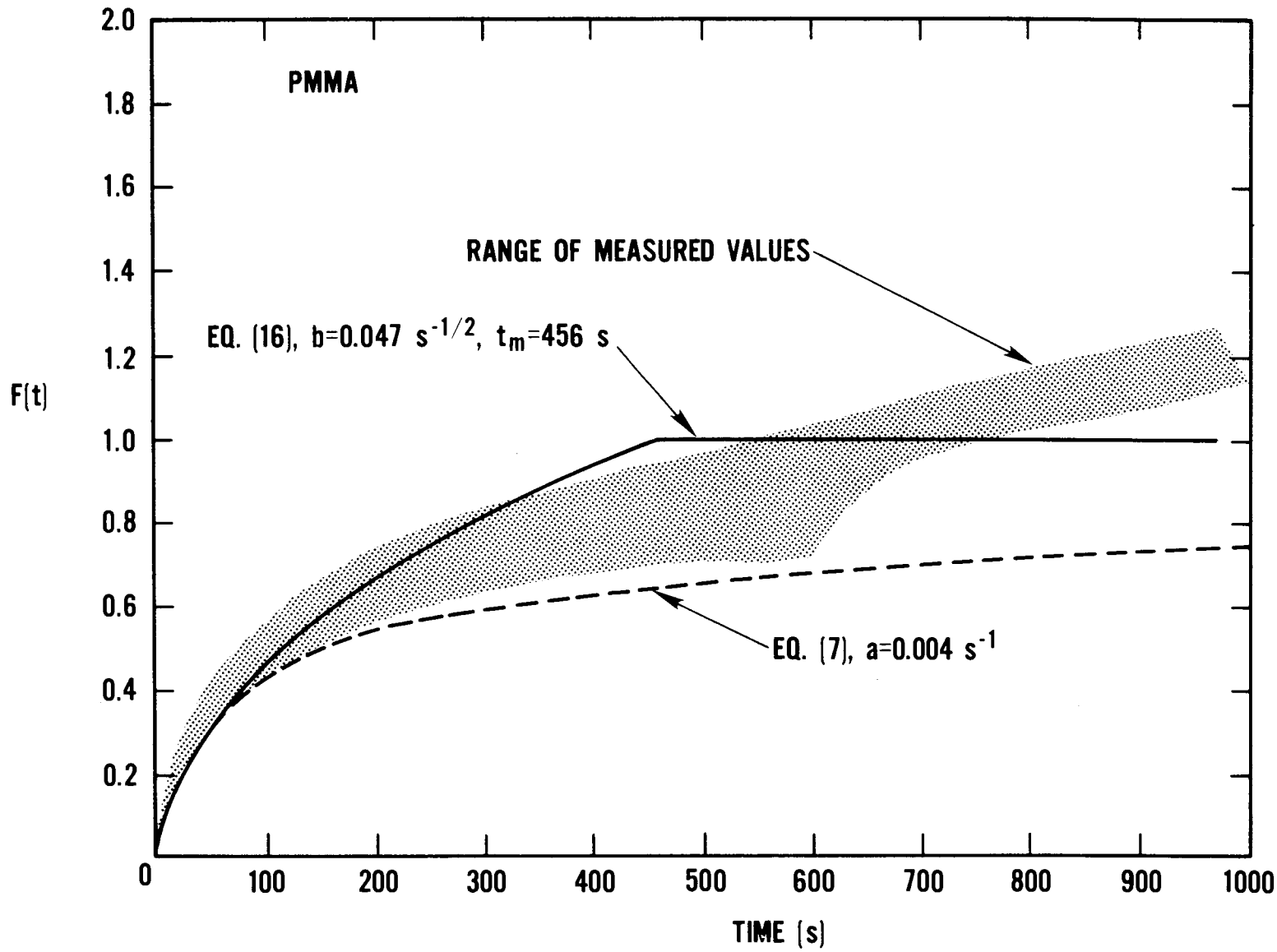

FIGURE 41. SURFACE TEMPERATURE PREDICTION FROM F(t) FOR PMMA

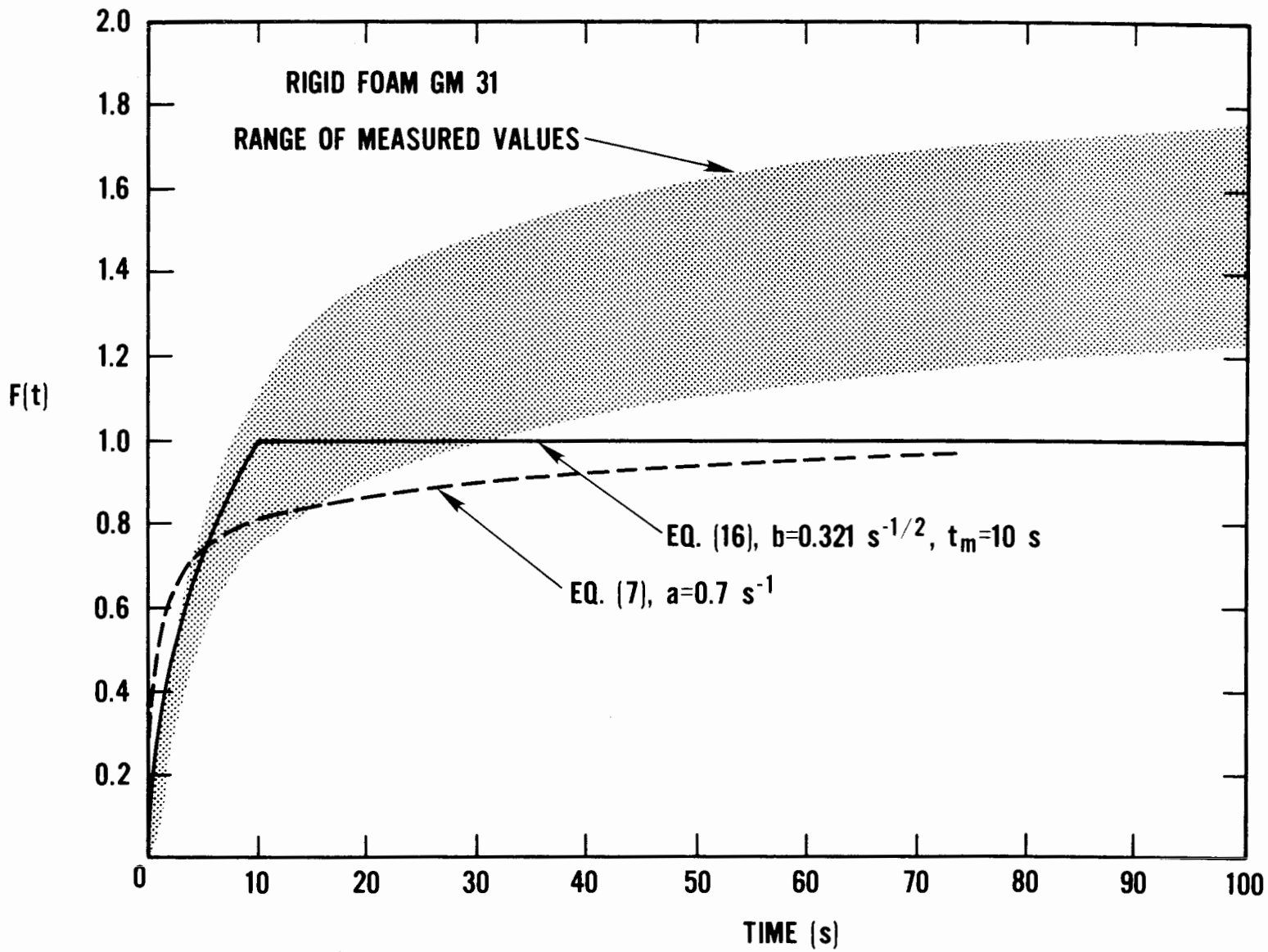

FIGURE 42. SURFACE TEMPERATURE PREDICTION FROM F(t) FOR RIGID FOAM

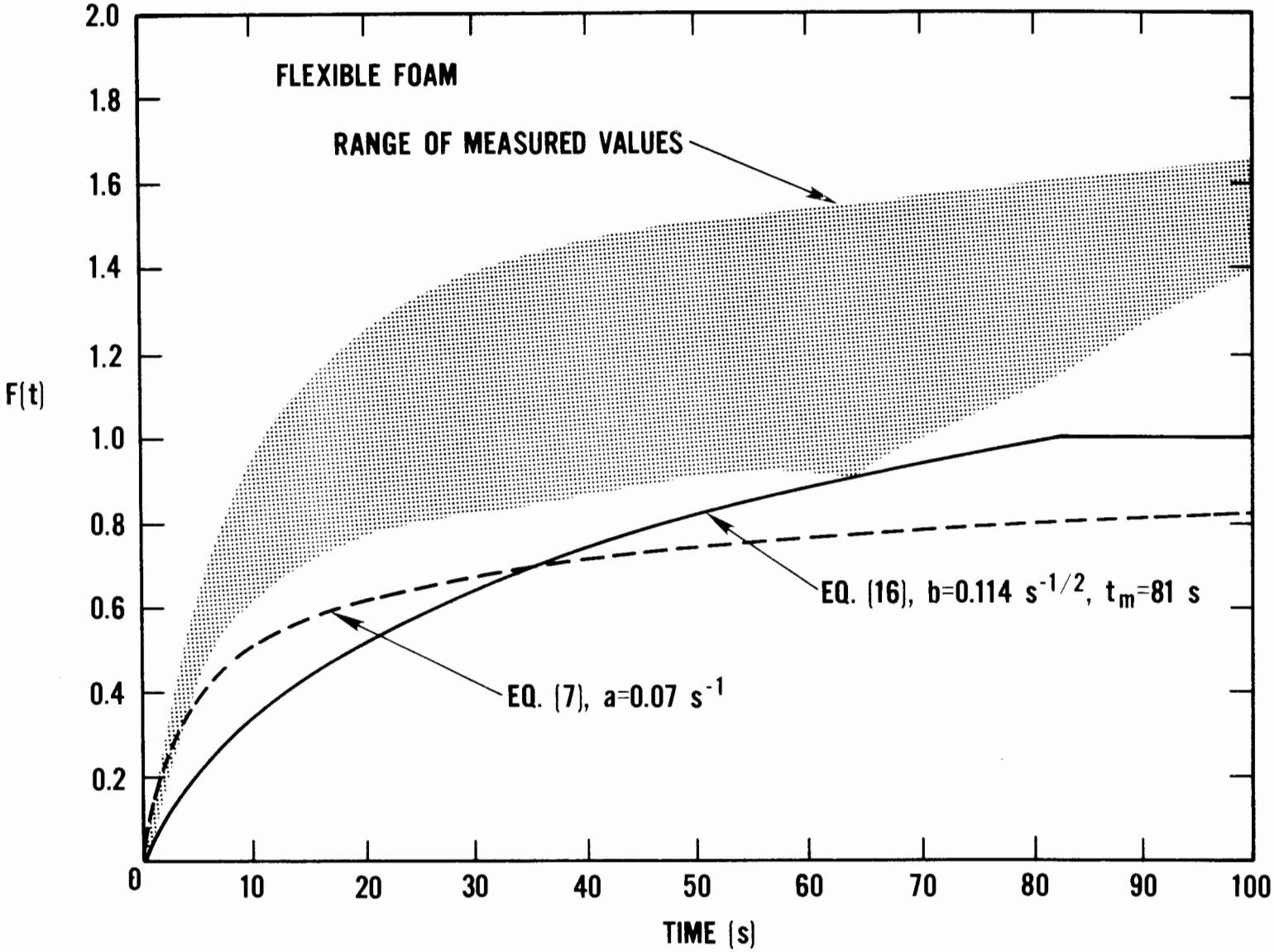

FIGURE 43. SURFACE TEMPERATURE PREDICTION FROM F(t) FOR FLEXIBLE FOAM

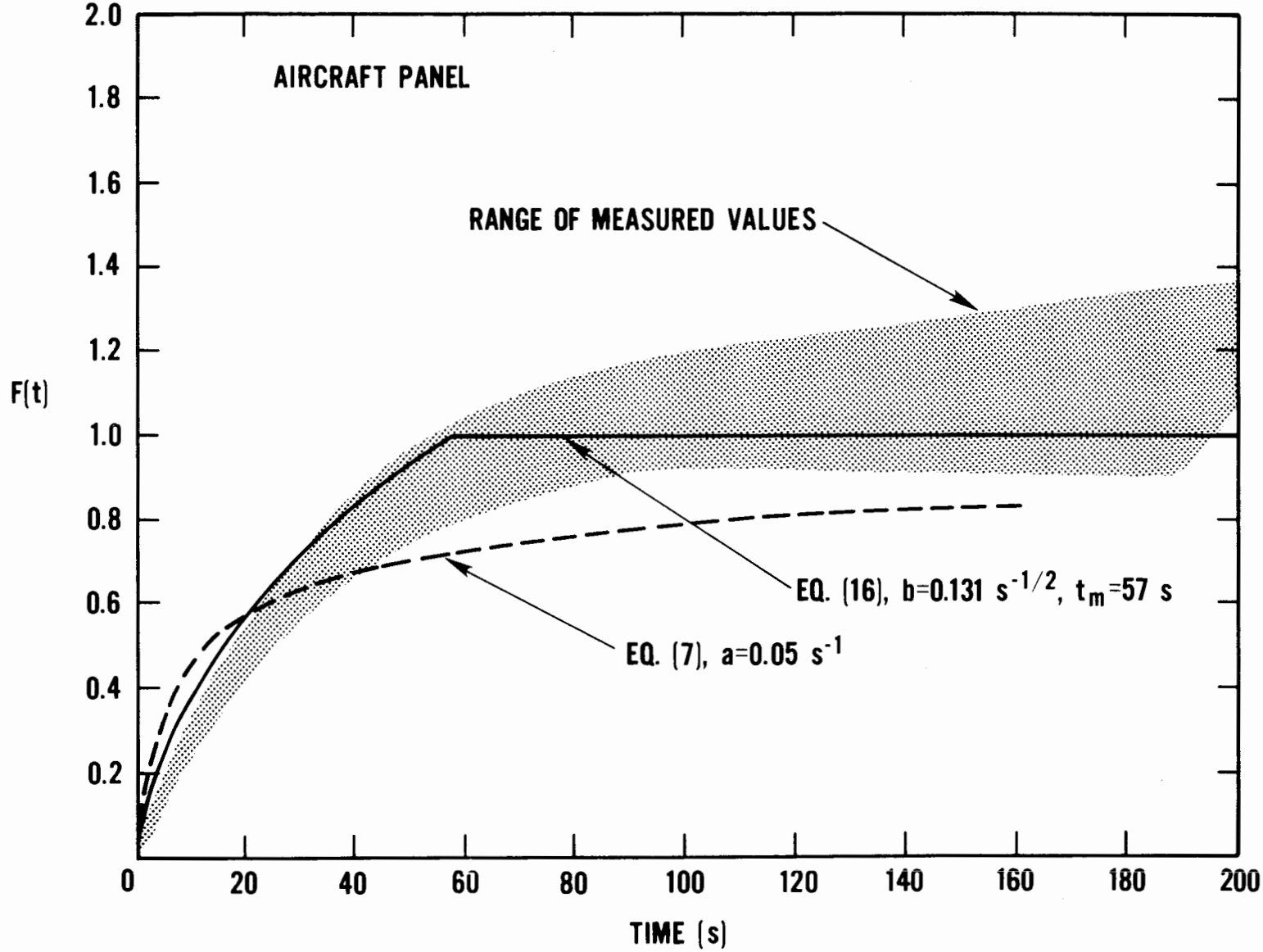

FIGURE 44. SURFACE TEMPERATURE PREDICTION FROM F(t) FOR AIRCRAFT PANEL